

**NOVEL PROBES BASED ON ORGANIC LIGANDS AND STUDY OF THEIR  
INTERACTIONS WITH SERUM ALBUMINS AND METAL IONS**

THESIS SUBMITTED TO  
**THE UNIVERSITY OF KERALA**  
FOR THE DEGREE OF  
**DOCTOR OF PHILOSOPHY**  
IN CHEMISTRY  
UNDER THE FACULTY OF SCIENCE

*By*  
**JISHA V. S.**

**PHOTOSCIENCES AND PHOTONICS  
CHEMICAL SCIENCES AND TECHNOLOGY DIVISION  
NATIONAL INSTITUTE FOR INTERDISCIPLINARY SCIENCE AND  
TECHNOLOGY (NIIST), CSIR  
TRIVANDRUM 695019, KERALA**

**OCTOBER 2010**

## STATEMENT

I hereby declare that the matter embodied in the thesis entitled: “**Novel Probes Based on Organic Ligands and Study of their Interactions with Serum Albumins and Metal Ions**” is the result of investigations carried out by me at the Photosciences and Photonics, Chemical Sciences and Technology Division of the National Institute for Interdisciplinary Science and Technology (*formerly*, Regional Research Laboratory), CSIR, Trivandrum, under the supervision of Dr. D. Ramaiah and the same has not been submitted elsewhere for a degree.

In keeping with the general practice of reporting scientific observations, due acknowledgement has been made wherever the work described is based on the findings of other investigators.

**(JISHA V. S.)**

National Institute for Interdisciplinary Science and Technology



**Photosciences and Photonics**  
**Chemical Sciences and Technology Division**  
Trivandrum 695019, India



**Dr. D. Ramaiah**  
Scientist

Tel: +91 471 2515362; Fax: +91 471 2490186

E-mail: rama@niist.res.in

---

October 18, 2010

### CERTIFICATE

This is to certify that the work embodied in the thesis entitled:  
**“Novel Probes Based on Organic Ligands and Study of their Interactions with Serum Albumins and Metal Ions”** has been carried out by Ms. JISHA V. S. under my supervision at the Photosciences and Photonics, Chemical Sciences and Technology Division of the National Institute for Interdisciplinary Science and Technology (NIIST), CSIR, Trivandrum and the same has not been submitted elsewhere for a degree.

(D. Ramaiah)

**Thesis Supervisor**

## ACKNOWLEDGEMENTS

*I have great pleasure in placing on record my deep sense of gratitude to Dr. D. Ramaiah, my thesis supervisor, for suggesting the research problem and for his guidance, support and encouragement, leading to the successful completion of this work.*

*I would like to express my sincere thanks to Professor M. V. George for his constant help and encouragement during the tenure of this work.*

*I wish to thank Dr. Suresh Das, Professor T. K. Chandrashekar and Dr. B. C. Pai, Directors of the National Institute for Interdisciplinary Science and Technology (NIIST) for providing me the necessary facilities for carrying out the work.*

*I sincerely thank Dr. A. Ajayaghosh, Dr. K. R. Gopidas, Dr. K. George Thomas and Dr. A. Srinivasan, Scientists of the Photosciences and Photonics, Chemical Sciences and Technology Division, for all the help and support extended to me. I sincerely thank Professor Dr. Bernd Epe, Institute for Pharmacy, University of Mainz, Germany for the help during my visit to the University of Mainz, Germany.*

*I thank all the members of the Photosciences and Photonics and in particular, Ms. R. R. Avirah, Dr. J. Joseph, Dr. K. T. Arun, Dr. M. Hariharan, Dr. E. Kuruvilla, Dr. J. Kuthanapillil, Dr. P. P. Neelakandan, Mr. A. K. Nair, Mr. S. C. Karunakaran, Mr. P. C. Nandajan, Mr. K. S. Sanju, Ms. T. J. Dhanya, Mr. N. Adarsh, Ms. M. Betsy, Mr. A. K. Paul, Mr. Harisankar, Ms. A. J. Thomas, Mr. K. V. Ratheesh, Mr. A. R. Ramesh and Mr. Anesh Gopal for their help and cooperation. I also thank members of other Divisions of NIIST for their help and cooperation. I would like to thank Mr. Robert Philip and Mrs. Sarada Nair for their help and support and also Ms. Saumini Shoji, Mr. A. Adarsh and Ms. S. Viji for NMR and mass spectral analyses.*

*I am deeply indebted to my parents, grand mother, brother, sister, in-laws and family members for their endless love, support and understanding. I am deeply grateful to my loving and encouraging husband Murali Das for his patience and support during the final stage of the thesis. I would also like to extend my thanks and appreciation to all my teachers for their help and blessings.*

*I sincerely thank the UGC-CSIR, DST and Government of India and DAAD, Germany for the financial support.*

**Jisha V. S.**

## CONTENTS

	Page
<b>Statement</b>	<b>i</b>
<b>Certificate</b>	<b>ii</b>
<b>Acknowledgements</b>	<b>iii</b>
<b>Contents</b>	<b>iv</b>
<b>Preface</b>	<b>vii</b>
<b>List of Figures</b>	<b>xi</b>
<b>List of Tables</b>	<b>xiv</b>
<b>List of Schemes</b>	<b>xv</b>
<b>List of Abbreviations</b>	<b>xvi</b>
<b>Chapter 1. Interactions of Ligands with Proteins and Metal Ions: An Overview</b>	
<b>1.1. Introduction</b>	<b>1</b>
<b>1.2. Proteins: Structure and Function</b>	<b>3</b>
<b>1.3. Classification of Proteins</b>	<b>7</b>
<b>1.4. Importance of Transport Proteins</b>	<b>9</b>
<b>1.5. Structural Features of Serum Albumins</b>	<b>10</b>
<b>1.6. Interactions of Ligands with Serum Albumins</b>	<b>14</b>
<b>1.7. Site Selective Binding Agents of Serum Albumins</b>	<b>18</b>
<b>1.8. Interactions of Ligands with Metal Ions</b>	<b>23</b>
<b>1.8.1. Fluorescent Sensors for Metal Ions Detections</b>	<b>24</b>
<b>1.9. Background for the Present Investigation</b>	<b>30</b>
<b>1.10. Objectives of the Present Investigation</b>	<b>33</b>
<b>Chapter 2. Study of Interactions of Squaraine Dyes with BSA and HSA</b>	
<b>2.1. Abstract</b>	<b>35</b>

2.2.	Introduction	36
2.3.	Results	42
2.3.1.	Synthesis, and Photophysical Properties	40
2.3.2.	Interactions of Squaraine Dyes with Serum Albumins	42
2.3.3.	Calculation of Association Constants	47
2.3.4.	Time-resolved and Circular Dichroism Studies	48
2.3.5.	Time-resolved Anisotropy and <sup>1</sup> H NMR Studies	52
2.3.6.	Morphology Studies	54
2.3.7.	Stability of the Dyes in presence of Serum Albumin	56
2.3.8.	Effect of Serum Albumin on Excited States	58
2.4.	Discussion	61
2.5.	Conclusions	63
2.6.	Experimental Section	64
<b>Chapter 3.</b>	<b>Site-Selective Binding Interactions of Squaraine Dyes with BSA, HSA and Other Selected Proteins</b>	
3.1.	Abstract	68
3.2.	Introduction	69
3.3.	Results	72
3.3.1.	Site- Selective Binding Ligand Displacement Method	72
3.3.2.	Circular Dichroism (CD) Studies	78
3.3.3.	Fluorescence Resonance Energy Transfer (FRET) Studies	83
3.3.4.	Interactions with Squaraine Dyes with Other Proteins	87
3.3.5.	Detection of Serum Albumins in Gel Electrophoresis	89
3.3.6.	Interaction of Squaraine Dyes with Modified Protein	90
3.4.	Discussion	94
3.5.	Conclusions	97
3.6.	Experimental Section	97

<b>Chapter 4.</b>	<b>Novel Naphthalimide–Dansyl Dyads and Study of their Interactions with Mono and Divalent Metal Ions</b>	
4.1.	Abstract	100
4.2.	Introduction	101
4.3.	Results	105
4.3.1.	Synthesis of the Dyads	105
4.3.2.	Absorption and Fluorescence Properties	108
4.3.3.	Interactions with Metal Ions	110
4.3.4.	Stoichiometry of the Complexation	114
4.3.5.	Reversibility of the Complexation	115
4.3.6.	Nature of the Complexation	116
4.3.7.	Selectivity of the Metal Ion Complexation	120
4.4.	Discussion	123
4.5.	Conclusions	125
4.6.	Experimental Section	125
	<b>References</b>	<b>129</b>
	<b>List of Publications</b>	<b>163</b>

## PREFACE

There is a widespread interest in studying the interactions of small molecules, including drugs, dyes and toxic compounds with biomolecules, especially proteins and metal ions because of their importance in medicinal and biochemical applications. Understanding the ligand-protein interactions would not only lead to the development of molecular probes for their recognition but also efficient drugs for biomedical applications. Among the various proteins, transport proteins such as serum albumins, play an important role as they facilitate the disposition and transportation of various ligands like drugs, amino acids, fatty acids, bilirubin, bile acids and thyroxine to the specific targets. The specific delivery of ligands by serum albumin originates from the presence of two major and structurally selective binding sites, namely, site I and site II, which are located in three homologous domains that form a heart-shaped protein. The binding affinity offered by site I is mainly through hydrophobic interactions, whereas site II involves a combination of hydrophobic, hydrogen bonding and electrostatic interactions.

Recently, it has been reported that sensitizers possessing higher affinity for serum albumin and showing preferential binding at site II are found to exhibit efficient photodynamic therapeutic applications (PDT). In this regard, the present thesis describes our efforts towards understanding the nature and selective binding interactions of various near infrared absorbing squaraine dyes with serum albumins and also the development of novel conjugates based on fluorescence resonance energy transfer for metal ions. The first Chapter of the

thesis presents a brief description of the structural features of proteins with a particular emphasis on the structures of human and bovine serum albumins (HSA and BSA) and a brief description of ligand-protein interactions. Further, a brief account on probes for metal ions, especially for copper ions is presented in this chapter along with the objectives of the present thesis.

The investigation of the interactions of squaraine dyes, with HSA and BSA through various photophysical, biophysical and microscopic techniques is the subject matter of the second chapter. Squaraines form a class of novel dyes possessing sharp and intense absorption in the red to near infrared region and hence are the object of intense investigations as molecular components of technological applications. Recently, we have proposed that squaraines as a possible new class of photosensitizers for PDT applications because of their highly favorable photophysical and *in vitro* photobiological properties. To evaluate the probable *in vivo* transportation pathways, we have investigated the interactions of a few selected squaraine dyes with serum albumins.

The addition of BSA and HSA to the squaraine dyes resulted in the increase in absorbance and fluorescence quantum yields of these dyes, along with significant bathochromic shifts in the absorption and fluorescence maxima. The picosecond time-resolved fluorescence studies indicate that the serum albumin-dye complex exhibits biexponential decay with significantly enhanced lifetimes when compared to the lifetime of the squaraine dyes in the absence of BSA or HSA. An interesting aspect of these investigations is the enhanced triplet excited state lifetimes and quantum yields observed for the halogenated dyes in the presence of serum albumins. The results presented in this chapter demonstrate that the

squaraine dyes interact efficiently with BSA and HSA and signal the binding event through dual mode 'visual color' change and 'turn on' fluorescence intensity and thereby their potential as NIR non-covalent protein labeling agents and as sensitizers in PDT applications.

The study of site selective binding of these dyes with serum albumins, investigated through ligand displacement assay, CD and FRET techniques forms the subject matter of the chapter 3. The fluorescence displacement assay and CD studies using the site specific reagents confirm that the squaraine dyes substituted with heavy atoms show high selectivity for site II, whereas the unsubstituted squaraine dye binds at site I of the protein. The binding of the unsubstituted squaraine dye was found to decrease the helical content of the protein, thereby leading to a reduction in the fluorescence intensity and lifetime of the Trp-214 residue present in native HSA and BSA, located in the same subdomain IIA of the protein. Interestingly, the binding of this dye at the same site results in an efficient fluorescence resonance energy transfer from Trp-214 to the squaraine dye. The distance between the Trp-214 and the squaraine dye calculated using Förster theory agrees well with the reported site I binding agent, such as dansylamine.

In contrast, no energy transfer was observed between Trp-214 in the serum albumins and bromo and iodo substituted dyes indicating that these derivatives bind less efficiently at the site I owing to steric constraints. The unsubstituted dye having hydrogen atoms and the molecular dimensions of 4.3 Å showed binding at both the sites with a marginal selectivity for site II. In contrast, the dye with bromine atoms and having dimensions of 5.5 Å exhibited *ca.* 90% selectivity for site II as against 10% at site I. Expectedly, on the basis of higher

molecular dimensions of 6.0 Å, the dye with iodine substitution, exhibited binding of *ca.* 95% at site II of both HSA and BSA. These studies indicate that these squaraine dyes exhibit substituent size-dependent selectivity at site II of the serum albumins with the iodo substituted dye exhibiting the maximum selectivity. These results demonstrate that the squaraine dyes under investigation interact selectively and efficiently with BSA and HSA as compared to other proteins and thereby act as selective probes for the detection of serum albumins in buffer and under gel electrophoresis conditions.

The study of interactions of a few novel donor-acceptor dyads with various metal ions is presented in the chapter 4 of the thesis. With the objective of understanding the ability of donor acceptor systems to function as bidentate ligands, we have synthesized a few novel dyads, having naphthalimide chromophore as the energy donor and dansyl moiety as the energy acceptor and investigated their interactions with various metal ions through various photophysical, and <sup>1</sup>H NMR techniques. The absorption spectra of these dyads in various solvents showed peaks corresponding to the individual naphthalimide and dansyl moieties in the near-UV region (300-400 nm), indicating that negligible interactions exist between these chromophores in the ground state. The fluorescence spectra exhibited emission in the visible region with two emission maxima at 376 and 525 nm. The emission at 376 nm corresponds to the naphthalimide moiety, while the emission observed at 525 nm is due to the intramolecular energy transfer (ET) process from the naphthalimide moiety, to the dansyl unit.

Investigation of the interactions with various metal ions indicate that these dyads exhibit unusual selectivity for  $\text{Cu}^{2+}$  ions as compared to  $\text{Na}^+$ ,  $\text{Li}^+$ ,  $\text{K}^+$ ,  $\text{Zn}^{2+}$ ,  $\text{Pb}^{2+}$ ,  $\text{Hg}^{2+}$ ,  $\text{Co}^{2+}$ ,  $\text{Fe}^{2+}$ ,  $\text{Cd}^{2+}$ ,  $\text{Mg}^{2+}$  and  $\text{Ba}^{2+}$  ions and signaled the binding event through inhibition of FRET mediated emission at 525 nm, with the concomitant enhancement in the emission intensity of the naphthalimide chromophore at 375 nm. Benesi-Hildebrand analysis of the fluorescence data along with the Job's plot gave a 2:1 stoichiometry for the complex between the dyads and  $\text{Cu}^{2+}$  ions with the association constants in the range  $2 - 2.6 \times 10^5 \text{ M}^{-1}$ . The complex formation between the dyads and  $\text{Cu}^{2+}$  ions was further confirmed through MALDI-TOF mass spectral analysis and NMR techniques. The uniqueness of these dyads is that they form stable 2:1 stoichiometric complexes involving the sulphonamide functionality and act as visual fluorescence ratiometric probes for the selective recognition of  $\text{Cu}^{2+}$  ions.

## List of Figures

		<b>Page</b>
<b>1.</b>	Figure 1.1	<b>4</b>
<b>2.</b>	Figure 1.2	<b>5</b>
<b>3.</b>	Figure 1.3	<b>6</b>
<b>4.</b>	Figure 1.4	<b>6</b>
<b>5.</b>	Figure 1.5	<b>10</b>
<b>6.</b>	Figure 1.6	<b>11</b>
<b>7.</b>	Figure 1.7	<b>12</b>
<b>8.</b>	Figure 1.8	<b>13</b>
<b>9.</b>	Figure 1.9	<b>16</b>
<b>10.</b>	Figure 1.10	<b>17</b>
<b>11.</b>	Figure 1.11	<b>22</b>
<b>12.</b>	Figure 1.12	<b>25</b>
<b>13.</b>	Figure 1.13	<b>26</b>
<b>14.</b>	Figure 2. 1	<b>38</b>
<b>15.</b>	Figure 2.2	<b>41</b>
<b>16.</b>	Figure 2.3	<b>43</b>
<b>17.</b>	Figure 2.4	<b>44</b>
<b>18.</b>	Figure 2.5	<b>45</b>

<b>19.</b>	Figure 2.6	<b>45</b>
<b>20.</b>	Figure 2.7	<b>46</b>
<b>21.</b>	Figure 2.8	<b>48</b>
<b>22.</b>	Figure 2.9	<b>49</b>
<b>23.</b>	Figure 2.10	<b>51</b>
<b>24.</b>	Figure 2.11	<b>52</b>
<b>25.</b>	Figure 2.12	<b>53</b>
<b>26.</b>	Figure 2.13	<b>54</b>
<b>27.</b>	Figure 2.14	<b>55</b>
<b>28.</b>	Figure 2.15	<b>57</b>
<b>29.</b>	Figure 2.16	<b>57</b>
<b>30.</b>	Figure 2.17	<b>58</b>
<b>31.</b>	Figure 2.18	<b>59</b>
<b>32.</b>	Figure 2.19	<b>60</b>
<b>33.</b>	Figure 2.20	<b>61</b>
<b>34.</b>	Figure 3. 1	<b>73</b>
<b>35.</b>	Figure 3.2	<b>74</b>
<b>36.</b>	Figure 3.3	<b>75</b>
<b>37.</b>	Figure 3.4	<b>76</b>
<b>38.</b>	Figure 3.5	<b>76</b>
<b>39.</b>	Figure 3.6	<b>77</b>
<b>40.</b>	Figure 3.7	<b>77</b>
<b>41.</b>	Figure 3.8	<b>78</b>

<b>42.</b>	Figure 3.9	<b>80</b>
<b>43.</b>	Figure 3.10	<b>81</b>
<b>44.</b>	Figure 3.11	<b>82</b>
<b>45.</b>	Figure 3.12	<b>82</b>
<b>46.</b>	Figure 3.13	<b>83</b>
<b>47.</b>	Figure 3.14	<b>84</b>
<b>48.</b>	Figure 3.15	<b>85</b>
<b>49.</b>	Figure 3.16	<b>86</b>
<b>50.</b>	Figure 3.17	<b>87</b>
<b>51.</b>	Figure 3.18	<b>88</b>
<b>52.</b>	Figure 3.19	<b>89</b>
<b>53.</b>	Figure 3.20	<b>93</b>
<b>54.</b>	Figure 3.21	<b>95</b>
<b>55.</b>	Figure 4. 1	<b>106</b>
<b>56.</b>	Figure 4.2	<b>109</b>
<b>57.</b>	Figure 4.3	<b>109</b>
<b>58.</b>	Figure 4.4	<b>111</b>
<b>59.</b>	Figure 4.5	<b>112</b>
<b>60.</b>	Figure 4.6	<b>113</b>
<b>61.</b>	Figure 4.7	<b>113</b>
<b>62.</b>	Figure 4.8	<b>115</b>
<b>63.</b>	Figure 4.9	<b>116</b>
<b>64.</b>	Figure 4.10	<b>117</b>

<b>65.</b>	Figure 4.11	<b>118</b>
<b>66.</b>	Figure 4.12	<b>119</b>
<b>67.</b>	Figure 4.13	<b>120</b>
<b>68.</b>	Figure 4.14	<b>121</b>
<b>69.</b>	Figure 4.15	<b>121</b>
<b>70.</b>	Figure 4.16	<b>122</b>
<b>71.</b>	Figure 4.17	<b>122</b>
<b>72.</b>	Figure 4.18	<b>124</b>

#### **List of Tables**

<b>1.</b>	Table 2.1	<b>47</b>
<b>2.</b>	Table 2.2.	<b>50</b>
<b>3.</b>	Table 4.1.	<b>108</b>

#### **List of Schemes**

<b>1</b>	Scheme 1.1	<b>29</b>
<b>2</b>	Scheme 2.1	<b>40</b>
<b>3</b>	Scheme 2.2	<b>40</b>
<b>4</b>	Scheme 2.3	<b>41</b>
<b>5</b>	Scheme 4.1	<b>105</b>

## List of Abbreviations

1. AFM- Atomic force microscopy
2. Ala- Alanine
3. Arg - Arginine
4. Asp- Aspartic acid
5. Ba(ClO<sub>4</sub>)<sub>2</sub> – Barium perchlorate
6. BSA- Bovine serum albumin
7. Ca(ClO<sub>4</sub>)<sub>2</sub> – Calcium perchlorate
8. CD- Circular dichroism
9. CD<sub>3</sub>CN - Acetonitrile
10. Cd(ClO<sub>4</sub>)<sub>2</sub> – Cadmium perchlorate
11. CMC - 1-Cyclohexyl-3-(2-morpholinoethyl) carbodiimide p-toluenesulfonate
12. Co(ClO<sub>4</sub>)<sub>2</sub> – Cobalt perchlorate
13. CoHA- Ammine cobalt (III) complexes
14. Cu(ClO<sub>4</sub>)<sub>2</sub> – Copper perchlorate
15. Cys- Cysteine
16. Cys-Cys- Cystine
17. Da- Dalton
18. D-A-D – Donor- acceptor- donor
19. DNA-Deoxyribonucleic acid
20. DNSA-Dansyl amide
21. DP-Dansyl L-proline
22. EDC –1-Ethyl-3-(3 dimethylaminopropyl) carbodiimide
23. ET – Energy transfer
24. FA- Folic acid
25. FR - Folate receptor
26. FRET – Fluorescence resonance energy transfer

27. FT-IR -Fourier transform infrared
28.  $\Delta G$  – Free energy change
29. GSH - Glutathione
30.  $\text{Hg}(\text{ClO}_4)_2$  – Mercury perchlorate
31. His-Histidine
32. HOMO – Highest occupied molecular orbitals
33. HSA-Human serum albumin
34. ICT-Intramolecular charge transfer
35. IR -Infrared
36.  $K_{ass}$  - Association constant
37. KBr – Potassium bromide
38. KCl – Potassium chloride
39.  $\text{KH}_2\text{PO}_4$ -Potassium dihydrogen phosphate
40.  $\text{kJM}^{-1}$  – Kilojoules per mole
41. LCFA – Long chain fatty acid
42.  $\text{LiClO}_4$  – Lithium perchlorate
43. LUMO – Lowest unoccupied molecular orbitals
44. Lys-Lysine
45. MALDI- Matrix-assisted laser desorption ionization
46.  $\mu\text{s}$ - microseconds
47.  $\text{mg/mL}$ -milligram per milliliter
48.  $\text{Mg}(\text{ClO}_4)_2$  - Magnesium perchlorate
49.  $\mu\text{M}$  – Micromolar
50. mM - Millimole
51. MRE -Mean residue ellipticity
52. MS -Mass spectrometer
53. ms-millisecond
54. MV-Methyl viologen
55. NaCl – Sodium chloride
56. Nd:YAG- Neodymium yttrium aluminum garnet
57. NIR-Near infrared

58. nm-nanometer
59. NMR- Nuclear magnetic resonance
60. ns-nanosecond
61.  $\text{Pb}(\text{ClO}_4)_2$  – Lead perchlorate
62. PDT – Photodynamic Therapy
63. PET - Photoinduced electron transfer
64. ppm – Parts per million
65. ps- picosecond
66. PVA-Pt-Poly vinyl alcohol -Platinum
67.  $\Phi_T$  - Quantum yields of triplet excited state
68.  $\Phi_f$  – Quantum yields of fluorescence
69. rHSA- Recombinant human serum albumin
70. rHSA(wt)-Wild type recombinant human
71. RNA – Ribonucleic acid
72. RSA – Rat serum albumin
73. SA - Serum albumin
74. SDS-PAGE- Sodium dodecyl sulphate –poly acrylamide gel electrophoresis
75. SQ-Squaraine
76. TCSPC- Time-correlated picosecond single photon counting
77. TEOA- Triethanolamine
78. TLC- Thin layer chromatography
79. TOF – Time of flight
80. Trp-Tryptophan
81. TX-100 – Triton X-100
82. Tyr-Tyrosine
83. UV-Ultraviolet
84. Vis-Visible
85.  $\text{Zn}(\text{ClO}_4)_2$  – Zinc perchlorate
86. ZnPP- Zn(II)-protoporphyrin IX
87.  $\text{ZnTMPyP}^{4+}$  - Tetrakis(1-methylpyridinium-4-yl)porphinatozinc(II)



# INTERACTIONS OF LIGANDS WITH PROTEINS AND METAL IONS: AN OVERVIEW

---

## 1.1. INTRODUCTION

Interactions of ligands with proteins and metal ions are fundamental processes underlying many aspects of cellular function. The biological function of a protein depends on its interactions with various ligand molecules. Examples are the interaction of hormone receptors with hormones, that trigger complicated signal cascades, or the interaction of certain proteins with nucleic acid sequences to regulate gene replication, transcription, or translation, or the highly specific interaction of cell-surface antigens with receptors located on other cells. Therefore, there have been many attempts aimed at accurately characterizing such processes with a variety of biophysical methods. Understanding the ligand recognition by the proteins on an atomic level is crucial to the biological function and of significant, practical importance in the discovery of new drugs and also in phototherapy (Gellman 1997, Kratochwil *et al.*, 1995).

A ligand can be broadly defined as anything to which a protein binds, either for purposes of catalysis, regulation, or transport. Classic examples of these ligands include proteins, nucleic acids, nucleotides, metabolic substrates, and enzyme cofactors (Voet *et al.*, 1995). Each of these ligands performs a specific role with regard to protein function. Enzymes bind the substrates on which they perform the catalytic function for which they have evolved, and often bind metabolic

intermediates or regulator molecules to attenuate that function (Banerjee *et al.*, 2005, Serganov *et al.*, 2005, Pal *et al.*, 2004, Dobson *et al.*, 1998, Balabin *et al.*, 2000, Balbach *et al.*, 1995, Borbat *et al.*, 2001, Lyon, *et al.*, 2002, Zhong, *et al.*, 2000, 2001). Proteins are responsible for the transport of biologically essential materials, either within the cell or between tissues of the body; a function that requires that these materials be bound and later released. Examples of biological ligand transport include the transport of lipids by albumin (Cohen *et al.*, 1980, Baldo-Enzi *et al.*, 1987), oxygen by haemoglobin (Collman *et al.*, 2004, Momenteau *et al.*, 1994) and glucose across the plasma membrane of the cell by the glucose transporter. Ligand binding therefore plays a critical role in cellular and physiological function.

Optical probes for the sensing and reporting of chemical species are of significant importance in chemical, biological and environmental sciences. Of particular interest has been the development of specific probes for the detection of proteins and transition metal ions because they play important roles in living systems (Beljaars *et al.*, 2000, Kurtzhals *et al.*, 1995, Sheffield, 2001). One convenient detection tool is the luminescent chemosensor, where the major challenge is the construction of sensors that exhibit a positive response upon analyte binding with high selectivity and sensitivity in water. Although a number of systems have been reported that can selectively interact with metal ions and proteins, only few of them exhibit 'turn on' fluorescence response. In this context, the design and development of organic ligands targeted at proteins and metal ions are of particular importance in the light of their potential applications in biology and medicine. This chapter describes briefly the structural aspects of proteins with particular emphasis on the

interaction of ligands with transport proteins and metal ions. Further, the objectives of the present investigations are also briefly described in this chapter.

## **1.2. PROTEINS: STRUCTURE AND FUNCTION**

The simple organic compounds, from which living organisms are constructed, known as biomolecules, are identical in all organisms and are related to each other and interact among themselves (Creighton 1992). The size, shape and chemical activity of biomolecules enable them not only to serve as the building blocks of cells, but also to participate in various dynamic, self-sustaining transformations of energy and matter. Depending on their chemical composition and function, biomolecules can be broadly classified as amino acids, proteins, enzymes, carbohydrates, lipids, nucleotides, nucleic acids and so on (Leninger 1984, Roberts 1989, Katchalski-Katzir 1986). Because of their inherent importance in biology, the structure and function of these biomolecules have been studied in detail. Our interest in this area is related to the study of interactions of small organic molecules having photodynamic activity with proteins because such studies are useful in the design of novel chemotherapeutics and in the development of probes useful in biology and medicine (Rodgers 1985, Davila *et al.*, 1989, Langlots *et al.*, 1986). In the following section, a brief description of the structure and functions of proteins is provided.

Proteins are nitrogen-containing organic compounds that are the basic units of life systems. These are polymers, or macromolecules, of amino acids containing from approximately 40 to several thousand amino acid groups joined by peptide linkages (Branden *et al.*, 1991, Richardson *et al.*, 1981, Dougherty 2000, Greenstein 1961,

Kreil 1997, Meister 1965). Of the numerous conformations possible for a protein, one or a few generally predominate under biological conditions. A protein, often has, multiple stable conformations which reflects the changes occurring in a protein as they bind to other. Proteins are classified into primary, secondary, tertiary, and quaternary structures and the structures of protein molecules determine the behaviour of proteins. An example is the recognition of the foreign substance by the immune system.

The order of amino acids in the protein molecule determines its primary structure. (Berman 1999, Brenner *et al.*, 1997, Fuchs *et al.*, 1998, McPherson *et al.*, 1989, Ponting *et al.*, 2002, Prockop *et al.*, 1995). The primary structure of a protein is the sequence of amino acid units in the chain and all the disulphide bridges (Figure 1.1). DNA codes the primary structure of the protein. Further folding of the protein molecules held in place by attractive forces between amino acid side chains gives proteins a secondary structure, which is determined by the nature of the amino acid R groups. *ie.*, Secondary structure of the protein results from the folding of polypeptide protein chains to produce maximum number of hydrogen bonds

**- Lys - Ala - His - Gly - Lys - Lys - Val - Leu - Gly - Ala -**

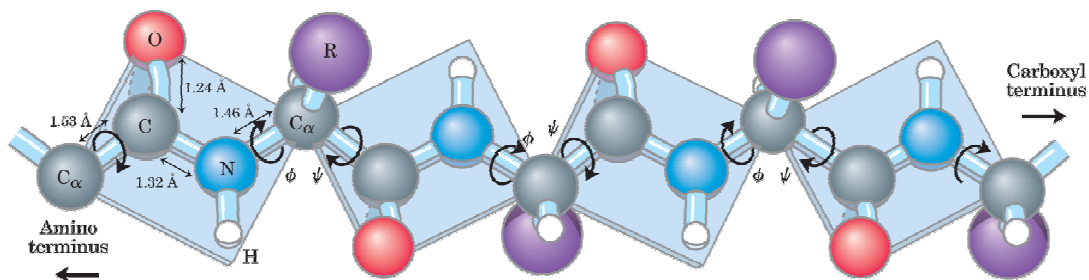


**Figure 1.1.** Primary structure of a protein.

between the peptide linkages. The most common secondary structures are the  $\alpha$ -helix, the  $\beta$ -conformation, and the  $\beta$ -turns (Figure 1.2).

The tertiary structure of the protein is formed by the twisting of  $\alpha$ -helices into specific shapes (Figure 1.3). These structures are stabilized by multiple weak interactions like hydrophobic interactions, which are the major contributors to

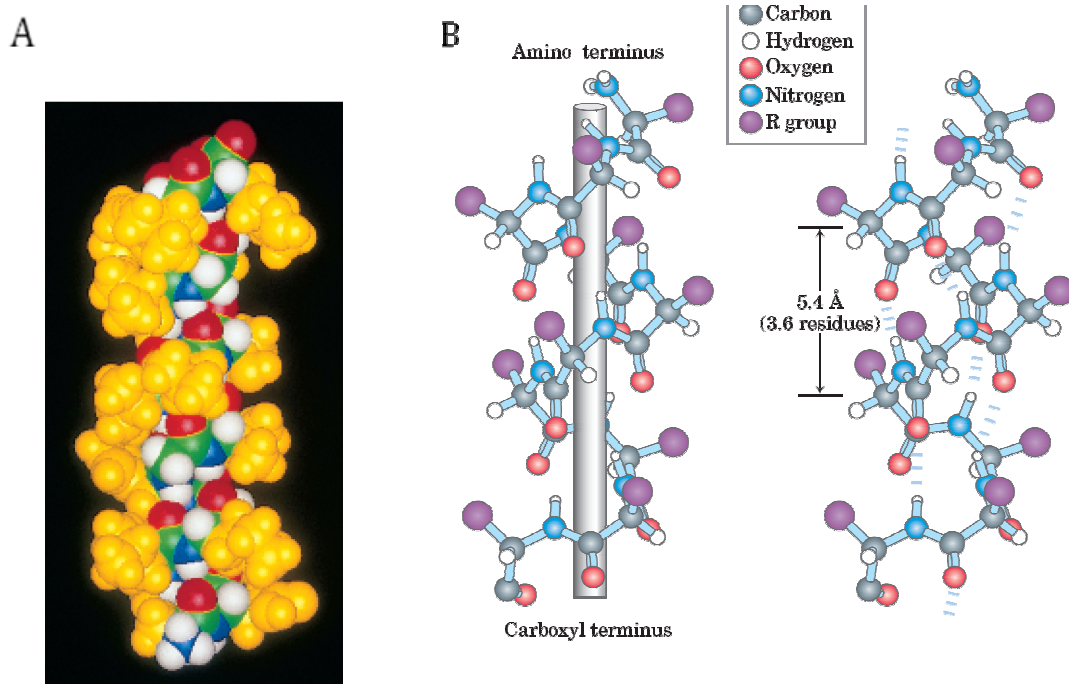


**Figure 1.2.** Secondary  $\alpha$ -helical structure of a protein (A) space filling and (B) ball and stick models.

stabilizing the globular form of most soluble proteins whereas hydrogen bonds and ionic interactions are optimizing the specific structures that make the protein thermodynamically more stable. Tertiary structure of protein is important because the enzyme and ligand molecules identify proteins based on this structure. This is exemplified by the antibodies, which recognize foreign proteins by their shape and react with them. Two or more protein molecules consisting of separate polypeptide

chains may be further attracted to each other to produce a quaternary structure (Figure 1.4). Knowledge of the three-dimensional structure of a protein is important for understanding how the protein functions. Proteins are dynamic molecules whose

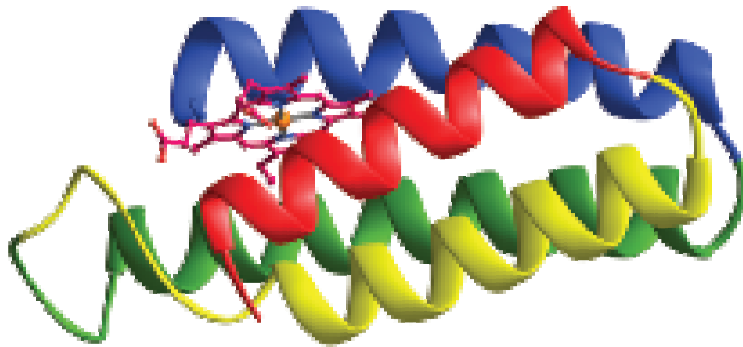


**Figure 1.3.** Tertiary structure of a protein.

functions depend on its interactions with other molecules, and these interactions are affected in physiologically important ways by the changes in its conformation. The functions of many proteins involve interactions with a variety of different molecules.

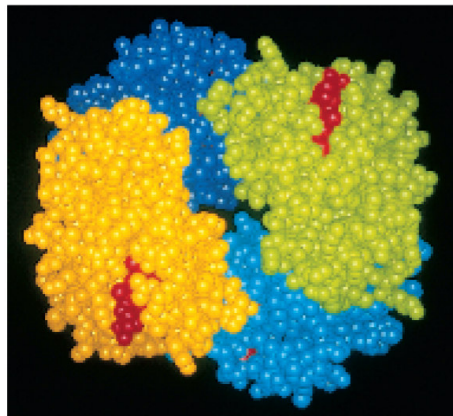


**Figure 1.4.** Quaternary structure of a protein.

Although these interactions are weak, they are the basis of complex physiological processes such as oxygen transport, immune function, and muscle contractions.

The function of many proteins depends upon the reversible binding with other molecules. The transient nature of protein-ligand interactions is critical to life, allowing an organism to respond rapidly and reversibly to changing environmental and metabolic circumstances. A ligand binds at a site on the protein called the binding site, which is complementary to the ligand in size, shape, charge, and hydrophobic or hydrophilic character. Furthermore, the interaction is specific: the protein can discriminate among the thousands of different molecules in its environment and selectively bind only one or a few. A given protein may have separate binding sites for several different ligands. These specific molecular interactions are crucial in maintaining high degree of order in a living system. The binding of a protein and ligand is often coupled to a conformational change in the protein that makes the binding site more complementary to the ligand, permitting tighter binding. In a multi subunit protein, a conformational change in one subunit often affects the conformation of other subunits. These conformational changes occurring in the protein upon ligand binding is, often, crucial for its various functions.

### **1.3. CLASSIFICATION OF PROTEINS**

Proteins are responsible for many different functions in the living cell. Based on their functions, the proteins may be classified into different types.

**Enzymes** are the proteins that catalyze chemical reactions within the cell and outside. During an enzymatic reaction, the substrates are converted into the product by the enzymes. Since enzymes are selective for their substrates and speed up only a few reactions from among many possibilities, the set of enzymes present within a cell

determines, which metabolic pathways occur in that particular cell. Some of the well known and very interesting examples are DNA- and RNA-polymerases etc.

**Hormones** act as chemical messengers in the cell and a small change in the level of hormones can change the cell metabolism. Eg. Insulin, growth factor, lipotropin, prolactin etc.

**Transport proteins** are globular proteins with the polar side groups tightly packed on the outside to enhance their solubility in water and the non-polar side groups folded to the inside to prevent water from getting in and unfold them. They are involved in the transportation or storage of chemical compounds and ions. Cytochrome *c*, haemoglobin, myoglobin and albumin are some of the examples of transport proteins.

**Structural proteins** are involved in the production of essential structural components for the cells and tissues. Collagen, elastin,  $\alpha$ -keratin and fibroin belong to this class of proteins.

**Motor proteins** convert chemical energy into mechanical energy. This class of proteins are able to move along the surface of a suitable substrate and are powered by the hydrolysis of ATP. Actin and myosin, responsible for muscular motion, are the prominent examples for this class.

**Receptors** are protein molecules present either in the plasma membrane or in the cytoplasm of the cells. Many functions of the human body are regulated by these receptors responding uniquely to specific molecules. Ligand-induced changes in receptors result in cellular changes, which constitute the biological activity of the ligands. These proteins are active only when they form complexes with low

molecular weight compounds. Very well known member of this protein family is the rhodopsin, a light detecting protein.

**Signalling proteins** are involved in the signalling of information during the metabolic processes. They undergo conformational changes in the presence of signalling molecules. These proteins can also act as enzymes. GTPases is an example.

**Storage proteins** are proteins that store metal ions and amino acids which are released during metabolic processes in the organism. Ferritin is an example of a storage protein that stores iron.

#### **1.4. IMPORTANCE OF TRANSPORT PROTEINS**

Among the different types of proteins, transport proteins play an important role as they are involved in the transportation of substances across the membrane. Serum albumin is the major transport protein in the blood plasma and is mainly involved in the transportation and metabolism of various exogenous and endogenous molecules. For example, these proteins transport water-insoluble lipids in the bloodstream and also involved in regulating the osmotic blood pressure (Carter *et al.*, 1990, Spector *et al.*, 1986, Wang *et al.*, 1993, Brock 1976, Roda *et al.*, 1982, Weisiger *et al.*, 1981, Forker *et al.*, 1981).

A well know example for transport protein is the hemoglobin (Leninger 1984, Ackers 1993, Dickerson 1993, di Prisco 1991, Perutz 1989) which carries oxygen from the lungs to the tissue (Figure 1.5.). Myoglobin performs a similar function in muscle tissue, taking oxygen from the hemoglobin in the blood and storing it or carrying it around until needed by the muscle cells. Another quite different group of

carrier molecules are the cytochromes (Figure 1.5) (Babcock *et al.*, 1992, Michel *et al.*, 1998). These are the electron carrier proteins that operate in the electron transport chain which is part of the respiratory process. The function and properties of these carrier proteins are affected by competitive inhibition. For example, cyanide binding

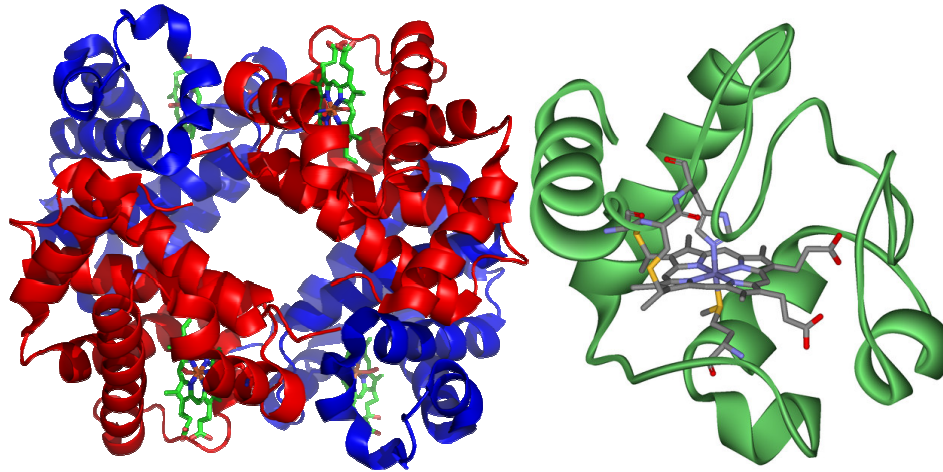


**Figure 1.5.** Structures of hemoglobin and cytochrome *c*.

to cytochrome inhibiting these proteins that are an integral part of the electron transport system in respiration. Similarly the carbon monoxide binding to haemoglobin also affects the organisms.

## **1.5. STRUCTURAL FEATURES OF SERUM ALBUMINS**

Serum albumin, the most abundant protein in the circulatory system, is one of the most extensively studied proteins (Brown 1975, Arvidson *et al.*, 1969, Sollenne *et al.*, 1979, Tanford, 1980, Peters, 1995). It is synthesized in the liver, exported as a non-glycosylated protein without prosthetic groups or other additives, and is present in the blood at around 40 mg/ml (~0.6 mM). It is the major transport protein for

unesterified fatty acids, but is also capable of binding diverse range of metabolites, drugs and organic compounds.

Human serum albumin (HSA), and bovine serum albumin (BSA) are monomeric proteins of 585 and 584 amino acid residues. These proteins have three structurally similar  $\alpha$ -helical domains I-III, which are further divided into subdomains A and B (He *et al.*, 1992). These proteins display approximately 80%

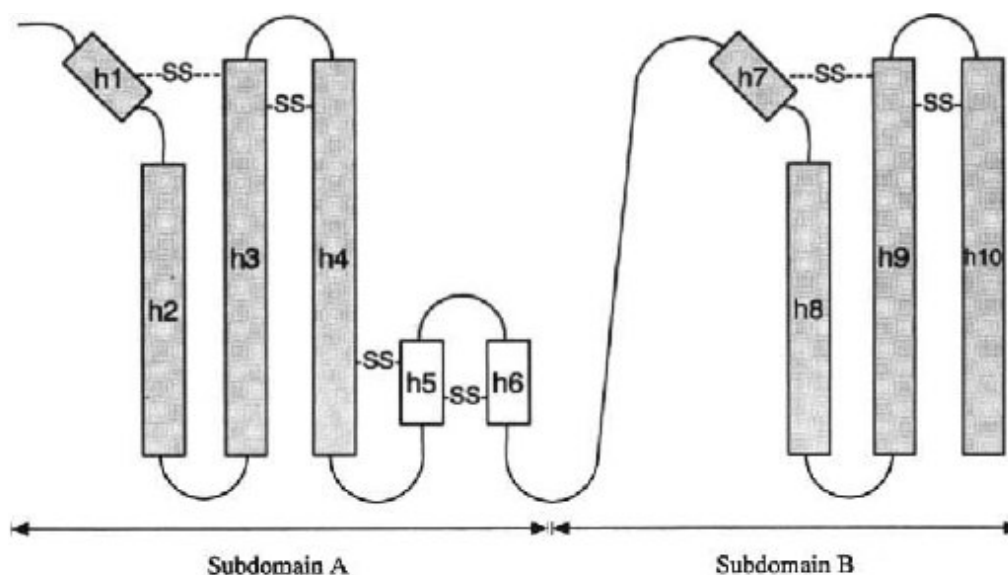


**Figure 1.6.** Topological illustration of the typical domains in HSA.

sequence homology and a repeating pattern of disulfides, which are strictly conserved. The molecular weights of BSA and HSA are 66 and 66.5 kD, respectively. From the spectroscopic point of view, one of the main differences between the two proteins is that BSA has two tryptophan residues (Trp-134 and Trp-212) and HSA has only one (Trp-214). This additional tryptophan residue in BSA is located at position 134, buried in a hydrophobic pocket, and it has been proposed to lie near the surface of the albumin molecule in the second helix of the first domain. Albumin

sequence is known to have 35 half-cystines, which form 17 disulfide bridges. Disulfide bonding is a characteristic of extracellular proteins and contributes to the stability of plasma proteins in circulation. The most unique structural feature of the albumins is their disulfide bonding pattern. A key to this pattern is the occurrence of eight Cys-Cys sequences involving nearly half of the 17 cystine residues.

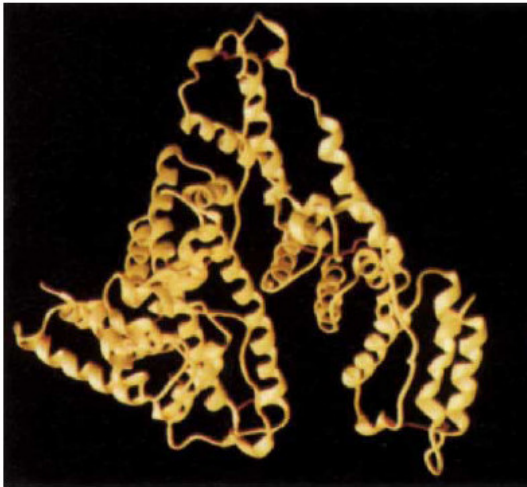


**Figure 1.7.** The stereoview of heart-shaped structure of HSA derived from X-ray crystallography (He and Carter *Nature* 358, 1992, 209-215).

The three-dimensional structure of serum albumin was reported by He and co-workers at a resolution of 2.8Å (He and Carter 1992). The tertiary structure of HSA is a heart-shaped or equilateral triangular molecule 80 Å on a side, with average thickness of 30 Å, and a calculated molecular volume of about 88,249 Å<sup>3</sup> (Carter and Ho 1994). The X-ray diffraction results show 67% of the residues of crystalline HSA to be involved in a total of 28  $\alpha$ -helical regions. The remainder of the chain is extended peptide chain with 10%  $\beta$ -turns. The helical pattern is similar in each of the three domains. Subdomain IIA is at the left and subdomain IIB is at the right. He and

Carter found that the helical bundles of subdomains form binding cavities for a number of aromatic small molecules (Carter and Ho 1994). The high affinity drug binding sites on HSA have been classified into two well-characterized groups, sites I and II, which are located in subdomains IIA and IIIA, respectively.

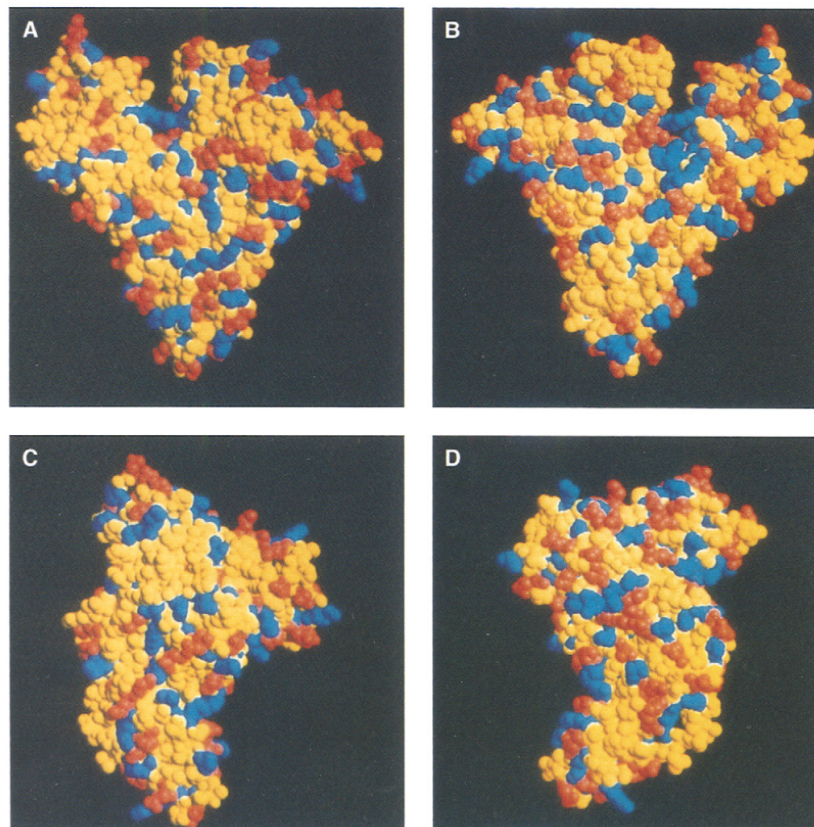


**Figure 1.8.** Space-filling model of HSA. (A) "Front," (B) "back," (C) left-hand side, (D) right-hand side. As in Fig. 1.6 the amino terminus is at the right in the "front" view. Basic residues are colored blue, acidic residues red, and neutral residues yellow.

Serum albumin adopts different secondary helical structures based on the environmental conditions and salt concentration. HSA can undergo pH dependent conformational transitions such as, the N-F transition between pH 5.0 and 3.5, the F-E transition between pH 3.5 and 1.2, and the N-B transition between pH 7.0 and 9.0.

The N-F isomerisation involves the unfolding and separation of domain III from rest of the molecule without significantly affecting rest of the molecule. For example, urea induced unfolding of HSA showed a two-step three state transition with accumulation of an intermediate around 4.8-5.2 M urea concentration (Chmelik *et al.*, 1988). In the first state unfolding of domain III together with partial but significant loss of native conformation of domain I takes place whereas; domain II of HSA remains unaffected in the intermediate state.

The calculated distribution of net charges in HSA shows a gradient along the molecule, with domain I having the highest net negative charge; domain II intermediate and domain III nearly neutral. The actual net charges may be altered by the suppression of ionization of some acidic or basic residues, but the calculated net charge at physiological pH for domains I, II, and III are -9, -8, and + 2, respectively, for HSA, -11, -7, and +1 for BSA, and -10, -5, and +3 for the rat protein. Domain I and sub-domain IIA combine to form one half of the protein and sub-domain IIB and domain III form the other half and the calculated net charges for these two halves at pH 7.4 are -14 and -1 for HSA, -12 and -5 for BSA, and - 13 and +1 for rat serum albumin (RSA).

## **1.6. INTERACTIONS OF LIGANDS WITH SERUM ALBUMINS**

One of the main functions of serum albumin is the transportation of different endogenous and exogenous agents, including drugs, in the blood stream. Interactions between ligands and albumin may be regulated, usually through specific interactions with one or more additional ligands. These ligands may cause conformational changes in the protein that affect the binding of the first ligand. The important forces

that involves in protein ligand binding are the H-bonding interactions, Van der Waals interaction, disulphide bonding and the hydrophobic interactions.

A hydrogen bond results from a dipole-dipole force between an electronegative atom and a hydrogen atom bonded to nitrogen, oxygen or fluorine (Emsely 1980). The energy of a hydrogen bond (5 to 30 kJ/mol) is comparable to that of weak covalent bonds (155 kJ/mol) and a typical covalent bond is only 20 times stronger than an intermolecular hydrogen bond. The hydrogen bond is strong compared to Van der Waals forces, but weaker than covalent, ionic and metallic bonds. Electrostatic interactions arise from electrostatic attraction between either partial charges arising from the differing electronegativities of atoms (e.g.  $\delta^+$  and  $\delta^-$ ) or full charges arising from ionized residues. These interactions are particularly important when the target molecules contain charged moieties such as amino acids or nucleic acids. Another important non-covalent interaction in protein-ligand interaction is the disulphide bonding, which is the interaction between free Cys-SH.

Hydrophobic interaction is the most important non-covalent force in protein-ligand interaction (Schenider *et al.*, 1990, 2008). The tendency of hydrocarbons to form intermolecular aggregates in an aqueous medium is known as hydrophobicity. At the molecular level, the hydrophobic effect is an important driving force for biological structures and is responsible for protein folding, protein-protein interactions, formation of lipid bilayer membranes, nucleic acid structures, and protein-small molecule interactions. Though a non-covalent bond is weaker than a covalent bond, the sum of different non-covalent interactions creates a large net stabilizing energy and the association between the protein and the ligand molecule is

usually stabilized by one or more of these non-covalent interactions.

Serum albumin has great affinity for small, negatively charged hydrophobic molecules. The flexibility of the albumin structure adapts it readily to ligands, and its three-domain design provides a variety of sites. The pioneering work by Sudlow and

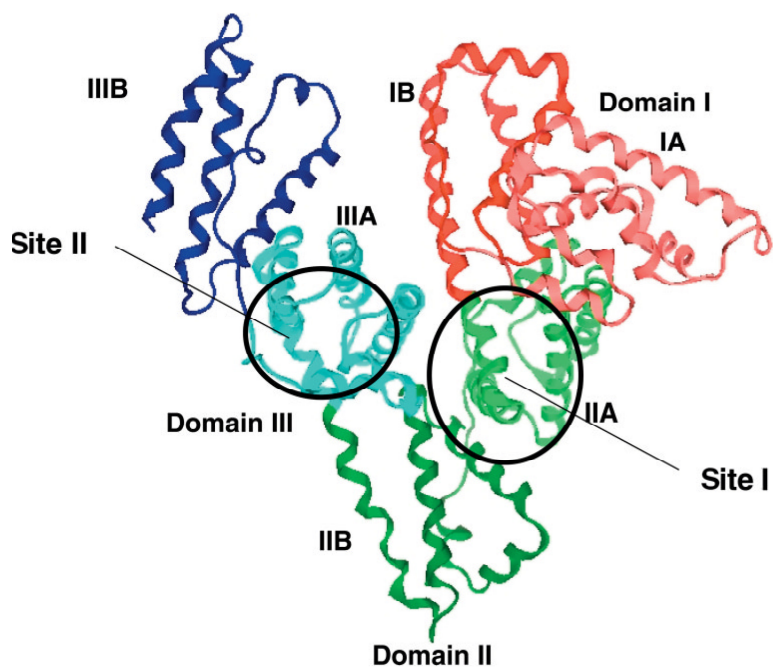


**Figure 1.9.** Major ligand binding sites in serum albumin.

co-workers revealed that albumin have two major and structurally selective binding sites for ligand molecules, which are named as site I and site II (Sudlow *et al.*, 1975, Sudlow *et al.*, 1976). Sudlow's site I is located in sub domain IIA, whereas Site II is in the sub-domain III A of the serum albumin. Site I ligands are heterocyclic anions with the charge situated in a fairly central position in the molecule. In contrast, the site II ligands are aromatic neutral molecules and the charge, if present, will be more on the peripheral part of the molecule. Although, more recent studies have found evidence supporting the existence of several sub-domains, consensus still exists that there are

basically two high affinity binding sites for small heterocyclic or aromatic compounds in this protein.

The drugs bind preferentially, and often stereoselectively, to site II of HSA by means of hydrogen bonding and electrostatic interactions, whereas hydrophobic interactions predominate at site I (Bennhold *et al.*, 1961, Spector *et al.*, 1975, 1986, Brown and Shockley, 1982, Honoré *et al.*, 1990, Kragh-Hansen *et al.*, 1990, Li *et al.*, 1988). Medium sized hydrophobic organic anions, long chain fatty acids, hematin, and bilirubin can bind strongly to serum albumin. Smaller and less hydrophobic compounds such as tryptophan and ascorbic acid are held less strongly but in a highly stereo selective manner, ie, the *L*-tryptophan binds 100-times as strong as the *D*-form.

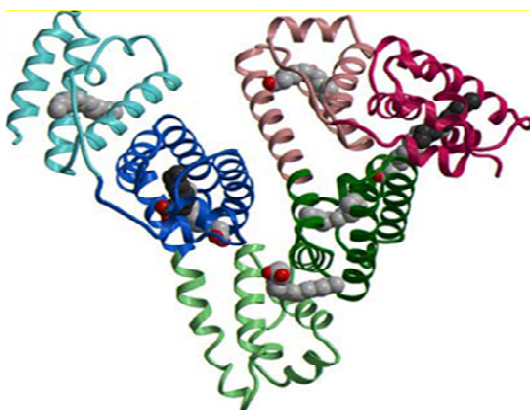


**Figure 1.10.** Crystal structure of HSA-myristate complex showing seven different binding sites.

The remarkable binding properties of albumin account for the central role it can play in both the efficacy and rate of delivery of drugs and other biomolecules, aided by the multiple hydrophobic binding sites provided by the protein. The crystallographic studies of a variety of drugs and biomolecules complexed with HSA

revealed the number and location of their binding sites on the protein. High-resolution crystal structures of FA/HSA complexes revealed a total of seven binding sites distributed heterogeneously throughout the protein and shared by medium-chain fatty acids and saturated, monounsaturated or polyunsaturated long-chain fatty acids (Curry *et al.*, 2005, Simard *et al.*, 2005, 2006).

Large number of compounds including therapeutic drugs is believed to bind at site I and site II of serum albumin. Understanding their binding interactions towards serum albumins is, therefore, important for elucidating their activity. As a result, various molecular systems have been developed for targeting proteins and a few examples are described in the following sections.

## **1.7. SITE SELECTIVE BINDING AGENTS OF SERUM ALBUMINS**

Sudlow *et al.*, (1975, 1976) have reported a few fluorescent probes based on the dansyl moiety and studied their site of binding. The non acid derivatives like dansyl *L*- proline (**1**) and dansyl *L*-tryptophan show high affinity for site II, whereas the derivative with carboxylic acid functionality like dansyl *L*-aspartic acid, dansyl *L*-glutamic acid and dansyl amine (**2**) showed high affinity for site I (Chart 1.1).

In another approach, Jimenez *et al.*, (2005) have investigated the binding interactions of arylpropionic acid derivative **3**, a group of nonsteroidal anti-inflammatory drug (Chart 1.2). The acid derivative of the drug binds preferentially and stereoselectively to site II of HSA through hydrogen bonding and electrostatic interactions. Interestingly, the ester derivative (**3-Me**) binds preferentially to site I, where hydrophobic interactions predominate. The authors have investigated

both(*R*)- and (*S*)-isomers to understand the stereoselectivity of HSA towards the drugs. A remarkable stereodifferentiation has been found in the triplet lifetimes within the protein microenvironment for (*R*)- and (*S*)-isomers.

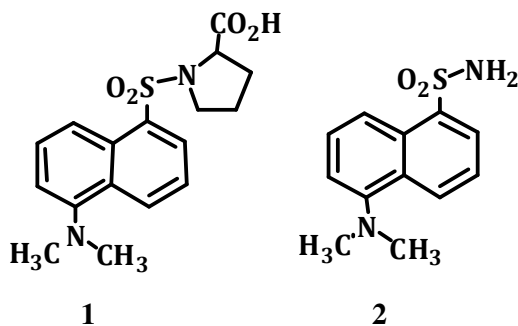


**Chart 1.1**

Kumar *et al.* have reported a chiral organic molecule **4** that cleave the serum albumin site-specifically (Kumar and Buranaprapuk 1997). This bifunctional molecule **4** was synthesised by covalently linking 4-(1-pyrenyl)-butyric acid with *L*-phenylalanine (Chart 1.2). The hydrophilic carboxylic acid functionality not only, ensures its

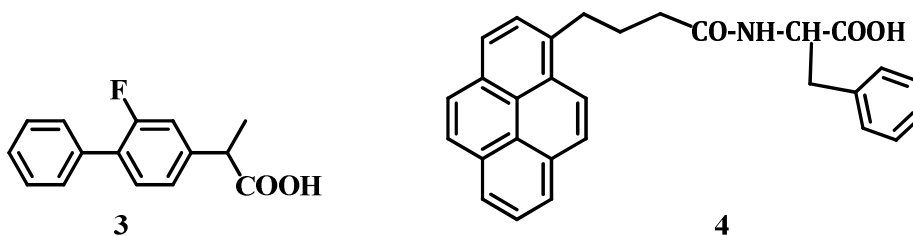


**Chart 1.2**

solubility in the aqueous medium, but also participates in H-bonding interactions. In addition, the hydrophilic amide functionality participates in electrostatic and hydrogen bonding interactions. Interestingly, the length of the linker was found to play an important role in the binding of the probes to proteins. It was found that

increase in the length of the linker and the size of the hydrophobic moiety increases the affinity of the probe towards the serum albumin. Further, the authors also studied the site-specific photocleavage of BSA on irradiating at 344 nm in the presence of **4** and ammine cobalt (III) complexes (CoHA), an electron acceptor. This site specific photocleavage was due to the efficient electron transfer from the long lived pyrene singlet excited state to CoHA. Further, the authors monitored the progress of the reaction by SDS-PAGE.

Fluorescent molecular probes **5** and **6** (Chart 1.3) having a hydroxystyryl and cyanopyranyl moieties for the detection of protein have been reported by Suzuki *et al.*, (2005). These fluorescent probes exhibited very weak fluorescence emission in the absence of protein. Interestingly, upon binding to BSA a large Stokes shift to the

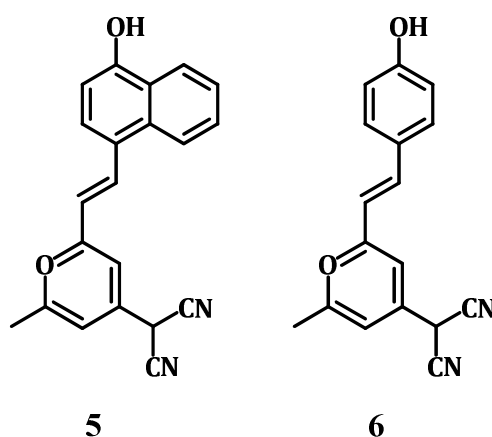


**Chart 1.3**

red region of the visible spectra and dramatic increase in the fluorescence intensity was observed. These changes in the emission spectra were attributed to the formation of strong complex with BSA, which is stabilized by the hydrophobic interactions and the intra molecular charge transfer (ICT) processes. The authors

also demonstrate the detection of the protein in SDS-PAGE. These experimental results clearly showed that these probes are good indicators of proteins and exhibit highly sensitive detection.

Recently, Komatsu *et al.*, have investigated the potential application of recombinant human serum albumin (rHSA) in the photosensitized reduction of water to hydrogen ( $H_2$ ) (Komatsu *et al.*, 2005). These studies were carried out by employing methyl viologen ( $MV^{2+}$ ) as an electron relay. The authors observed that ZnPP (Zn(II)-protoporphyrin IX) binds in the sub-domain IB of wild-type rHSA [rHSA(wt)] by an

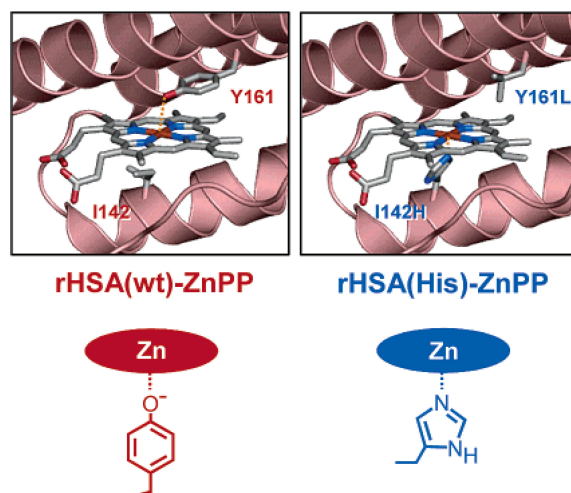


**Chart 1.4**

axial coordination of Tyr-161 and, in the rHSA (I142H/Y161L) mutant [rHSA(His)], by a His-142 coordination (Chart 1.4). Both the rHSA (wt)-ZnPP and rHSA (His)-ZnPP complexes showed a long-lived photoexcited triplet state with lifetimes ( $\tau_T$ ) of 11 and 2.5 ms, respectively. The accommodation of ZnPP into the protein matrix efficiently eliminated the collisional triplet self-quenching process. A significant quenching in the triplet lifetime was observed in the presence of electron acceptor,  $MV^{2+}$ . The

transient absorption spectrum revealed the oxidative quenching of rHSA-3ZnPP\* by  $MV^{2+}$ . In the presence of colloidal PVA-Pt as a catalyst and triethanolamine (TEOA) as a sacrificial electron donor, the photosensitized reduction of water to  $H_2$  takes place. The efficiency of the photoproduction of  $H_2$  was greater than that of the system using the well-known organic chromophore, tetrakis(1-methylpyridinium-4-yl)porphinatozinc (II) ( $ZnTMPyP^{4+}$ ), under the similar conditions. This example showed that apart from the physiological functions, BSA also has immense potential in material applications.

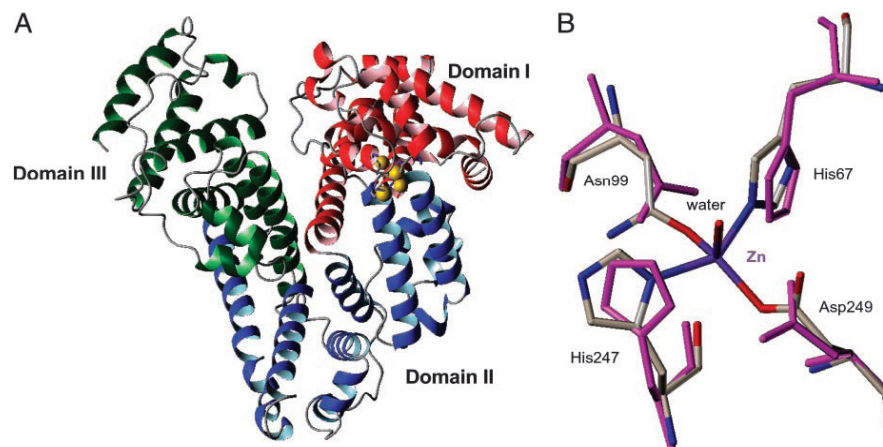


**Figure 1.11.** Proposed  $Zn^{2+}$ -binding site in HSA. (A) Domain structure of albumin. Domain I is coloured red (residues 1–181), domain II is blue (residues 188–373), domain III is green (residues 380–571). (B) Overlay of the  $Zn^{2+}$ -binding site.

In addition to the organic ligands, serum albumin can also bind to various heavy metal ions (Peters, 1995, Stewart *et al.*, 2003). They possess a variety of metal sites with different specificities. The best characterized metal sites on albumin are those of  $Cu^{2+}$  ions and  $Ni^{2+}$  ions, which bind strongly to a square-planar site of four nitrogen ligands from Asp-1-Ala-2-His-3 at the N terminus, and for  $Au^+$  ions (from

antiarthritic drugs), which binds to the thiolate sulfur at Cys-34. Circular dichroism studies suggested that the major  $Zn^{2+}$  site is also a secondary binding site for  $Cu^{2+}$  ions and  $Ni^{2+}$  ions. Early  $^{113}Cd$  NMR experiments on BSA demonstrated the existence of two  $Cd^{2+}$  binding sites, A and B. Later, competition experiments on BSA and HSA have shown that the site A binds  $Zn^{2+}$  ions more strongly than  $Cd^{2+}$  ions.

## **1.8. INTERACTIONS OF LIGANDS WITH METAL IONS**

Molecular recognition is a subject of considerable interest because of its implications in many fields such as chemistry, biology, medicine and environmental science. It requires the molecular receptor to discriminate and specifically bind a substrate among a group of structurally related molecule. The substrate may be a cation, anion or a neutral molecular species. A successful and selective receptor-substrate or host-guest recognition results when the two species which are complementary to each other both in size, shape and interact to form a complex. This complementarity is elegantly demonstrated by biological systems through enzyme-substrate interactions, biosynthesis of proteins and antigen-antibody reactions. Molecular recognition between a host and guest becomes useful when the binding event is signaled through a measurable property of the host termed as chemosensors. Thus, chemosensors are molecules of abiotic origin that are able to bind selectively and reversibly to an analyte of interest with a concomitant change in one or more properties of the system.

A typical chemosensor consists of a molecular recognition unit (receptor) and a signal transducing moiety (chromophore), which is integrated through a spacer.

The receptor is responsible for the selective analyte binding, whereas the chromophore is an active unit, which signals the binding event *via* changes in the absorption or emission (photochemical sensing) or redox potentials (electrochemical sensing). In the following section a brief discussion on different types of signaling processes and a few examples of ratiometric chemosensors for cation recognition are presented.

### **1.8.1. FLUORESCENCE SENSORS FOR METAL ION DETECTION**

Fluorescent sensors consist of a fluorophore linked to an ionophore and is thus called a fluoroionophore. The signaling moiety acts as a signal transducer, usually organic chromophores or dyes that have strong absorption or emission, which converts the information (recognition event) into an optical signal, expressed as the change in the photophysical characteristics of the fluorophore (Valeur 1994). These changes may be due to the perturbation of the photoinduced processes such as electron transfer, charge transfer, energy transfer, excimer or exciplex formation. In photoinduced electron transfer (PET) the fluoroionophore plays the role of an acceptor. Upon excitation of the fluorophore, an electron of the highest occupied molecular orbital (HOMO) is promoted to the lowest unoccupied molecular orbital (LUMO), which enables photoinduced electron transfer from the HOMO of the donor (belonging to the free cation receptor) to that of the fluorophore, causing fluorescence quenching of the latter (Figure 1.12). Upon cation binding, the redox potential of the donor is raised so that the relevant HOMO becomes lower in energy than that of the fluorophore. Consequently, the donating ability of the receptor is

reduced, which, in turn renders PET less favourable and the fluorescence emission is reinstated. The changes in the fluorescence emission intensity associated with this process have been used successfully as the signaling event for metal ion detection (de silva *et al.*, 1986, 1997, Turfan *et al.*, 2002, Nishizawa *et al.*, 1999).

In addition to the PET, photoinduced intermolecular energy transfer between linked donor- acceptor systems has also been widely employed for selective detection of cations. For example, the binding of the cation to the donor may result in the increase in the distance between donor and acceptor and thus resulted in the

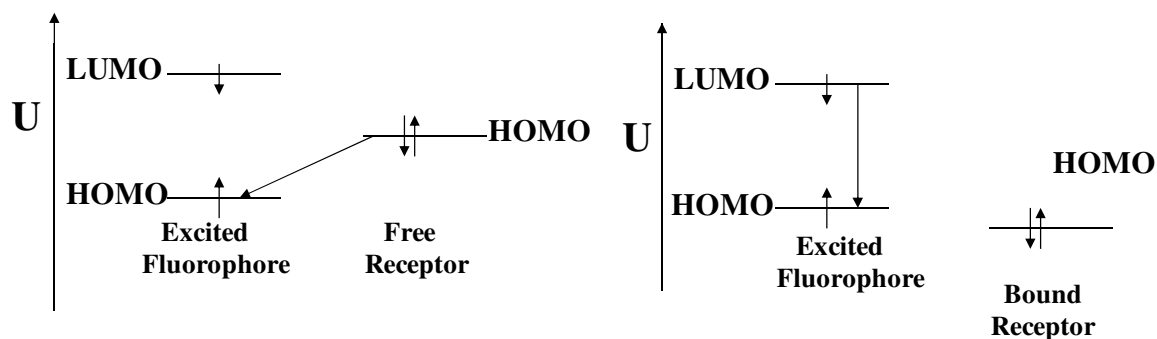


**Figure 1.12.** Energy level diagram showing the mechanism of the photoinduced electron transfer.

decrease in energy transfer or *vice versa* (Figure 1.13). This is reflected as the occurrence of the emission from the donor, in contrast to the acceptor emission in the absence of cation binding. The efficiency of this energy transfer process depends

$$\Phi_T = 1/[1 + (R/R_0)^6] \quad (\text{eq. 1.1})$$

on the distance between the donor and acceptor according to Forster's theory and is given by the equation 1.1, where, R is the distance between the two fluorophore and  $R_0$  is the Förster critical radius. As  $\Phi_T$  varies inversely with the sixth power of  $R/R_0$ , a

relatively small variation in the distance could lead to a large increase in energy transfer efficiency, provided that the interchromophoric distance is larger than the Förster critical radius in the free ligand and lower in the complex.

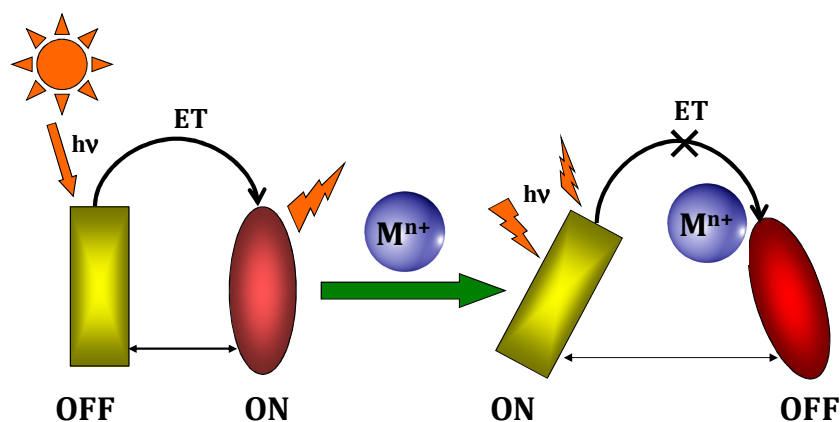


**Figure 1.13.** Schematic representation of inhibition of the photoinduced energy transfer mechanism upon cation binding.

Valeur *et al.* have reported the first bifluorophoric cation sensor **7**, which works according to the principle of photoinduced energy transfer (Chart 1.5) (Valeur *et al.*, 1992). This system consists of two coumarins linked by a short flexible chain (pentakis(ethylene oxide)), capable of forming complexes with Pb<sup>2+</sup> ions. Binding with Pb<sup>2+</sup> ions in acetonitrile resulted in significant changes in absorption, excitation, and emission spectra, whereas alkali and alkaline–earth metal ions caused negligible effect. The emission spectrum of the amino substituted coumarin donor strongly overlaps with the absorption spectrum of the coumarin acceptor, which indicates an efficient electronic energy transfer between the two units, resulting in formation of a new fluorescence emission band due to the energy transfer emission.

Interestingly, significant increase in the rate of energy transfer for the [7-Pb<sup>2+</sup>] complex was observed in acetonitrile, whereas no change was observed in propylene carbonate. This was attributed to the different structures of the metal-ligand complex in the two solvents. The [7-Pb<sup>2+</sup>] complex has a stoichiometry of 1:1 in acetonitrile, whereas a 1:3 complex is formed in propylene carbonate. Upon ligand

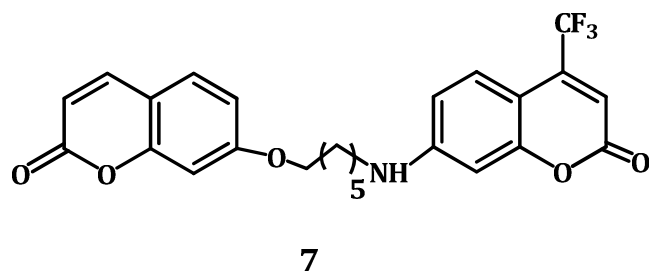


**Chart 1.5**

complexation, a significant increase in efficiency and rate of energy transfer for the complex is observed in acetonitrile due to the helical wrapping of the ligand around the cation. This causes a decrease in the distance between the donor and acceptor units resulting in the enhancement of fluorescence resonance energy transfer, whereas no conformational change was observed in propylene carbonate causing negligible changes in the FRET emission.

Another interesting example was reported by de Silva *et al.*, where both PET and EET (electronic energy transfer) processes were used to signal the metal ion binding event in a terpyridyl diester-based sensor (Chart 1.6) (de Silva *et al.*, 1997). The terpyridyl moiety strongly binds Eu<sup>3+</sup> ions, whereas the crown moiety potentially binds K<sup>+</sup> ions. Upon complexation the excitation energy transfer from the ligand to metal takes place. In the absence of K<sup>+</sup> ions, the luminescence is quenched due to PET

from the nitrogen atom of the crown. Binding of  $K^+$  ions causes a very large enhancement of the luminescence quantum yield as expected from cation-induced

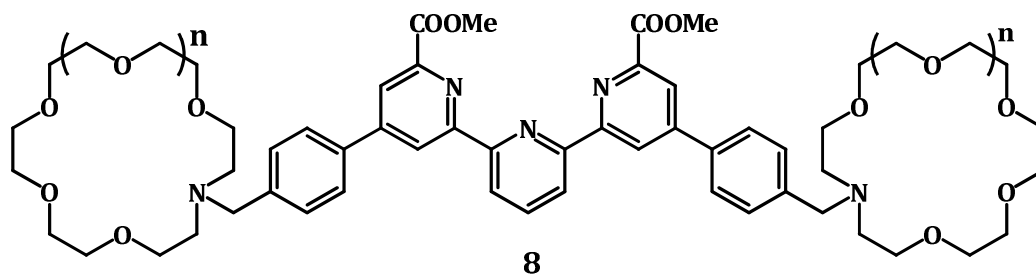


**Chart 1.6.**

reduction of the PET efficiency. This was the first example of a chemosensor based on metal triggered metal-centered emission.

In the coumarin-conjugated porphyrins, reported by Lin *et al.*, the excitation energy of the coumarin donor is efficiently transferred to the porphyrin acceptor (Chart 1.7) (Lin *et al.*, 2008). The emission spectrum of coumarin strongly overlaps with the absorption spectra of the porphyrin which is very critical for EET. The

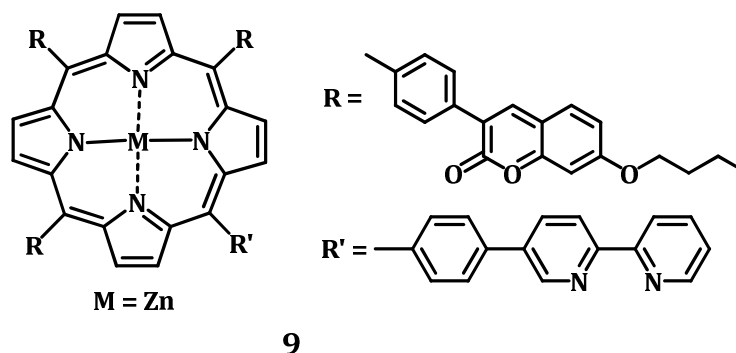
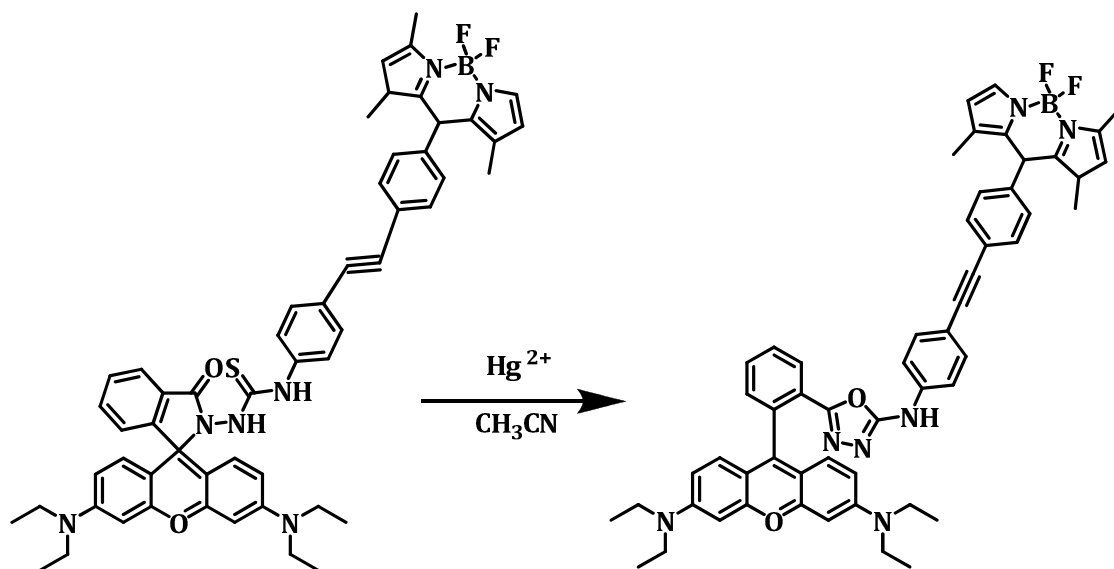


**Chart 1.7**

authors have further modified the system by introducing a bipyridyl group and developed a coumarin-zinc-porphyrin-bipyridine probe for the selective detection of

cobalt ions. Upon binding to cobalt ions, the energy transfer efficiency of the molecule decreases which resulted from the decrease in the molar absorption of porphyrin acceptor. The emission spectra showed marked decrease in the zinc porphyrin acceptor emission intensity and a significant increase in the coumarin donor fluorescence intensity. This change in the emission maxima is used as a tool for the detection of cobalt ions.



**Scheme 1.1.**

Recently, Zhang *et al.*, reported a BODIPY-rhodamine (BODIPY boron-dipyrromethene) FRET “off-on” system as a ratiometric and intracellular  $\text{Hg}^{2+}$  sensor (Zhang *et al.*, 2008). As shown in the scheme 1.1, the highly efficient ring-opening reaction induced by  $\text{Hg}^{2+}$  generates the long-wavelength rhodamine fluorophore, which acts as the energy acceptor. The acceptor rhodamine and the donor BODIPY were linked via a rigid and conjugated phenyl-ethynyl-phenyl bridging group. The  $\text{Hg}^{2+}$  ions induced ring opening and which changes the emission maximum from 514

nm (the characteristic peak of BODIPY) to 589 nm (the characteristic peak of rhodamine). This wavelength shift allows the ratiometric detection of Hg<sup>2+</sup> ions both in solution and in living cells.

The few examples given above demonstrate that the inhibition/induction of photoinduced energy transfer can be a valuable tool in the design and development of sensors for metal ions detection. The primary advantage of the energy transfer mechanism is the ratiometric detection of the analyte of interest, in addition to the advantages offered by the fluorescence techniques. Thus, the development of fluorescence based molecular receptors through the photoinduced energy transfer mechanism holds great promise as a tool for the selective detection of metal ions.

## **1.9. BACKGROUND FOR THE PRESENT INVESTIGATION**

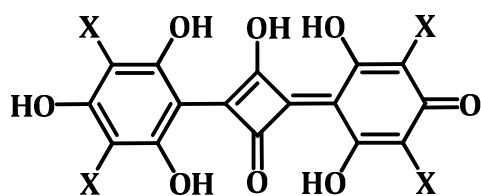
Squaraines form a class of dyes possessing sharp and intense absorption bands ( $\epsilon \sim 1-5 \times 10^5 \text{ cm}^{-1} \text{ M}^{-1}$ ), in the red to near infrared region. Squaraine dyes, in general can be considered as an acceptor in conjugation with two donors D-A-D. The donor molecules can be the same or different giving rise to symmetrical and unsymmetrical dyes (Bigelow *et al.*, 1986, Law 1987, Kamat *et al.*, 1992, Oswald *et al.*, 1999). These dyes are usually prepared by the condensation between squaric acid and electron-rich aromatic, heteroaromatic, or olefinic compounds in a one-step reaction. The success of the reaction depends on the nucleophilicity of the aryl species, wherein only the highly nucleophilic species was found to undergo the condensation reaction.

The S<sub>0</sub>-S<sub>1</sub> electronic excitation of these dyes involves a charge transfer process,

which is primarily confined to the central cyclobutane ring. The intramolecular CT character of this transition combined with the extended conjugated  $\pi$ -electron network present in squaraines gives rise to the sharp and intense absorption bands in the visible to infrared region. The photochemical and photophysical properties of these dyes have been studied extensively. Squaraines are highly suitable for a number of industrial applications, including photogeneration pigments for photoreceptors, in copiers and laser printers, photoconductors in organic solar cells, and IR absorbers in organic optical disks. However, the biological applications of squaraines, especially their potential use as sensitizers in PDT, have not been explored. This is due to the very low intersystem crossing efficiency of these dyes, rendering them less efficient in generating reactive species required for cellular damage. Recently, biological applications of squaraine-N-hydroxysuccinamide esters as long wavelength fluorescent labels have been reported in the literature (Oswald *et al.*, 1999).

Since suitably substituted squaraine dyes possess favourable absorption properties i.e. absorption in the photodynamic window, we felt that by enhancing their intersystem crossing efficiency, these dyes could function as sensitizers for use in PDT. In this regard, we have synthesized squaraine dyes substituted with heavy atoms like bromine and iodine (Chart 1.8). The heavy atoms are known to enhance intersystem crossing efficiency and populate the triplet excited state by virtue of spin orbital coupling (Ramaiah *et al.*, 1997). Laser flash photolysis studies of **11** and **12** have revealed that triplet excited states were the main transient intermediates involved. The singly deprotonated forms of **11** and **12** exhibit reasonable triplet

lifetimes ( $\tau_T = 132$  and  $36 \mu\text{s}$ ) and significant quantum yields of triplet excited states ( $\Phi_T = 0.22$  and  $0.50$ ), respectively. Furthermore, these dyes generate singlet oxygen in good yields ( $\Phi(^1\text{O}_2) = 0.13$  and  $0.47$  for **11** and **12**, respectively). The photobiological studies have indicated high photocytotoxicity both in mammalian cells and bacterial strains for **11** and **12** with relatively little toxicity in the dark as compared to the non halogenated derivative (Ramaiah *et al.*, 2002, 2004, Patent No. US 6770787). Mutagenicity studies showed that these dyes are non-mutagenic in the dark, but induce non-negligible mutations in the presence of visible light (oxidative



**10) X = H; 11) X = Br; 12) X = I**

**Chart 1.8**

damage). As was mentioned above, reactive oxygen species generated in the photodynamic processes are able to damage membranes, DNA and other cellular targets. DNA strand breaks at guanine and thymine positions in particular, as well as DNA-DNA and DNA-protein cross links have been observed as consequences of the photodynamic reactions.

Serum albumin can bind with drug molecules reversibly and with very high affinity. The formation of this complex decreases the concentration of unbound molecule in the plasma and thereby affects the ligand's distribution, pharmacokinetics, toxicity, and ultimately its rate of excretion. Previous studies on

various photosensitizers like porphyrins and chlorins revealed the well-correlated relationship between photodynamic activity and HSA site-II binding affinity to drugs, i.e. the photodynamically active compounds were generally found to bind to site II of HSA. Because of the clinical and pharmaceutical importance, the interaction of serum albumins with the phloroglucinol based squaraine dyes has been studied extensively in this thesis.

### **1.10. OBJECTIVES OF THE PRESENT INVESTIGATION**

Development of organic molecules that exhibit selective interactions with serum albumins and bind selectively at Site II has immense significance in biochemical and medicinal applications. In this context, our main objective has been to study the interaction of serum albumins with phologlucinol based squaraine dyes. Since the triplet state of the photosensitizer play a prominent role in photodynamic activity it was also our interest to understand how the triplet state properties of the squaraine dyes are altered in the presence of serum albumins. Another objective of the thesis has been to understand how the steric factors influence the site-selective binding interactions of squaraine dyes, with a view towards evaluating the probable *in vivo* transportation pathways of the halogenated and non-halogenated squaraine dyes.

Yet another objective of the thesis was to establish the binding sites of the squaraine with the protein through ligand displacement studies using site specific binding agents. It has been well established that folate receptor are over expressed in tumour cells. In this context, it was of our interest to modify the serum albumins with

folic acid and investigate the ability to folate modified serum albumin as a sensitizer delivery system. Yet another objective of the thesis has been to synthesis donor-acceptor systems and to investigate their interactions with various metal ions.

We have investigated the interactions of squaraine dyes with serum albumins employing photophysical, chiroptical, biophysical, and microscopic techniques and demonstrated that these dyes interact selectively with serum albumins with high association constants involving a combination of hydrophobic, hydrogen bonding, and electrostatic interactions. Our results reveals that these dyes show substituent size-dependent selectivity at site II of serum albumins and signal the binding event through “turn on” fluorescence intensity as well as enhanced triplet excited state lifetimes and quantum yields, thereby indicating their potential use in NIR non-covalent protein labeling and as sensitizers in photodynamic therapeutic agents. In addition, our investigations on the metal ion binding of donor-acceptor systems showed that these systems exhibited unusual selectivity for  $\text{Cu}^{2+}$  ions and form stable 2:1 stoichiometric complexes involving sulphonamide functionality and act as visual fluorescence ratiometric probes for the selective recognition of  $\text{Cu}^{2+}$  ions.

# STUDY OF INTERACTIONS OF SQUARAIN DYES WITH BSA AND HSA

---

## 2.1. ABSTRACT

With the objective to evaluate the potential applications of the squaraine dyes in photodynamic therapeutic (PDT) applications, we have studied the interactions of polyhydroxyl substituted squaraine dyes **1-3** with bovine serum (BSA) and human serum (HSA) albumins through various photophysical, spectroscopic, chiroptical and microscopic techniques. These dyes showed good solubility in the aqueous medium and exhibited favorable photophysical properties such as strong absorption in the photodynamic therapeutic window (600 – 850 nm), high quantum yields of triplet excited states and singlet oxygen.

The addition of serum albumin resulted in increase in the absorbance and fluorescence quantum yields of the squaraine dyes, along with significant bathochromic shifts in the absorption and fluorescence maxima. Half-reciprocal analysis of the absorption data gave a 1:1 stoichiometry for the complex between the serum albumins and squaraine dyes with high association constants ( $K_{ass}$ ) in the range  $10^5 - 10^6 \text{ M}^{-1}$ . The [**1**-HSA] complex showed a  $K_{ass}$  of  $1.8 \times 10^6 \text{ M}^{-1}$  and free energy change ( $\Delta G$ ) of  $-36 \text{ kJmol}^{-1}$ , whereas for the [**1**-BSA] complex, we obtained the values of  $K_{ass} = 1.4 \times 10^6 \text{ M}^{-1}$  and  $\Delta G = -35 \text{ kJmol}^{-1}$ . Similarly, the bromo substituted dye **2** with HSA and BSA exhibited association constants of  $K_{ass} = 6 \times 10^6$  and  $4.9 \times 10^6 \text{ M}^{-1}$  and  $\Delta G$  value of  $-38.6$  and  $-38.1 \text{ kJmol}^{-1}$ , respectively. On the other hand, the dye **3**

having iodine substitution showed significantly reduced association constants of  $9.9 \times 10^5$  and  $4.1 \times 10^5 \text{ M}^{-1}$  for HSA and BSA and  $\Delta G$  of -34 and -32  $\text{kJmol}^{-1}$ , respectively.

The complex formation of the squaraine dyes with the serum albumins were further confirmed by the observation of induced CD signal corresponding to the squaraine chromophore, up-field shift ( $\sim \Delta\delta$  0.1 ppm) of the aromatic protons of the dye in the  $^1\text{H}$  NMR spectra and the increase in the fluorescence anisotropy of dye on binding to albumins. The picosecond time-resolved fluorescence studies indicated that the serum albumin-dye complexes exhibit a bi-exponential decay with significantly enhanced fluorescence lifetimes. In addition, a regular change in the BSA morphology by varying the size of the dyes **1-3** in the AFM analysis of serum albumin-dye complex was observed. Laser flash photolysis studies of the dyes **2** and **3** in the presence of HSA indicated *ca.* 2 - 2.5 fold enhancements in the triplet excited state quantum yields and lifetimes, when compared to that obtained in buffer. Interestingly, the [squaraine-serum albumin] complex showed high stability and is found to be resistant to chemical and photochemical degradation. The uniqueness of these molecular systems is that these dyes interact selectively with serum albumins and signal the binding event through dual mode recognition of 'visual color' change, 'turn on' fluorescence intensity and enhancements in triplet excited state quantum yields. Thus, results demonstrate the application of these dyes as potential NIR protein non-covalent labeling agents and sensitizers in PDT applications.

## **2.2. INTRODUCTION**

Serum albumin (SA), the major extracellular multifunctional protein in

mammals, is a multifunctional protein involved in many critical physiological processes. These processes include the binding and transport of exogenous and endogenous ligands, maintenance of colloidal osmotic pressure, free-radical scavenging (Caraceni *et al.*, 1994), and regulation of acid–base balance, coagulation processes and vascular permeability. Despite its rigid structure secured by 17 disulfide bonds, albumin can undergo structural modifications via oxidative and non-oxidative pathways (Iglesias and Levine 2001), leading to anomalous conformations and changes in its binding properties. The alternations in albumin structure have been linked with cirrhosis (Watanabe *et al.*, 2004), diabetes, renal disease (Ivanov *et al.*, 2002), aging, acute and chronic inflammation, acute schizophrenia (Gryzunov *et al.*, 2000) and cancer (Kazmierczak *et al.*, 2006). Therefore, the understanding of the structural perturbation of albumin could provide early manifestation of a disease and prevent serious complications.

The specific delivery of ligands by serum albumin originates from the presence of two major and structurally selective binding sites, namely, site I and site II, which are located in three homologous domains that form a heart-shaped structure for the protein. The binding interactions at site I is mainly through hydrophobic interactions whereas, site II involves a combination of hydrophobic, hydrogen bonding and electrostatic interactions. Recently, it has been reported that molecules possessing higher affinity for serum albumin and showing preferential binding at site II are found to exhibit efficient PDT activity. In addition, by virtue of their capacity to reversibly bind a large variety of drugs, serum albumins play a predominant role in drug pharmacokinetics and pharmacodynamics (Foster *et al.*, 1977, Vijai and Foster

1967). Therefore, the understanding the nature and selective binding interactions of ligands with serum albumin is important for the design of efficient drugs and sensitizers for use in PDT applications (Szacilowski *et al.*, 2005, Pandey *et al.*, 1997, Bonnett 2000, Moser 2006, Henderson *et al.*, 1992, Cottrell *et al.*, 2006, Wieder *et al.*, 2006).

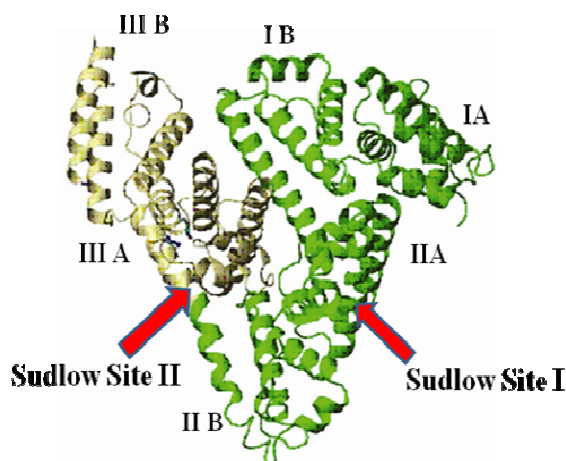


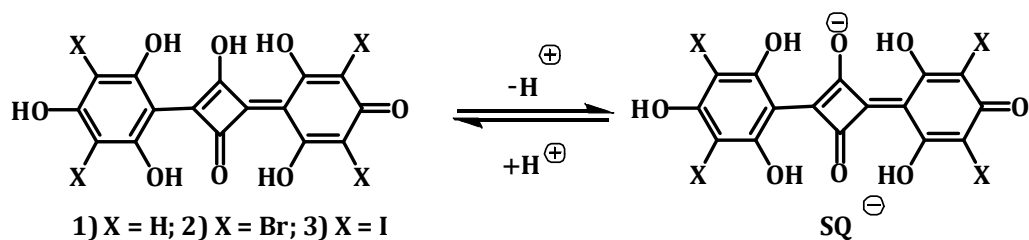
**Figure 2.1.** Crystal structure of HSA showing the major ligand binding sites (Sudlow Site I and Sudlow Site II) and the structure was obtained from the Protein Data Bank (ID code 1ha2).

In this context, it was of our interest to develop novel squaraine based systems as sensitizers for PDT applications. The squaraine dyes can be generally described as compounds containing two donor moieties (D) connected to a central  $C_4O_2$  electron withdrawing group (A) forming a donor-acceptor-donor (D-A-D) system. The intramolecular charge transfer character of the  $S_0-S_1$  transition combined with an extended  $\pi$ -electron network, gives rise to the observed sharp and intense bands in the visible to infrared region for these dyes (Bigelow *et al.*, 1986, Dirk *et al.*, 1995, Farnum *et al.*, 1974, Kobayashi *et al.*, 1986, Bernstein and Goldstein 1988). The

squaraines are the object of intense investigations as molecular components for technological applications (Fabian *et al.*, 1992, Law 1993). These include, electrophotography, optical data storage, solar cells, ion and molecular sensors, (Zhong *et al.*, 2002, Wallace *et al.*, 2005, Ros-Lis *et al.*, 2004, Martinez-Manez *et al.*, 2003, Avirah *et al.*, 2007, 2008) and nonlinear optics (Kolev *et al.*, 2004). However the biological applications of the squaraines, especially their potential use as sensitizers in PDT, have not been explored. This is due to very low intersystem crossing efficiency of these dyes, rendering them less efficient in generating reactive species required for cellular damage. Recently we have proposed the appropriately substituted squaraines as a possible new class of photosensitizers for PDT, because of their highly favourable photophysical properties and *in vitro* photobiological properties (Arun *et al.*, 2005, Jyothish, *et al.*, 2004, Ramaiah *et al.*, 2002, 2004).

The heavy atoms substituted squaraine dyes **2** and **3** showed enhanced intersystem crossing efficiency and thereby triplet excited state yields by virtue of spin orbital coupling (Ramaiah *et al.*, 1997) (Scheme 2.1). The photobiological studies showed that **2** and **3** exhibit high photocytotoxicity both in mammalian cells and bacterial strains and relatively little toxicity in the dark as compared to the non halogenated derivative **1**. The mutagenicity studies showed that these dyes are non-mutagenic in the dark, but induce non-negligible mutations (oxidative damage) in the presence of visible light. In this context, we have selected the squaraine dyes **1-3** and investigated their interactions with serum albumins under different conditions through photophysical, chiroptical and biophysical techniques. Our results demonstrate that these dyes bind with protein effectively, with high association

constants involving a combination of hydrophobic, hydrogen bonding and electrostatic interactions. Interestingly, the halogenated dyes exhibit enhanced triplet



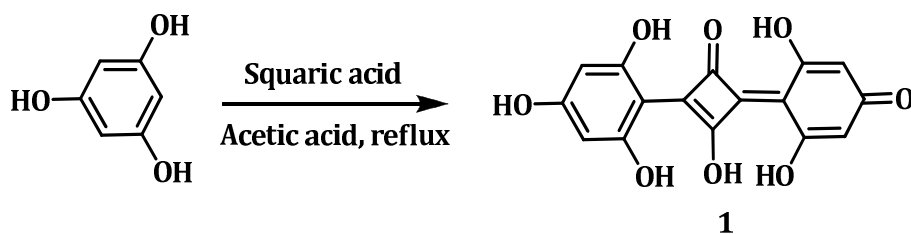
**Scheme 2.1**

excited state lifetimes and quantum yields in the presence of serum albumins. The binding can be visualized through dual mode recognition of visible color change and ‘turn on’ fluorescence intensity and hence these dyes can have potential use as non-covalent labeling agents of serum albumins and as sensitizers in PDT applications.

## 2.3. RESULTS

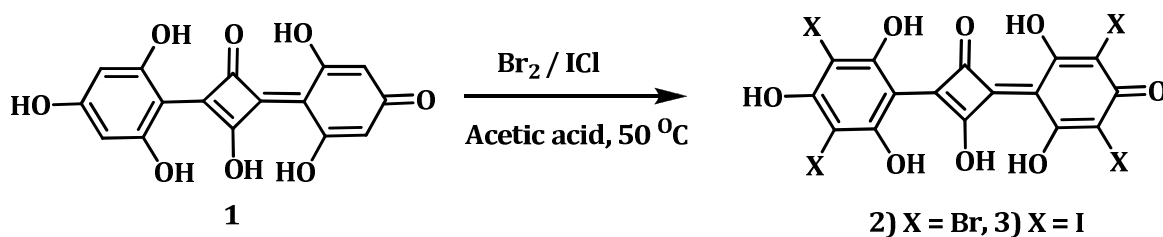
### 2.3.1. SYNTHESIS AND PHOTOPHYSICAL PROPERTIES

The synthesis of the squaraine dyes **1-3**, was carried out via the reported procedure as shown in Schemes 2.2 and 2.3. The squaraine dye **1** was prepared in 67% yield by the reaction of phloroglucinol with squaric acid (Triebes and Jacob1965). The reaction of **1** in glacial acetic acid with bromine or iodine



**Scheme 2.2.** Synthesis of the squaraine dye **1**.

monochloride in glacial acetic acid at 50 °C gave the dyes **2** and **3** in 80% and 71% yields respectively. The squaraine dyes **1-3** exist in solution in the protonated, neutral, singly deprotonated or doubly deprotonated forms, depending on the pH of the solution (Ramaiah *et al.*, 1997). Figure 2.2 shows the absorption and emission spectra of the singly deprotonated form of the squaraine dyes **1-3** in 2% ethanol



**Scheme 2.3.** Synthesis of the squaraine dyes **2** and **3**.

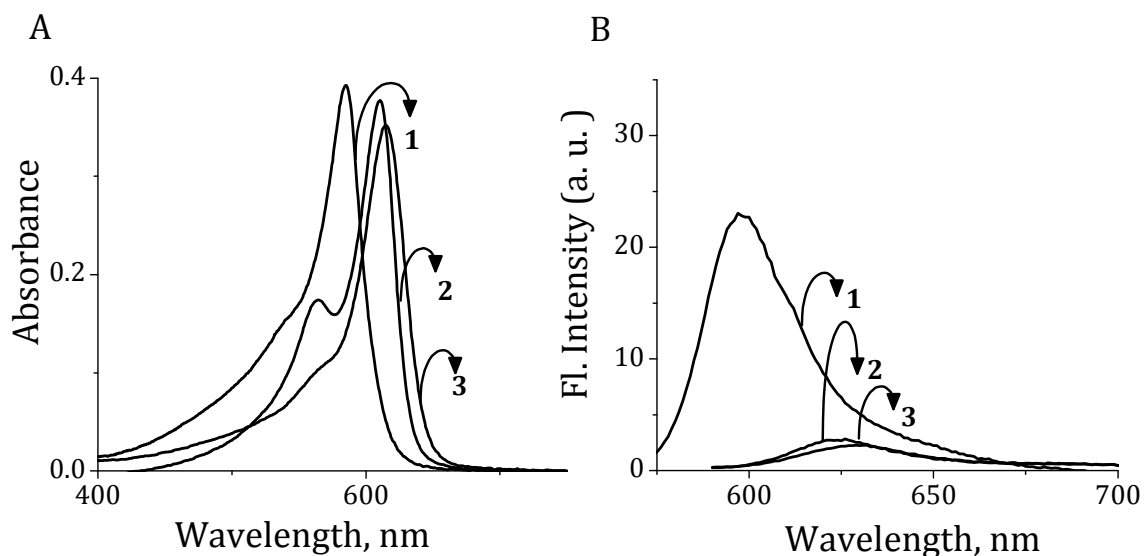


**Figure 2.2.** Absorption (A) and emission (B) spectra of the dyes **1-3** (3.0  $\mu\text{M}$ ) in 2% ethanol-phosphate buffer mixture. Excitation wavelengths, 560 (dye **1**) and 575 nm (dyes **2** and **3**).

buffer. The singly deprotonated forms of **1**, **2** and **3** showed relatively intense sharp bands at 584, 610 and 613 nm, respectively, wherein the absorption maxima of

dyes **2** and **3** are red shifted by about 12-30 nm, as compared to **1** (Das *et al.*, 1992). Of the two halogenated derivatives, the iodo derivative showed larger bathochromic shift than the bromo derivative. Figure 2.2B shows the emission spectra of the singly deprotonated forms of the dyes **1-3** in 2% ethanol-buffer mixture. The emission maximum of the iodo derivative **3**, showed a bathochromic shift of 9 nm, as compared to **2** in 2% ethanol-buffer solutions. The  $\lambda_{\text{max}}$  and fluorescence quantum yields of the singly deprotonated forms of **1-3** are summarized in Table 2.1. The quantum yields of fluorescence ( $\Phi_f$ ) in 2% ethanol-buffer for **2** and **3** are found to be lower than **1**. This is attributed to the enhanced intersystem crossing efficiency due to the heavy atom effect in these systems (Turro 1978, Detty *et al.*, 1990, Ramaiah *et al.*, 1997, Detty, *et al.*, 1988, Cincotta *et al.*, 1987, Gandin *et al.*, 1983, Ueno *et al.*, 1991).

### **2.3.2. INTERACTIONS OF SQUARINE DYES WITH SERUM ALBUMINS**

Since the squaraine dyes exhibited favourable photophysical properties, we were interested in understanding their binding ability towards serum albumins. The binding interactions were monitored by the changes in the absorption and emission spectra of these derivatives with the addition of increasing concentration of serum albumin. Figure 2.3 shows the changes in the absorption spectra of **1** (3.0  $\mu\text{M}$ ) with increasing concentration of HSA in 2% (vol/vol) ethanol-buffer mixture. The absorption spectra of the squaraine dye **1** alone showed the absorption and emission maxima at 584 and 600 nm, respectively. With increase in concentration of HSA, a decrease in absorbance of **1** at 584 nm was observed upto 1.5  $\mu\text{M}$  of HSA. Further

increasing in HSA concentration to 7  $\mu\text{M}$  resulted in the formation of new band at 610 nm, with a bathochromic shift of about 26 nm. Similar decrease in the extinction coefficients with bathochromic shifts in their absorption maxima were observed for the dyes **2** and **3**. The formation of the bathochromically-shifted band, interestingly

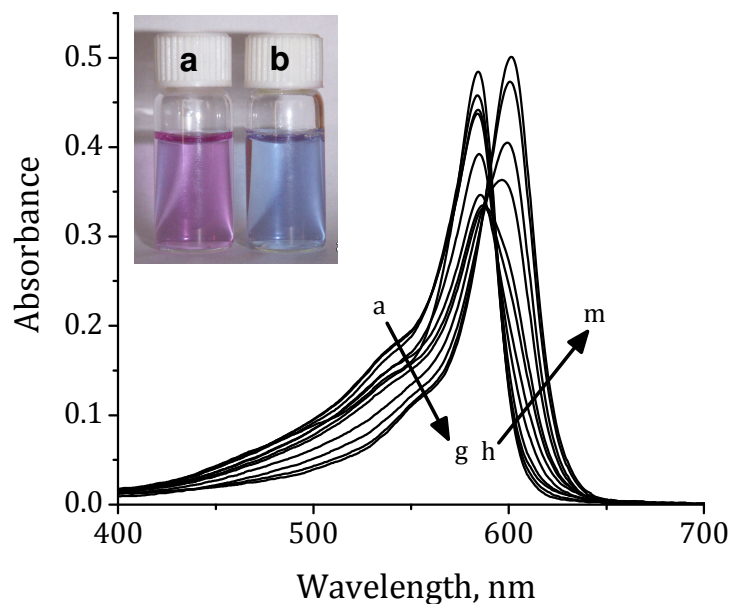


**Figure 2.3.** Changes in the absorption spectra of the dye **1** (3.0  $\mu\text{M}$ ) with the addition of HSA in 2% ethanol-phosphate buffer (pH=8.4). [HSA] (a) 0, (g) 1.5, (h) 1.8 and (m) 7  $\mu\text{M}$ . Inset shows the visible detection of HSA, a) pinkish-red, **1** alone; b) bluish in color, **1** in presence of HSA (7  $\mu\text{M}$ ).

resulted in naked eye visualization of color change from pinkish-red (**1** alone) to blue in presence of HSA. Figure 2.4 shows the absorption changes of **2** (3.0  $\mu\text{M}$ ) with the addition of HSA in 2% ethanol-buffer. The absorption spectra of the squaraine dye **2** in 2% (vol/vol) ethanol-buffer, exhibits a sharp absorption at 610 nm with a weak shoulder at 525 nm. The initial addition of HSA (upto 0.19  $\mu\text{M}$ ) led to a decrease in the absorbance at 610 nm, corresponding to the squaraine chromophore.

However, the subsequent additions (0.19-7  $\mu\text{M}$ ) resulted in the formation of a new band at 624 nm with significant hypochromism. Similar observations have been made for the dye **3** (3.0  $\mu\text{M}$ ) in the presence of HSA. Figure 2.5 shows the corresponding changes in fluorescence spectra of **1** with increasing concentration of

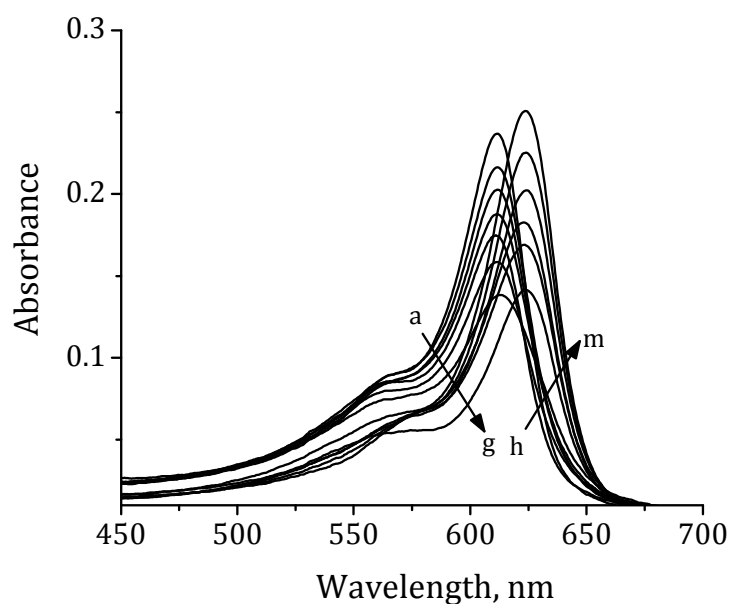


**Figure 2.4.** Changes in the absorption spectra of **2** (3.0  $\mu\text{M}$ ) with the addition of HSA in 2% ethanol-phosphate buffer (pH=6.8). [HSA] (a) 0, (g) 0.19, (h) 0.28 and (m) 7  $\mu\text{M}$ .

HSA. The dye **1** alone in 2% ethanol-buffer showed an emission maximum at 600 nm. Upon the addition of HAS, a gradual enhancement in fluorescence intensity, with a bathochromic shift in emission maxima from 600 to 623 nm was observed. The changes in the fluorescence spectra of **2** with increasing concentration of HSA are shown in Figure 2.6. As observed for dye **1**, a gradual enhancement in fluorescence intensity with a bathochromic shift of 15 nm was observed in the fluorescence spectra of **2** upon the addition of HSA. The subsequent additions yielded significant

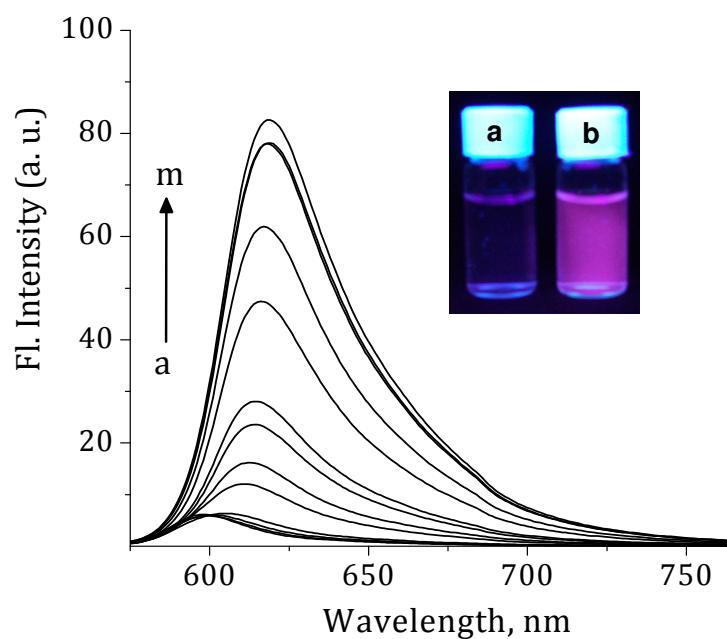


**Figure 2.5.** Fluorescence intensity changes of the dye **1** ( $3 \mu\text{M}$ ) with increasing addition of HSA (pH=8.4). [HSA] (a) 0 and (m)  $7 \mu\text{M}$ . Excitation wavelength, 560 nm. Inset shows the 'turn on' fluorescence, a) **1** alone and b) **1** in presence of HSA.

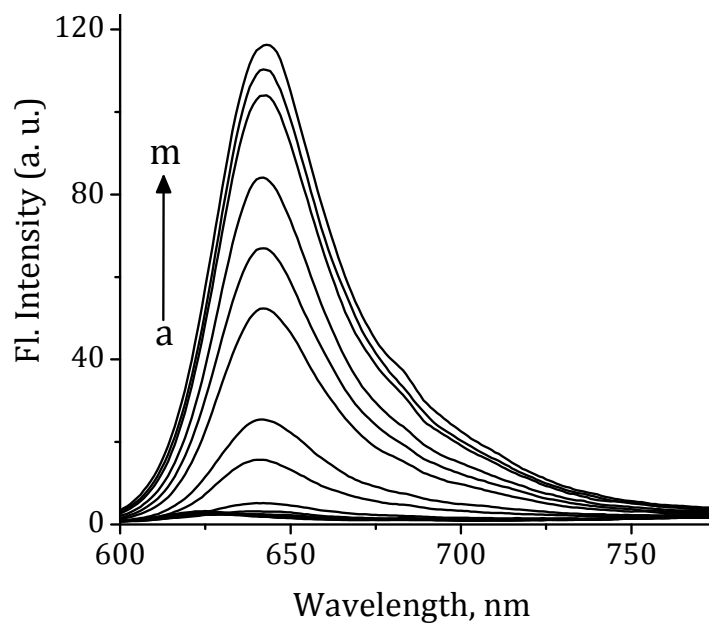


**Figure 2.6.** Fluorescence intensity changes of the dye **2** ( $3.0 \mu\text{M}$ ) with increasing addition of HSA 2% ethanol-phosphate buffer (pH=6.8). [HSA] (a) 0 and (m)  $7 \mu\text{M}$ . Excitation wavelength, 575 nm.

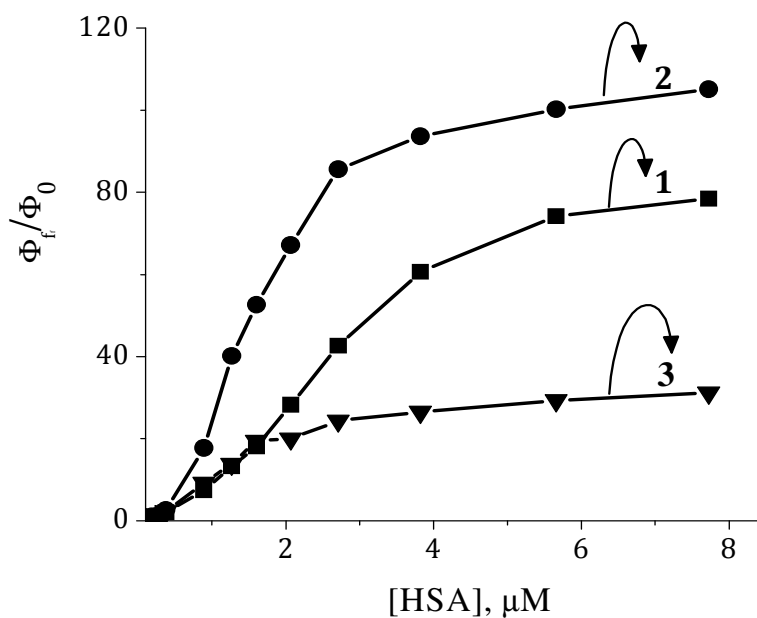


**Figure 2.7.** Relative changes in the fluorescence quantum yields of the dyes **1-3** (3 μM) with increasing concentration of HSA (0-7 μM) in 2% ethanol-phosphate buffer.

changes, and finally, *ca.* 104-fold enhancement in fluorescence quantum yields was observed at 7 μM of HSA. Similar fluorescence changes were made for the squaraine dye **3** in the presence of HSA with *ca.* 35-fold enhancement in the fluorescence quantum yields (Figure 2.7). This significant ‘turn on’ fluorescence intensity with bathochromic shift of 15-20 nm on binding to HSA, led to the visual observation of fluorescence intensity (inset of Figures 2.5). Table 2.1 summarizes the absorption and emission changes of the squaraine dyes **1-3** in 2% ethanol-buffer in the absence and presence of HSA and BSA. Interestingly, the encapsulation of the dyes within the hydrophobic environment of the protein results in significant enhancement in the fluorescence quantum yields. The quantum yields of the dye-serum albumin complexes were determined to be  $12 \times 10^{-2}$ ,  $2.5 \times 10^{-2}$  and  $0.63 \times 10^{-2}$  for the [1+HSA], [2+HSA] and [3+HSA] respectively. Similar observations were obtained for BSA also.

**Table 2.1.** Absorption and emission properties of squaraine dyes **1-3** in the absence and presence of BSA and HSA in 2% (vol/vol) ethanol-phosphate buffer.

Dye	$\lambda_{ab}$ , nm <sup>a</sup>	$\lambda_{em}$ , nm <sup>b</sup>	$\Phi_f(10^{-2})$ <sup>c</sup>
<b>1</b>	584	600	0.14
<b>1 + HSA</b>	610	623	12
<b>1+ BSA</b>	610	620	11
<b>2</b>	610	625	0.018
<b>2+ HSA</b>	624	640	2.5
<b>2 + BSA</b>	624	643	2
<b>3</b>	613	634	0.023
<b>3+ HSA</b>	628	646	0.65
<b>3 + BSA</b>	628	645	0.7

<sup>a</sup>Absorption ( $\lambda_{ab}$ , nm), <sup>b</sup>fluorescence ( $\lambda_{em}$ , nm), <sup>c</sup>Fluorescence quantum yields were calculated using cresyl violet as the standard ( $\Phi_f = 0.52$ ) in methanol.

### 2.3.3. CALCULATION OF ASSOCIATION CONSTANTS

To quantify the binding affinities of the squaraine dyes with the serum albumins, the binding isotherms using the half-reciprocal method (Kumar and Buranaprapuk, 1997) were plotted using the absorption data. The binding plot derived from the absorption titration data of compound **1** with HSA is shown in Figure 2.8. The binding constant ( $K_{ass}$ ) and corresponding change in free energy estimated for the [**1**-HSA] complex was  $1.8 \times 10^6 \text{ M}^{-1}$  and  $-36 \text{ kJmol}^{-1}$ , respectively (Table 2.2). Similarly, an association constant of  $1.4 \times 10^6 \text{ M}^{-1}$  and the change in free

energy of  $-35 \text{ kJmol}^{-1}$  was obtained in the case of the dye **1** with BSA. Interestingly, the dye **2** with HSA and BSA exhibited nearly same association constant ( $K_{\text{ass}} = 6 \times 10^6$  and  $4.9 \times 10^6 \text{ M}^{-1}$  and  $\Delta G = -38.6$  and  $-38.1 \text{ kJmol}^{-1}$ ), whereas, the dye **3** showed significantly reduced association constants of magnitude (one order less) than that of dyes **1** and **2** ( $9.9 \times 10^5$  and  $4.1 \times 10^5 \text{ M}^{-1}$  for HSA and BSA respectively) with  $\Delta G$  value of  $-34$  and  $-32 \text{ kJmol}^{-1}$  respectively.

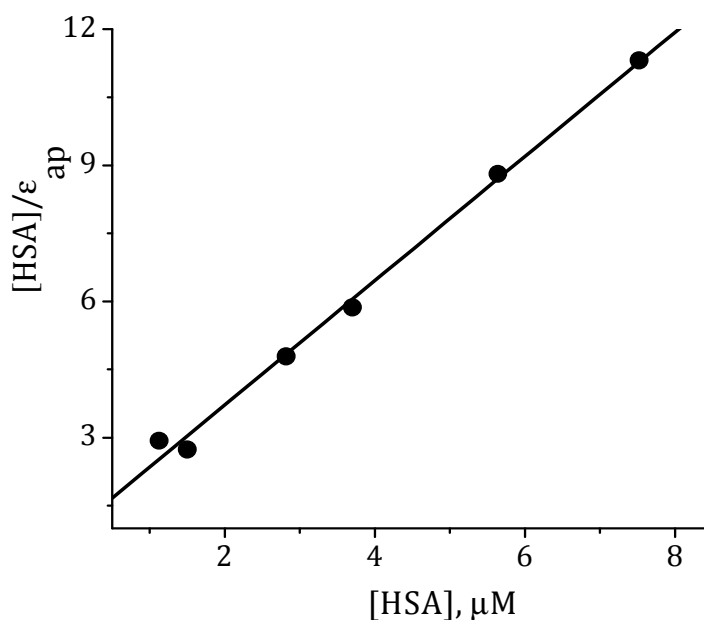


**Figure 2.8.** Half-reciprocal plot obtained from absorption data for **1** with increasing concentration of HSA.

#### 2.3.4. TIME-RESOLVED AND CIRCULAR DICHROISM STUDIES

To have a better understanding of fluorescence changes observed for the dyes **1-3** in the presence of HSA and BSA, we have analyzed their interactions through picosecond time-resolved fluorescence technique (Hariharan *et al.*, 2006, Neelakandan *et al.*, 2008). Figure 2.9 shows the decay profile of **1** with increasing concentration of BSA. The squaraine dye **1** alone exhibited a monoexponential decay

with lifetime of 121 ps, whereas biexponential decay with significantly increased lifetimes of 0.5 ns (60%) and 1.5 ns (40%) was observed in the presence of BSA. Similarly, in the presence of HSA, **1** exhibited fluorescence lifetimes of 0.6 ns (60%) and 1.0 ns (40%). Similar observations were made with the dyes **2** and **3**. The dyes **2** which showed very low fluorescence lifetime ( $< 50$  ps) in the absence of HSA,

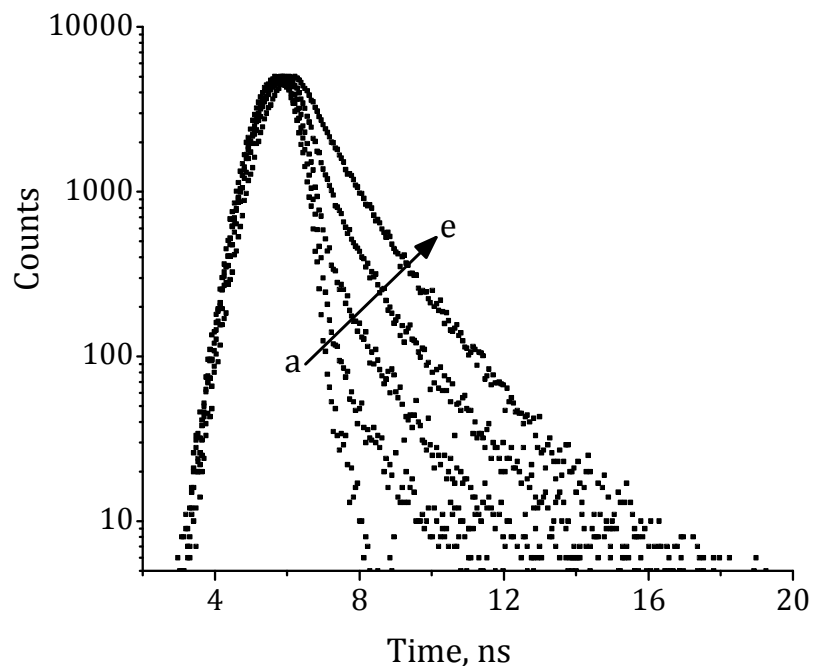


**Figure 2.9.** Time-resolved fluorescence decay profiles of **1** ( $3 \mu\text{M}$ ) with the increase in addition of BSA. [BSA] (a) 0, (b) 0.18, (c) 0.37, (d) 0.75 and (e)  $7 \mu\text{M}$ . Excitation wavelength 560 nm, decay collected at 620 nm.

exhibited biexponential decay with lifetimes of 0.3 ns (90%) and 1.3 ns (10%) when bound to HSA. Similarly, **3** showed biexponential decay with lifetimes of 0.3 ns (95%) and 1.5 ns (5%) in the presence of HSA. The values of non-radiative decay rate constants ( $k_{nr}$ ) for the dye **1** have been calculated using the fluorescence quantum yields and lifetimes. In the case of **1**, the rate constants are found to be  $8.3 \times$

$10^9 \text{ s}^{-1}$  and  $7.6 \times 10^8 \text{ s}^{-1}$ , respectively, in the absence and presence of BSA. Table 2.2 summarizes the lifetimes and binding parameters for **1-3** in the presence and absence of HSA and BSA in phosphate buffer.

**Table 2.2** . Lifetimes and binding parameters for the dyes **1-3** in the presence and absence of HSA and BSA in phosphate buffer.<sup>a</sup>

Dye	$\tau$ (ns)	$K_{ass}, \text{M}^{-1}$	$-(\Delta G)$ $\text{kJmol}^{-1}$
<b>1</b>	0.121	-	-
<b>1 + HSA</b>	0.4 (60%), 1 (40 %)	$1.8 \times 10^6$	36
<b>1 + BSA</b>	0.5 (60 %), 1.5 (40%)	$1.4 \times 10^6$	35
<b>2</b>	<0.05	-	-
<b>2 + HSA</b>	0.3 (90%), 1.3 (10%)	$6 \times 10^6$	38.6
<b>2 + BSA</b>	0.4 (90%), 1.4 (10%)	$4.9 \times 10^6$	38.1
<b>3</b>	<0.05	-	-
<b>3 + HSA</b>	0.3 (95%), 1.5 (5%)	$9.9 \times 10^5$	34
<b>3 + BSA</b>	0.3 (95%), 1.1(5%)	$4.1 \times 10^5$	32

<sup>a</sup>Serum albumin association constant ( $K_{ass}$ ), free energy change ( $\Delta G$ ), fluorescence lifetimes ( $\tau$ ). The data are the average of more than two independent experiments and the error is ca.  $\pm 5\%$  .

Circular dichroism studies are useful in understanding the complex formation of organic ligands in a chiral environment (Harata *et al.*, 1975, Dalglish *et al.*, 1971, Nordén *et al.*, 1982, Kubista *et al.*, 1988, Rodger *et al.*, 1997, Siam *et al.*, 1998). Binding of an achiral molecule within a chiral environment can lead to the induced optical activity of the bound species. The method of induced CD (ICD) is based on the

observation that an optical activity arises from dissymmetry in the ligand induced by its binding to the protein, since the free ligand has either no asymmetric centre or is a racemic mixture and therefore gives no signal in solution. Thus, squaraine dyes when bound to serum albumin is expected to give an ICD signal due to the local asymmetric environment provided by the amino acid residues at the dye binding

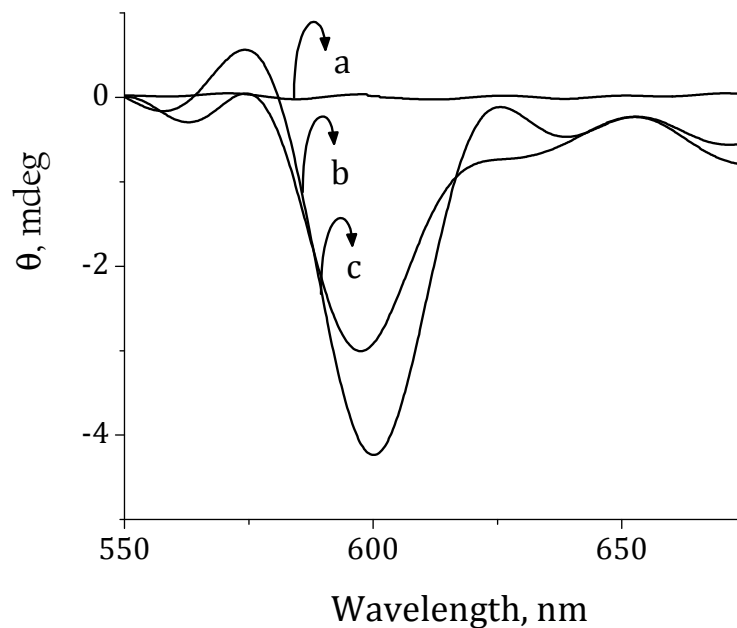


**Figure 2.10.** Changes in the CD spectra of the dye **1** in the presence of HSA in 2% ethanol-phosphate buffer (pH=8.4). [HSA] (a) 0.0, (b) 0.19  $\mu\text{M}$  and (c) 7.44  $\mu\text{M}$ .

sites. Figure 2.10 shows the ICD signal of the dye **1** with increasing concentration of HSA. These dyes alone, being achiral, does not give any optical signal. Interestingly, the addition of HSA to the squaraine dyes **1-3** resulted in the ICD signal at the chromophore absorption region. At lower protein concentration, the dye **1** showed an ICD signal at 594 nm. Further increase in the concentration of HSA caused a shift of the signal to 604 nm. Similar changes were observed in the CD spectra of the squaraine dyes **2** and **3** with the addition of HSA, wherein, the initial ICD signal

observed at 634 nm shifted to 638 nm at 7.44  $\mu\text{M}$  of HSA (Figure 2.11). These results clearly demonstrate the chiral microenvironment surrounding the squaraine chromophore.

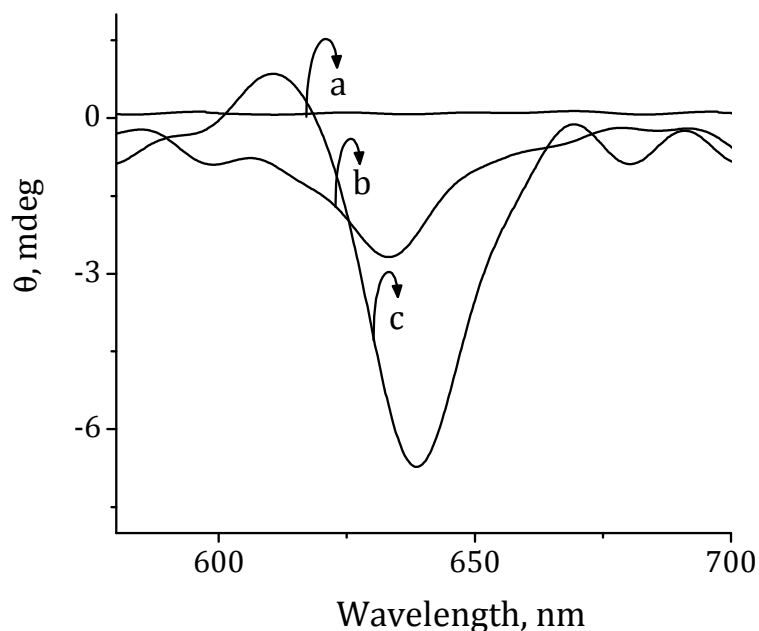


**Figure 2.11.** Induced CD spectra of the dye **3** in presence of HSA in 2% ethanol-phosphate buffer (pH=6.8). [HSA] (a) 0.0, (b) 1.5  $\mu\text{M}$  and (c) 7.44  $\mu\text{M}$ .

### 2.3.5. TIME-RESOLVED ANISOTROPY AND $^1\text{H}$ NMR STUDIES

The complex formation between the dye **1** and serum albumin was further analyzed through time-resolved anisotropy, and  $^1\text{H}$  NMR techniques. Fluorescence anisotropy gives a physical insight into the extent of restriction imposed by the microenvironment on the dynamics of the molecule and, thus, can be exploited for confirming the formation of stable inclusion complex (Mazzaglia *et al.*, 2005, Sen *et al.*, 2005, Mallick *et al.*, 2005). An increase in the rigidity of the surrounding environment of a fluorophore results in an increase in the time-resolved anisotropy.

In addition, polarization measurements can give details about association or binding phenomenon. We have monitored the fluorescence anisotropy of the dye **1** with increasing concentration of BSA at 620 nm. Figure 2.12 shows the changes in the fluorescence anisotropy ( $r$ ) of **1** at 620 nm as a function of BSA concentration. The plot shows a marked increase in the anisotropy value with increasing concentration of BSA, implying motional restriction in the protein environments.

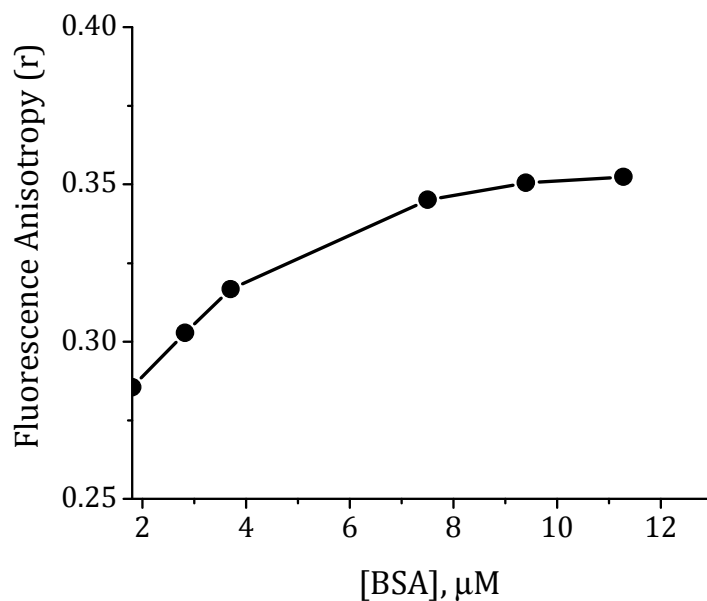


**Figure 2.12.** Variation in the time-resolved fluorescence anisotropy of **1** ( $3 \mu\text{M}$ ) with increasing concentration of BSA in 2% ethanol-phosphate buffer ( $\text{pH} = 8.4$ ). Decay collected at 620 nm.

Similarly, binding of a ligand to protein can affect the chemical shifts of both the ligand and protein NMR signals (Meyer and Peter 2003, Lucas *et al.*, 2004). Figure 2.13 shows the  $^1\text{H}$  NMR spectrum of dye **1** in  $\text{CD}_3\text{OD}-\text{D}_2\text{O}$  mixture. The four aromatic proton of the dye appears as singlet at 5.845 ppm in  $\text{CD}_3\text{OD}-\text{D}_2\text{O}$  mixtures. With the addition of BSA in  $\text{D}_2\text{O}$ , the peaks corresponding to the aromatic proton

undergoes broadening together with an up-field shift  $\Delta\delta = 0.1$  ppm, indicating the interaction of the dyes with the protein.

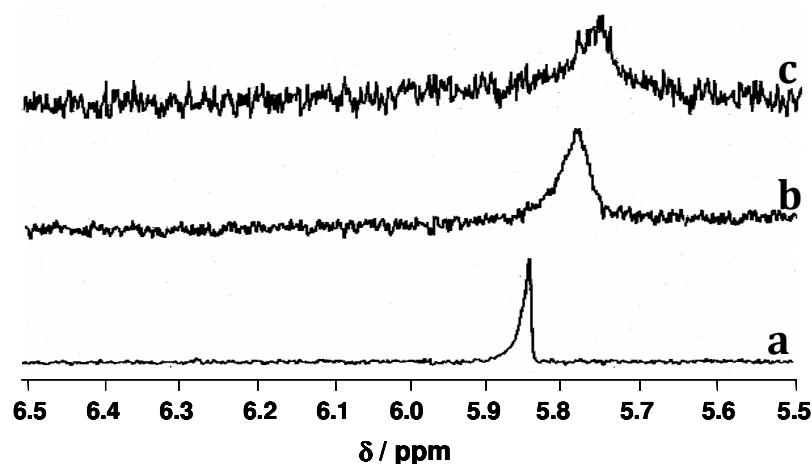


**Figure 2.13.**  $^1\text{H}$  NMR spectra of **1** (60 mM) in  $\text{CD}_3\text{OD-D}_2\text{O}$  with the increasing concentration of BSA. [BSA] (a) 0, (b) 7 and (c) 14 mM.

### 2.3.6. MORPHOLOGY STUDIES

Understanding the interaction of molecules at the atomic level is gaining much attention in the recent years (Binnig, et al., 1986, Ruger, et al., 1990, Xu *et al.*, 2005, Samori 2006). Among the various techniques, atomic force microscopy (AFM) has been instrumental in imaging the soft materials such as organic molecules and biological samples. To understand the effect of variation in size of the substituents, and thereby the role of steric factors in the formation of complexes between serum albumin and squaraine dyes, we have analyzed the surface morphology of BSA (18  $\mu\text{M}$ ) in the absence and presence of the dyes **1-3** (9.4  $\mu\text{M}$ ) through tapping mode atomic force microscopy (TM-AFM).

The AFM images of BSA alone showed a regular structure with a mean roughness of  $2 \pm 0.1$  nm (Figure 2.14 A). However, upon complexation with the dyes

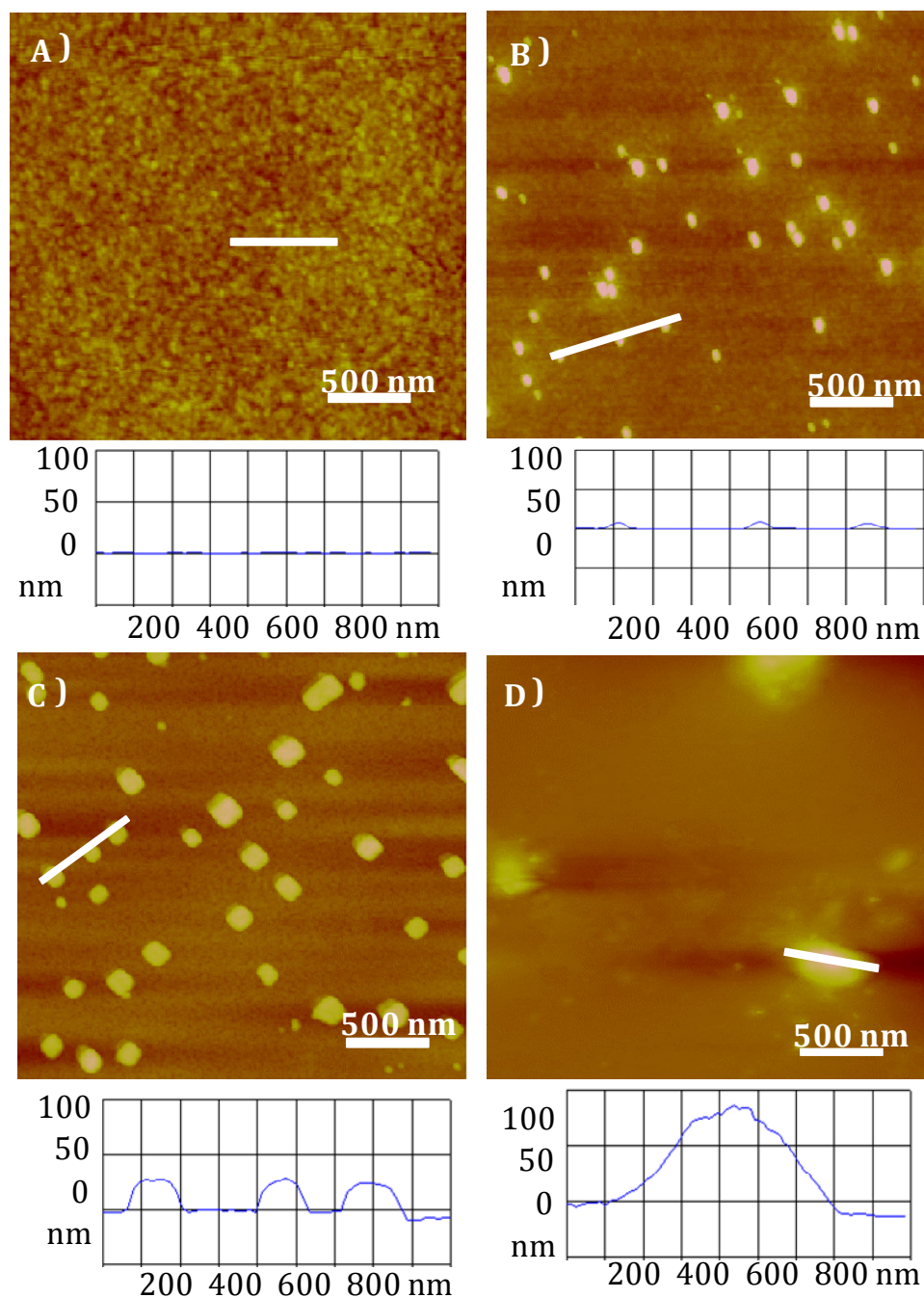


**Figure 2.14.** Atomic force microscopic (AFM) images and cross section profiles of **1-3** -BSA complexes on mica surface, **1-3** ( $9.4 \mu\text{M}$ ). (A) BSA ( $18 \mu\text{M}$ ) alone, (B) **1**-BSA, (C) **2**-BSA, and (D) **3**-BSA.

**1-3**, the regular structure of BSA has changed drastically resulting in the formation of substitution size dependent evenly distributed structures (Figures 2.14 B-D). The [1-BSA] complex showed uniform structures, but with a relatively smaller width of  $75 \pm 10$  nm (Figure 2.14 B). Similarly, the AFM analysis of the [2-BSA] complex gave uniform structures with a width of  $250 \pm 12$  nm (Figure 2.14 C), whereas structures with a width of  $450 \pm 15$  nm were observed for the complex [3-BSA] complex (Figure 2.14 D). The regular increase in the dimensions of uniform structures with the increase in size of the dyes **1-3**, indicates the fact that steric factors ( $3 > 2 \gg 1$ ) play a major role in the formation of the non-covalent complexes as well as in the site selective binding interactions of these dyes with the serum albumins.

### **2.3.7. STABILITY OF THE DYES IN PRESENCE OF SERUM ALBUMIN**

The utility of the squaraine dyes in various biological applications is severely limited due to the nucleophilic attack on the squaryl ring by thiol containing biomolecules and formation of aggregates under aqueous conditions. These two drawbacks result in the change in their photophysical properties, eventually affecting their applicability. Recently, it has been reported that the encapsulation of the squaraine dye as a rotaxane (Arunkumar *et al.*, 2005), protects the dye from aggregation and nucleophilic attack. In this regard, it was our interest to study efficiency of the [dye-serum albumin] complex in protecting the dye from nucleophilic attack. With this view, we have investigated the interaction of the dyes with aminothiols like cysteine (Cys), cystine and glutathione (GSH) in the absence and presence of serum albumin. Figures 2.15 and 2.16 show the changes in the

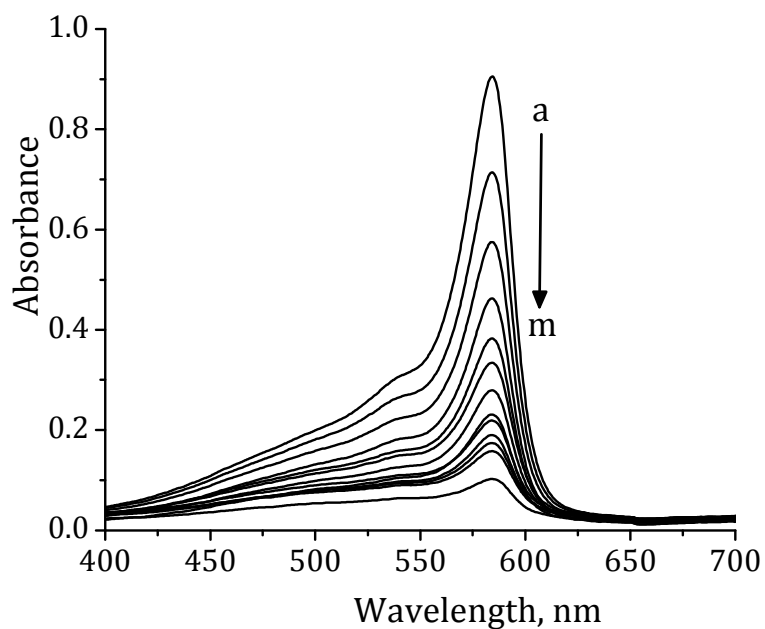


**Figure 2.15.** Effect of Cysteine (Cys) on the absorption spectra of the dye **1** ( $6 \mu\text{M}$ ). [Cys] (a) 0 and (m) 0.72 mM.

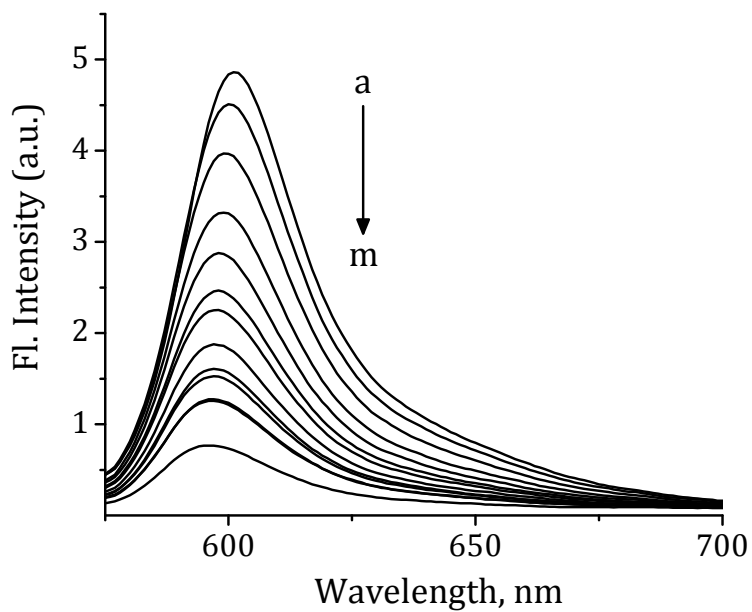


**Figure 2.16.** Effect of Cysteine on the emission spectra of the dye **1** ( $6 \mu\text{M}$ ). [Cys] (a) 0 and (m) 0.72 mM. Excitation wavelength, 560 nm.

absorption and emission spectra of the dye **1** with addition of Cys in 2% ethanol-phosphate buffer. As can be seen from the Figure 2.15, on adding 0.72 mM of Cys to a

solution of **1** in 2% ethanol-buffer, the absorbance and emission decreases pointing to the nucleophilic attack on the squaraine by the -SH group of cysteine. Similar observations were made in the case of glutathione and cystine. Interestingly, in the presence of BSA no appreciable decrease in the absorbance could be seen indicating that BSA blocks the attack by the thiol group thereby protecting the dye (Figure 2.17).

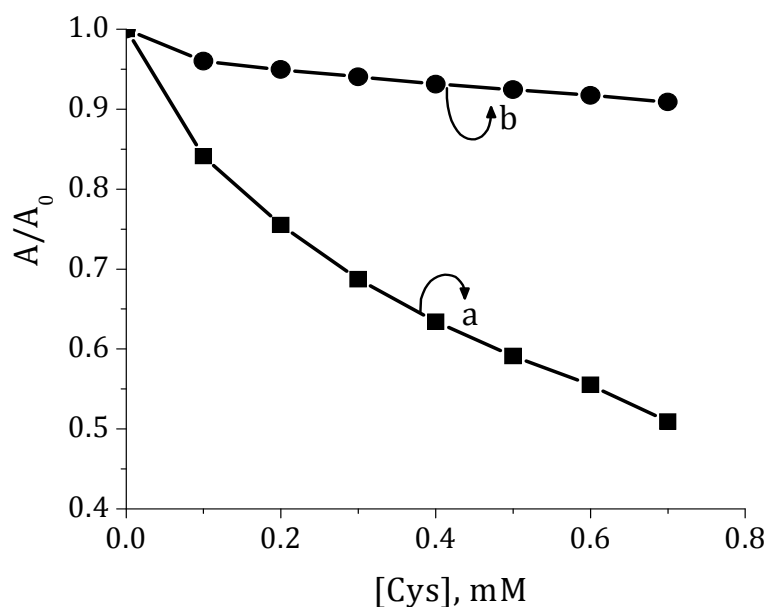


**Figure 2.17.** Change in absorbance of **1** (6  $\mu\text{M}$ ) in 2% ethanol phosphate buffer with addition of cysteine in the (a) absence and (b) presence of BSA (14  $\mu\text{M}$ ).

### 2.3.8. EFFECT OF SERUM ALBUMIN ON EXCITED STATES

The *in vitro* photodynamic efficacy of a photosensitizer, particularly via the type II mechanism, is determined by its triplet excited state quantum yield and triplet excited state lifetime. To evaluate the consequences of the binding of the dyes **2** and **3** with the serum albumins and thereby their use as PDT agents, we have quantified the

formation of their triplet excited states through nanosecond laser flash photolysis studies. Laser flash photolysis studies provide information on the triplet excited state properties of the dyes (Vaya, 2006, Baptista and Indig, 1998, Bohne *et al.*, 1992). The dyes, in ethanol-phosphate buffer, were excited at 532 nm using the second harmonic of the Nd:YAG laser. Excitation of the dyes **2** and **3** by 532 nm laser pulses (10 ns, 50

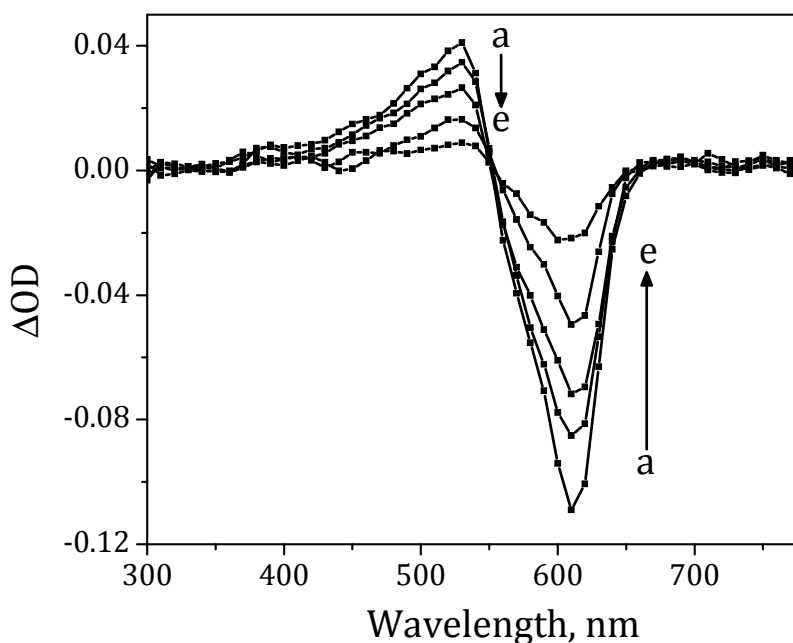


**Figure 2.18.** Transient absorption spectra obtained at a) 1, b) 10, c) 20 d) 40 and e) 80  $\mu$ s immediately after 532 nm laser excitation of argon saturated solution of squaraine dye **2** in the ethanol-phosphate buffer.

mJ/pulse) led to the formation of a transient absorption with bleach in the region corresponding to the ground state absorption spectra. The time-resolved transient spectra following the laser photolysis of squaraine dyes **2** and **3** were investigated in argon sample in the absence and presence of HSA (Figures 2.18 and 2.19). The transients observed in the case of **2** and **3** could be assigned to the triplet excited states on the basis of quenching studies with molecular oxygen and  $\beta$ -carotene as

well as literature evidence (Kumar *et al.*, 1989). The triplet excited states of **2** and **3** showed significantly enhanced lifetimes of 109 and 59  $\mu\text{s}$ , respectively, in the presence of HSA as compared to those observed in buffer (46 and 26  $\mu\text{s}$ , respectively). This can be attributed to the slower deactivation of the excited state via the non-radiative processes due to the restriction imposed on the degrees of

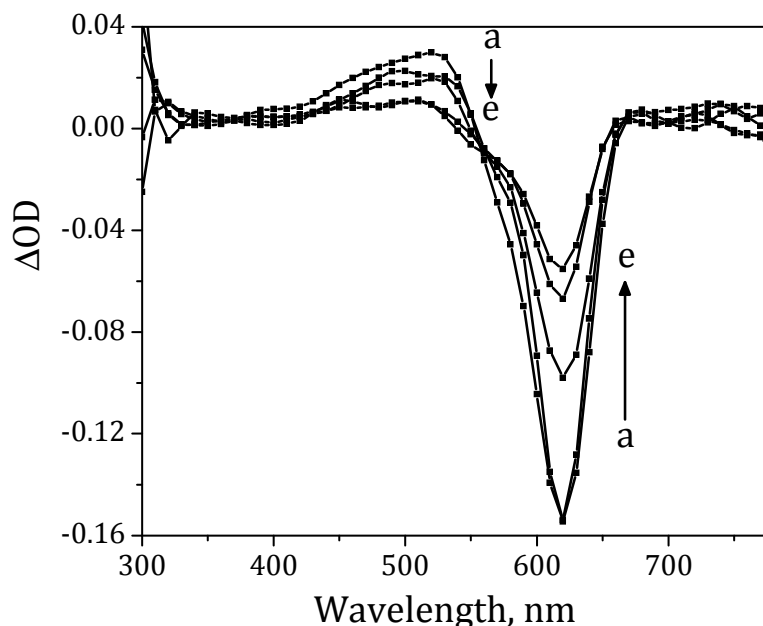


**Figure 2.19.** Transient absorption spectra obtained immediately at a) 1, b) 10, c) 20 d) 40 and e) 80  $\mu\text{s}$  after 532 nm laser excitation of argon saturated solution of [2-HSA] complex in the ethanol-phosphate buffer.

freedom inside the HSA binding sites. Figure 2.20 shows the decay curves of **2** and **3** in the absence and presence of HSA at 500 nm. By using the method of triplet-triplet energy transfer, we have estimated the quantum yields of triplet excited states. In the presence of HSA, we obtained significantly increased triplet quantum yields of ( $\Phi_T$ ) 0.54 and 0.7, respectively, for the dyes **2** and **3**, as compared to the yields (0.14 and 0.4, respectively) obtained in buffer. This enhancement in the triplet excited

state lifetime and quantum yields of **2** and **3** in HSA indicates that the serum albumin may be exploited as a drug delivery agent for the squaraine dyes for applications in biology.

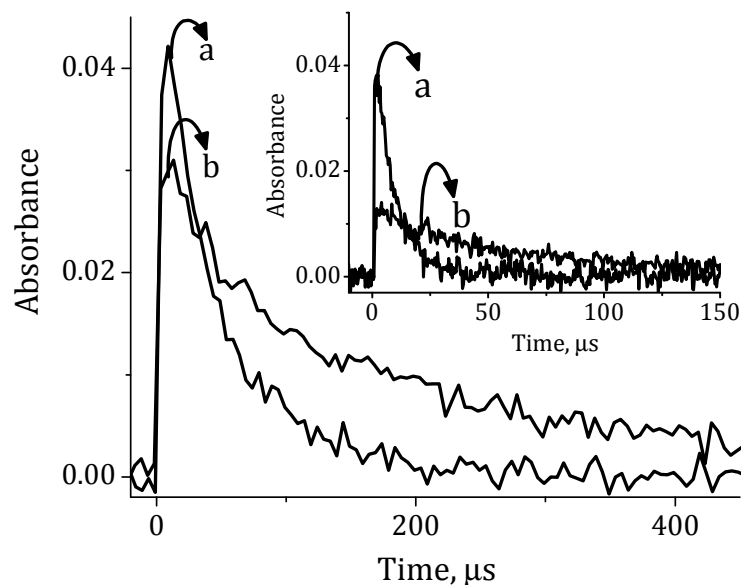


**Figure 2.20.** The transient decay monitored at 500 nm for **2** and **3** (inset) in the absence (a) and presence of (b) HSA.

## 2.4. DISCUSSION

The squaraine dyes **1**, **2** and **3**, under investigation, are quite soluble in buffer and interact efficiently with serum albumin. The absorption of the squaraine chromophore is very sensitive to the environment it experiences, and can undergo large changes upon binding to protein. Initial decrease in the absorbance of the squaraine chromophore could be attributed to the formation of a tight complex with HSA and BSA at site I and the partial  $\pi$ -stacking of the aromatic amino acid like tryptophan located at site I with the aromatic ring of the squaraines. However, at higher concentrations of serum albumins (above 1.5, 0.19, and 0.08  $\mu\text{M}$ , respectively,

for **1**, **2**, and **3**), we observed a quantitative increase in absorbance and fluorescence yields. The subsequent enhancement with a large red shift and hyperchromism in the absorption suggests that squaraine chromophore experiences a hydrophobic environment in the site II of serum albumin. The formation of a relatively loose complex at this site led to the observation of significant bathochromic shifts in absorption and fluorescence emission. The squaraine dye experiences a combination of hydrophobic, hydrogen bonding, and electrostatic interactions at site II.

The picosecond time-resolved fluorescence studies indicated that the complex [BSA-**1**] complex exhibits biexponential decay with significantly enhanced lifetimes of 0.5 (60%) and 1.5 ns (40%) when compared to the lifetime of **1** ( $\tau = 121$  ps) in the absence of BSA. Similarly, dyes **2** and **3** exhibited biexponential decay with enhanced lifetimes albeit, with different amplitudes. The two different components observed indicate that the dye binds at two different sites within the protein. The minor component (5-40%) observed with relatively longer lifetimes of 1.08-1.5 ns in the case of dyes **1-3** in the presence of BSA indicates the localization of the dyes at a rigid environment, whereas the major component of 60-95% having a relatively shorter lifetime of 0.3-0.5 ns indicates the dye bound at site II.

The complex formation was further confirmed by observation of induced CD signal corresponding to the squaraine dyes at the dye absorption region, up-field shift (about  $\Delta\delta$  0.1 ppm) of aromatic protons of dye in  $^1\text{H}$  NMR spectra and the restriction in the rotational motion of the dye measured by fluorescence anisotropic measurements. The motion of the dye in the presence of the serum albumin depends not only on its size but also on the nature of the attachment, three-dimensional shape

and motion of the protein, and the global Brownian movement of the dye protein aggregate. Since the overall dimension of the protein-bound probe is logically much larger than that of the unbound species, there is a marked reduction in the motion of the dye molecules, resulting in an increase in the anisotropy value. This is demonstrated in the anisotropy values obtained for the 620 nm emission of **1** with increasing concentration of BSA.

The observation of distinct AFM morphological changes of the protein, when complexed with the dyes **1-3**, further, confirms the binding of the dyes with protein. Moreover, binding of these dyes within the protein cavity protects the dyes from aminothiols such as cysteine and glutathione. The efficient complexation of the dyes **2** and **3** with serum albumins is reflected in the quantitative increase in the triplet excited state lifetimes and quantum yields of the dye-serum albumin complex. This observation could be attributed to the microencapsulation of the dyes by the serum albumins resulting in the restriction of rotational freedom of guest molecules and increased intersystem crossing efficiency.

## **2.5. CONCLUSIONS**

In summary, the squaraine dyes **1-3** exhibit favorable solubility in the aqueous medium and absorption in the near infrared region. These dyes exhibit selective and efficient interactions with serum albumins such as HAS and BSA, and show significant enhancement in emission quantum yields and lifetimes. Binding of these squaraine dyes with serum albumins provide significant chemical stabilization, in addition to the enhancement in their triplet quantum yields. The uniqueness of the

squaraine dyes is that they interact with BSA and HSA very efficiently and signal the binding event through dual mode ‘visual color’ change and ‘turn on’ fluorescence intensity. These results clearly demonstrate their potential application as novel NIR non-covalent labels in immunochemical assay, biophysical studies and as sensitizers in photodynamic therapeutic applications.

## 2.6. EXPERIMENTAL SECTION

### 2.6.1. GENERAL TECHNIQUES

All melting points are uncorrected and were determined on a Mel-Temp II melting point apparatus. The electronic absorption spectra were recorded on a Shimadzu UV-3101PC UV-VIS-NIR scanning spectrophotometer (Sajimon *et al.*, 2007, Jyothish *et al.*, 2007, Kuruvilla *et al.*, 2007, Jisha *et al.*, 2009, Nair *et al.*, 2009). The fluorescence spectra were recorded on a SPEX-Fluorolog F112X spectro-fluorimeter. The <sup>1</sup>H and <sup>13</sup>C NMR spectra were obtained using a Bruker DPX-300 MHz spectrometer. The mass spectra were recorded on a JEOL AX503 mass spectrometer. The pH measurements were carried out using ELICO Model L1-120 digital pH meter, which was calibrated using standard buffer solutions of pH 4 and 9.2. The fluorescence quantum yields were determined by using optically matched solutions. The quantum yields of fluorescence were calculated using the equation 1.1.

$$F_u = \frac{A_s F_u n_u^2}{A_u F_s n_s^2} F_s \quad (\text{eq. 1.1})$$

cresyl violet ( $\Phi_f = 0.52$ ) in methanol was used as the standard where,  $A_s$  and  $A_u$  are the absorbance of standard and unknown, respectively.  $F_s$  and  $F_u$  are the areas of

fluorescence peaks of the standard and unknown and  $n_s$  and  $n_u$  are the refractive indices of the solvents used for the standard and unknown, respectively.  $\Phi_s$  and  $\Phi_u$  are the fluorescence quantum yields of the standard and unknown compounds. Fluorescence lifetimes and fluorescence anisotropy were measured using a IBH picosecond single photon counting system. The fluorescence decay profiles were deconvoluted using IBH data station software V2.1, and minimizing the  $\chi^2$  values of the fit to  $1 \pm 0.1$ . Circular dichroism (CD) spectra were recorded on Jasco Corporation, J-810 spectropolarimeter. Laser flash photolysis experiments were carried out in an Applied Photophysics Model LKS-20 Laser Kinetics Spectrometer using the second harmonic (532 nm) of a Quantum Ray GCR-12 series pulsed Nd:YAG laser. Doubly distilled water was used in all the studies. All experiments were carried out at room temperature ( $25 \pm 1^\circ\text{C}$ ), unless otherwise mentioned.

## 2.6.2. MATERIALS AND METHODS

Bovine serum albumin and human serum albumin were obtained from Aldrich and were used without further purification.

### 2.6.2.1. Synthesis of bis (3,5-dibromo-2,4,6-trihydroxyphenyl)squaraine (**2**)

The squaraine dye **1** (100 mg, 0.3 mmol) was dissolved in glacial acetic acid (85 mL) by stirring the solution at  $50^\circ\text{C}$  for 90 min. After cooling the solution to room temperature, bromine (215 mg, 1.3 mmol) in glacial acetic acid (15 mL) was added dropwise, over a period of 1 h. The reaction mixture was kept in the refrigerator for 4 h to yield 160 mg (80%) of **2**, mp  $315^\circ\text{C}$ , which was recrystallized from a mixture (4:1) of water and isopropanol. IR (KBr)  $\nu_{\text{max}}$  3413, 1622, 726 and 519

cm<sup>-1</sup>; HRMS-ESI Calcd for C<sub>16</sub>H<sub>6</sub>O<sub>8</sub>Br<sub>4</sub>: 642.6874; Found: 642.6879.

### 2.6.2.2. Synthesis of bis (3,5-diiodo-2,4,6-trihydroxyphenyl)squaraine (3)

The squaraine dye **1** (100 mg, 0.3 mmol) was dissolved in glacial acetic acid (85 mL) by stirring the solution at 50 °C for 90 min. After cooling the solution, iodine monochloride (218 mg, 1.34 mmol) in glacial acetic acid (15 mL) was added dropwise, over a period of 1 h. The reaction mixture was further stirred for 1 h. Water (15 mL) was added to the reaction mixture and kept in the refrigerator for 5 h. The solid precipitate was filtered to give 180 mg (71%) of **3**, mp 270 °C, which was recrystallized from a mixture (4:1) of methanol and isopropanol. IR (KBr)  $\nu_{\max}$  3383, 1603, 726 and 508 cm<sup>-1</sup>; HRMS-ESI Calcd for C<sub>16</sub>H<sub>6</sub>O<sub>8</sub>I<sub>4</sub>: 834.6320. Found: 834.8360.

### 2.6.2.3. Atomic Force Microscopy (AFM) Analysis

Samples for the imaging were prepared by drop casting the BSA solution in the absence and presence of dyes **1-3** on freshly cleaved mica. AFM images were recorded under ambient conditions using a Digital Instrument Multimode Nanoscope IV operating in the tapping mode regime. Micro-fabricated silicon cantilever tips (MPP-11100-10) with a resonance frequency of 299 kHz and a spring constant of 20-80 Nm<sup>-1</sup> were used. The scan rate varied from 0.5 to 1.5 Hz. AFM section analyses was done offline.

### 2.6.2.4. Calculation of association constant ( $K_{ass}$ )

The intrinsic binding constant ( $K_{ass}$ ) was determined from the half reciprocal

plot of  $D/\Delta\varepsilon_{ap}$  vs  $D$ , where  $D$  is the concentration of BSA,  $\Delta\varepsilon_{ap} = [\varepsilon_a - \varepsilon_F]$  and  $\Delta\varepsilon = [\varepsilon_b - \varepsilon_F]$ . The apparent extinction coefficient,  $\varepsilon_a$ , is obtained by calculating  $A_{[obsd]} / [Dyes]$ .  $\varepsilon_b$  and  $\varepsilon_F$  correspond to the extinction coefficient of the bound form of dye and the extinction coefficient of free dye, respectively. The data were fitted to equation 1.2, with a slope equal to  $1/\Delta\varepsilon$  and y-intercept equal to  $1/\Delta\varepsilon K_{ass}$ .  $\varepsilon_b$  was determined from  $\Delta\varepsilon$ , and  $K_{ass}$  was obtained from the ratio of the slope to the y-intercept.

$$\frac{D}{D\varepsilon_{ap}} = \frac{D}{D\varepsilon} + \frac{1}{D\varepsilon K_{ass}} \quad (\text{eq. 1.2})$$

#### 2.6.2.5. Calculation of change in free energy ( $\Delta G$ )

Change in free energy ( $\Delta G$ ) associated with the complexation between SQ and BSA, was determined using the equation 1.3, where  $K_{ass}$  is the association constant.

$$\Delta G = -2.303RT \log K_{ass} \quad (\text{eq. 1.3})$$

#### 2.6.2.6. Calculation of non-radiative decay rate constant ( $k_{nr}$ )

In order to calculate the non-radiative decay rate constant ( $k_{nr}$ ), the equation 1.4 and 1.5 was used,

$$k_{nr} = k_r \left[ \frac{1}{\Phi_f} - 1 \right] \quad (\text{eq. 1.4})$$

$$k_r = \frac{\Phi_f}{\tau_f} \quad (\text{eq. 1.5})$$

where,  $k_r$  is radiative decay rate constant,  $\Phi_f$  = fluorescence quantum yield of squaraine dyes,  $\tau_f$  is lifetime of dye and  $\Phi_f$  = fluorescence quantum yield of dye.

# SITE-SELECTIVE BINDING INTERACTIONS OF SQUARINE DYES WITH BSA, HSA AND OTHER SELECTED PROTEINS

---

### 3.1. ABSTRACT

Site-selective binding of squaraine dyes with serum albumin (SA) was investigated through fluorescence displacement assay using site specific reagents like dansylamide and dansylproline, circular dichroism and energy transfer studies. The Squaraine dyes substituted with heavy atoms (**2** & **3**) show high selectivity towards site II, sub-domain IIIA of the protein, whereas the squaraine dye **1** binds at site I, sub-domain IIA of the protein. The binding at site I decrease the helical content of the protein, leading to a reduction in the fluorescence intensity and lifetime of the Trp-214 residue in native HSA and BSA, located in the same sub-domain IIA. Interestingly, an efficiency energy transfer was found to occur from the Trp-214 to the squaraine dye **1**. The distance between the donor and acceptor was calculated using Försters theory and the value was found to be 27 and 30 Å for BSA and HSA, respectively. The measured lifetimes of HSA (3.1 ns (20%) and 6.6 ns (79%)) are typical of tryptophan in a polar environment and are reduced upon interaction with the squaraine **1**. The squaraine dyes showed selective interactions with serum albumins as compared to other proteins such as globulins, ferritin, transferin, fibrinogen, lysozyme, carboxy peptidase A and ribonuclease A. Further, we have synthesized folic acid-BSA conjugate as a targeted carrier system for the dyes. Our investigations revealed that these dyes interact effectively with the folic acid-BSA conjugate indicating that the

folate linked protein can be used as an efficient delivery vehicle for these dyes. The uniqueness of these dyes is that they show substituent size dependent selectivity at site II of serum albumins, wherein the iodo substituted squaraine dye showed the maximum selectivity selectively and can be used as probes for the detection of serum albumins under gel electrophoresis conditions.

### **3.2. INTRODUCTION**

Protein-ligand interactions are important in biological processes such as enzyme-substrate recognition, hormone action, signal transduction, and cell communication (Peters 1996, Gellman 1997, Berde *et al.*, 1979, Schneider *et al.*, 2008, Pal *et al.*, 2004, Lyon *et al.*, 2002). Of all the proteins, serum albumin is found abundantly in the bloodstream and is principally characterized by its remarkable ability to bind and transport a wide range of endogenous and exogenous ligands like drugs, amino acids, fatty acids, bilirubin, bile acids, and thyroxin (Fasano *et al.*, 2005, Ascenzi *et al.*, 2006, Ghuman *et al.*, 2005, Simard *et al.*, 2005, Simard *et al.*, 2006). Because of the ability of the serum albumins to interact with a wide variety of molecules, it is of current interest to exploit its various favourable properties for the development of novel therapeutic agents (Beljaars *et al.*, 2000, Kurtzhals *et al.*, 1995, Sheffield 2001, Kragh-Hansen 1981).

Even though, a number of studies have been carried out to identify and characterize the location and structure of drug binding sites in the serum albumin, several aspects are not yet well understood. For example, Fehske *et al.* proposed that

site I of HSA consisted of two regions, called the warfarin- and azapropazone-regions, of which only the warfarin binding region was affected on modifying the tryptophan residue (Fehske *et al.*, 1978). However, studies on the binding characterization of ligand pairs such as warfarin-azapropazone, warfarin-phenylbutazone, acenocoumarol-phenylbutazone and phenprocoumon-phenylbutazone revealed that several warfarin-region binding drugs are able to competitively displace azapropazone-region binding drugs. These findings indicate that the detailed construction of the drug binding sites of HSA is complicated and largely unknown. Nevertheless, it is well accepted that, the specific physiological activity of the ligands upon complexation with serum albumin originates from the presence of two major and structurally selective binding sites, namely, site I and site II, which are located in three homologous domains. (Carter *et al.*, 1990, He *et al.*, 1992, Dockal *et al.*, 1999, Carter *et al.*, 1994, Lopicque *et al.*, 1993, Sudlow *et al.*, 1975, Sudlow *et al.*, 1976, Zhong *et al.*, 2000, Chuang *et al.*, 2006).

The crystal structure of the drug binding region has identified that site I is dominated by the presence of 16 hydrophobic residues including tryptophan (Try-214), lysine (Lys-199), and histidine (His-242) which play an important role in the protein-ligand interactions. The most important amino acid residues of the IIIA sub-domain (site II) binding site are tyrosine (Tyr-411) and arginine (Arg-410). The extensive studies on drug binding have identified that binding site I is dominated by strong hydrophobic interactions. The ligands bound at this site are located in the immediate vicinity of tryptophan (Trp-214), which can serve as an efficient energy

donor. In contrast, the interactions at site II involve a combination of hydrophobic, hydrogen bonding, and electrostatic interactions. Of all the amino acid residues, tyrosine (Tyr- 411) is the most probable candidate for the complex formation at this site since its phenolic hydroxyl group can undergo effective hydrogen bonding with the bound ligands (Rahman *et al.*, 1993, Kumar *et al.*, 2002, Duff *et al.*, 2006, Bhasikuttan *et al.*, 2007, Lhiaubet-Vallet *et al.*, 2004, Jimenez *et al.*, 2005, Kumar *et al.*, 2000, Kumar *et al.*, 1999, Kumar *et al.*, 2005, Kumar *et al.*, 1993).

It has been reported that photosensitizers possessing higher affinity for serum albumin and showing preferential binding at site II are found to exhibit efficient photodynamic therapeutic (PDT) applications (Tsuchida *et al.*, 1997, Pandey *et al.*, 1997). In this context, the design of novel functional molecules that can undergo selective interactions with serum albumin exclusively at site II and exhibit efficient photodynamic activity has been challenging because such molecules can have potential use as drugs and sensitizers in PDT applications (Bonnett 2000, Moser 1998). As mentioned in the chapter 2 of the thesis, the squaraine dyes, bis-(2,4,6-trihydroxyphenyl)squaraine (**1**), bis-(3,5-dibromo-2,4,6-trihydroxyphenyl)squaraine (**2**), and bis-(3,5-diiodo-2,4,6 trihydroxy-phenyl)squaraine (**3**), based on the phloroglucinol moiety (Chart 3.1), undergo efficient interactions with serum albumins with an enhancement in the triplet quantum yield and lifetimes (Jisha *et al.*, 2006). Since the ligands having affinity towards the site II showed high potential as PDT drugs, it was our objective to investigate their site selective binding interactions with human (HSA) and bovine serum albumins (BSA) using site specific reagents. In

the present study, we have used 5-dimethylaminonaphthalene-1-sulfonamide (DNSA) as the site I binding agent and dansylproline (DP) as the site II binding agent (Pandey *et al.*, 1997). Our results demonstrate that the halogenated squaraine dyes **2** and **3** exhibit high selectivity (>90%) toward site II of serum albumins with a high association constant ( $10^5$ - $10^6\text{M}^{-1}$ ) involving hydrogen bonding and electrostatic

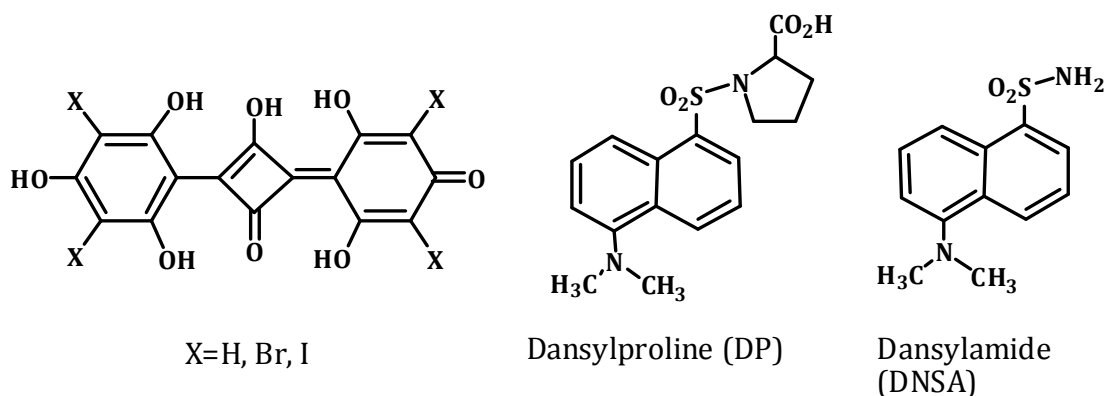


**Chart 3.1**

interactions in contrast to the marginal selectivity observed with the unsubstituted dye **1**. The site selective binding was further confirmed by energy transfer studies between tryptophan and squaraine as well as circular dichroism studies. The uniqueness of these dyes is that they exhibited high selectivity for HSA and BSA when compared to other proteins, thus, demonstrating their usefulness as fluorescence probes for serum albumins in buffer and under gel electrophoresis conditions.

### 3.3. RESULTS

#### 3.3.1. SITE-SELECTIVE BINDING LIGAND DISPLACEMENT METHOD

Titration of the squaraine dyes with serum albumins (HSA and BSA) showed

that these dyes show efficient interactions with these transport proteins in buffer and signal the event through changes in absorption and emission properties. In order to understand the site of binding in HSA and BSA we have employed ligand displacement method utilising site specific binding reagents like DNSA and DP. DNSA is known to bind specifically at site I, whereas DP binds specifically at site II of the protein. Since DNSA and DP show high binding affinity to site I and site II, they can effectively displace any ligand bound to protein at site I and site II, respectively. The absence of displacement with a site selective agent, thus, indicates the improbability of drug binding to that particular site. Conversely, the decrease in the fluorescence intensity of the dye-serum albumin complex when the competitor is added can be interpreted as the displacement of the probe from its binding site. The major

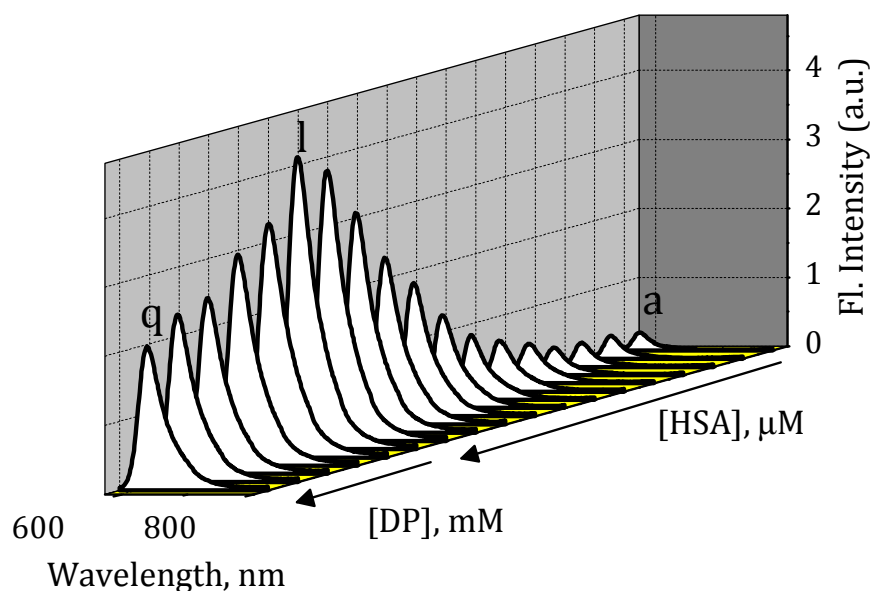


**Figure 3.1.** Effect of HSA on the fluorescence spectra of the dye **1** ( $3 \mu\text{M}$ ) and followed by the addition of dansylproline (DP). [HSA] (a)  $0.0$  and (l)  $7 \mu\text{M}$ . [DP] (l)  $0.0$ , and (q)  $0.6 \text{ mM}$ . Excitation wavelength,  $560 \text{ nm}$ .

requirement for the success of this assay is that the affinity between the site specific binding reagent and the protein should be comparable to that between the dye and the protein.

Figure 3.1 shows the changes in the intensity of the dye **1** with the consecutive addition of HSA and DP. As seen in the Figure 2.5, the addition of HSA and BSA to a solution of squaraine dye **1** in buffer resulted in the regular increase in the

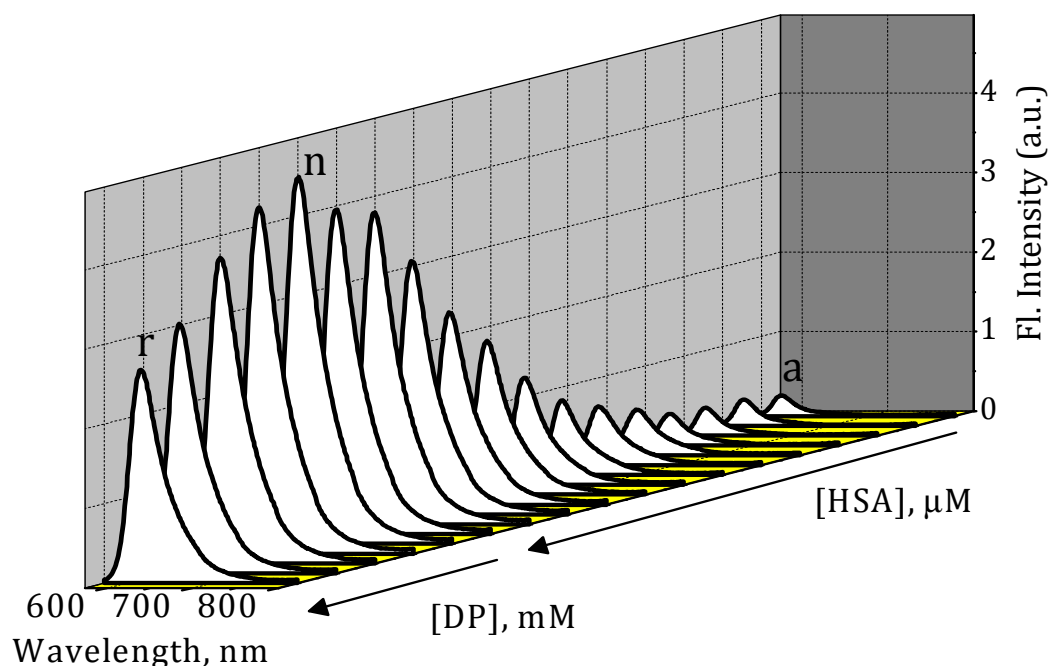


**Figure 3.2.** Effect of HSA on the fluorescence spectra of the dye **1** ( $3 \mu\text{M}$ ) and followed by the addition of dansylamide (DNSA) [HSA] (a)  $0.0$  and (n)  $7 \mu\text{M}$ . [DNSA] (n)  $0.0$ , and (r)  $0.71 \text{ mM}$ . Excitation wavelength,  $560 \text{ nm}$ .

fluorescence intensity followed by saturation at *ca.*  $7 \mu\text{M}$  of HSA. When DP, a known site II specific reagent was gradually added to this [**1**-HSA] complex, we observed regular decrease in the emission spectra of dye **1** confirming thereby the effective displacement of the dye **1** by DP. These fluorescence changes reached saturation at

0.6 mM of DP and an effective displacement of around 60% was observed. Figure 3.2 shows the changes in the fluorescence spectra of [1-HSA] complex with addition of DNSA. The effective displacement in the case of DNSA was found to be around 40%,

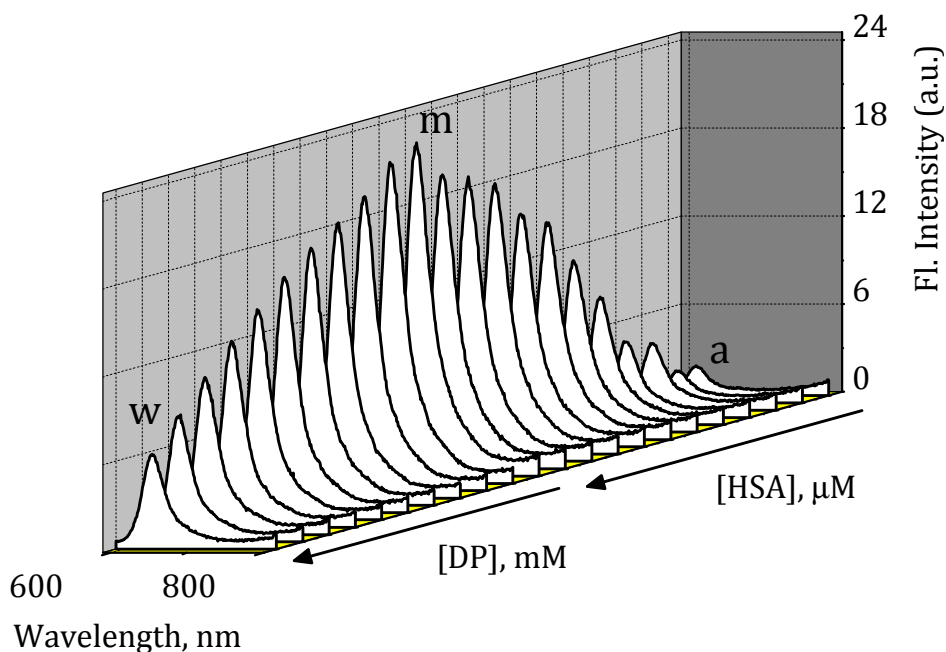


**Figure 3.3.** Effect of HSA on the fluorescence spectra of the dye **2** ( $3 \mu\text{M}$ ) and followed by the addition of dansylproline (DP) [HSA] (a)  $0.0$  and (m)  $7 \mu\text{M}$ . [DP] (m)  $0.0$ , and (w)  $0.6 \text{ mM}$ . Excitation wavelength,  $575 \text{ nm}$ .

as compared to the 60% obtained with DP. Similar experiments were carried out with the dyes **2** and **3**. Addition of DP to a solution of [2-HSA] complex resulted in the gradual decrease of fluorescence intensity, which reached saturation at  $0.6 \text{ mM}$  of DP, with an effective displacement of about 90% (Figure 3.3). Similar results were obtained with DNSA; however the effective displacement was found to be only around 10% (Figure 3.4). On the other hand, [3-HSA] complex with increasing concentration of DP exhibited an effective displacement (95%) of the dye **3**, whereas

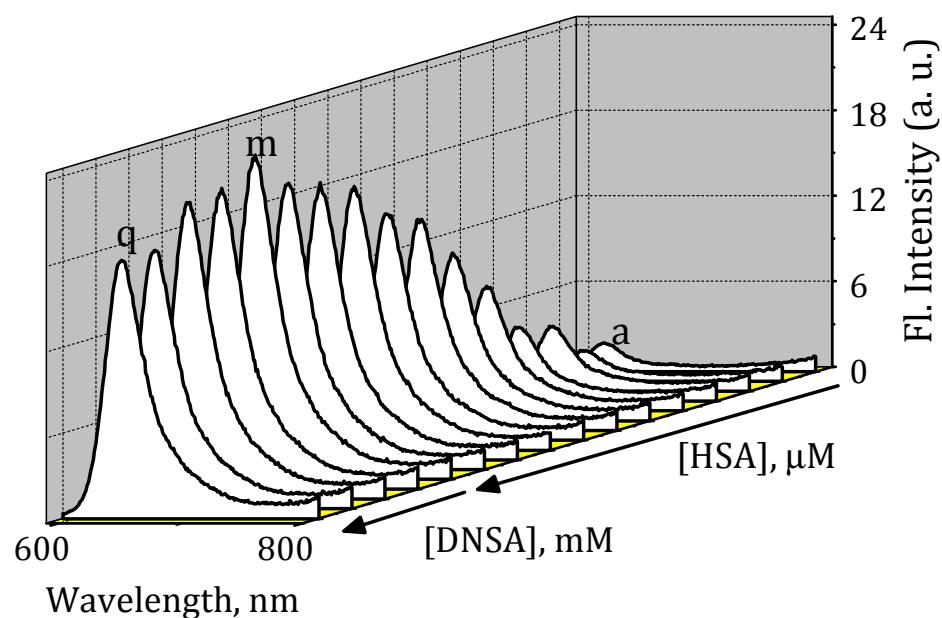


**Figure 3.4.** Effect of HSA on the fluorescence spectra of the dye **2** (3  $\mu$ M) and followed by the addition of dansylamide (DNSA). [HSA] a) 0.0 and (m) 7  $\mu$ M. [DNSA] m) 0.0, and q) 0.71 mM. Excitation wavelength, 575 nm.

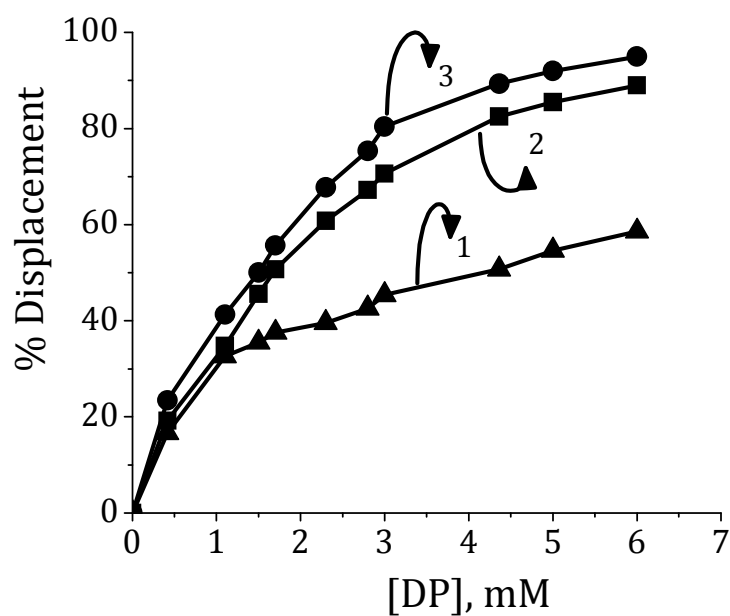


**Figure 3.5.** Relative percentage of displacement of the dyes **1**, **2** and **3** from [HSA-Dye] complexes by the addition of site II binding agent DP.

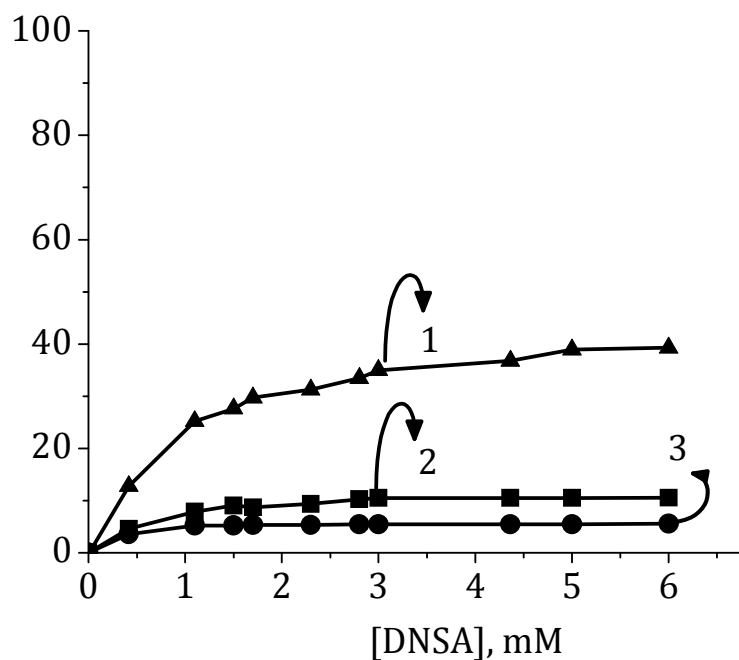


**Figure 3.6.** Relative percentage of displacement of the dyes **1**, **2** and **3** from [Dye-HSA] complexes by addition of site I binding agent DNSA.

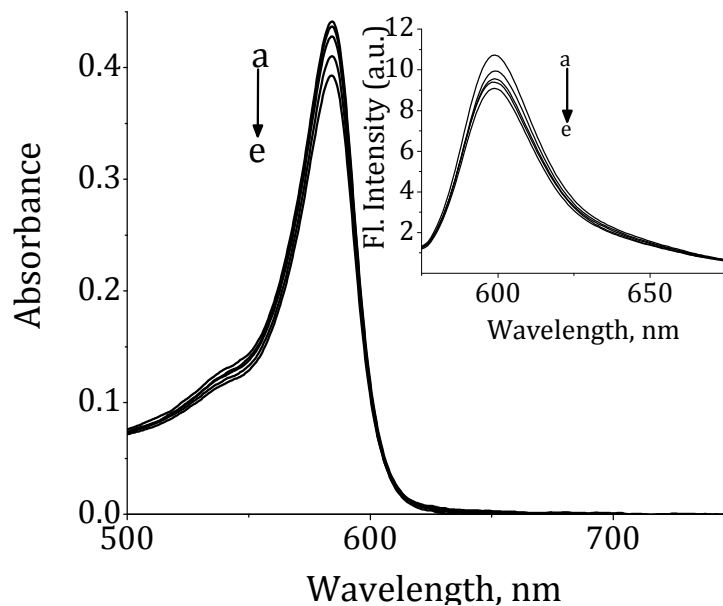


**Figure 3.7.** Effect of dansylproline (DP) on the absorption and emission (inset) spectra of the dye **1** ( $3 \mu\text{M}$ ). [DP]: (a) 0.0, (b) 0.16, (c) 0.30, (d) 0.44 and (e) 0.6 mM. Excitation wavelength, 560 nm.

DNSA showed only 5% displacement efficiency. Figures 3.5 and 3.6 shows the percentage of displacement of the various squaraine dyes **1-3** with addition of DP and DNSA to the dye-SA complex. The titrations of DP and DNSA with the dyes **1-3**

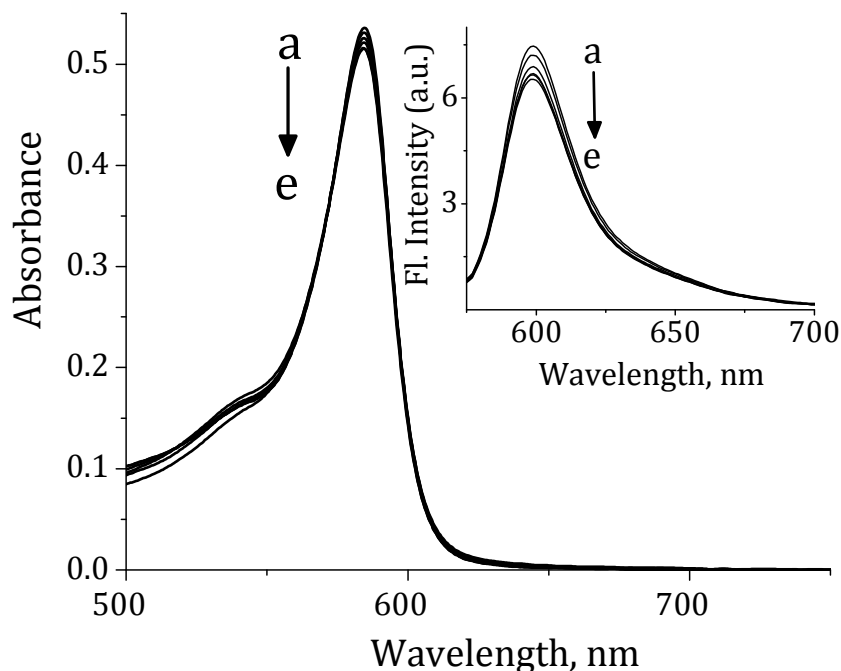


**Figure 3.8.** Effect of dansylamide (DNSA) on the absorption and emission (inset) spectra of the dye **1** ( $3.0 \mu\text{M}$ ). [DNSA]: (a) 0.0, (b) 0.22, (c) 0.43, (d) 0.62 and (e) 0.71 mM. Excitation wavelength, 560 nm.

alone, showed negligible changes in the absorption and emission properties, indicating thereby that the changes observed with the [dye-SA] complex were mainly due to the displacement of the dyes **1-3** from the complex by the competitive binding ligands such as DP and DNSA (Figures 3.7 and 3.8).

### 3.3.2. CIRCULAR DICHROISM (CD) STUDIES

Circular dichroism is a sensitive technique to monitor the conformational secondary structure, and the value at 222 nm is a signature of its helical content. HSA

contains ~68%  $\alpha$ -helix with 32% contribution from domain I, 34% from domain II, and 34% from domain III (Sugio *et al.*, 1999, Amisha Kamal *et al.*, 2004, Muller *et al.*, 1976). Any changes in the CD signal upon dye binding can be correlated to the conformational changes in the SA. The absorption and fluorescence spectra of the three dyes are nearly the same, whereas their CD spectra varied dramatically with the site of binding (Johnson 1999, Dockal *et al.*, 2000). The CD spectra, therefore, provides a clear method to distinguish between the dye binding sites.

To ascertain the possible influence of the dye binding on the secondary structures of BSA and HSA, we have performed far-UV circular dichroism studies of HSA and BSA in the absence and presence of the dyes **1-3**. The CD spectra of native SA exhibits two negative minima in the ultraviolet region at 208 and 222 nm, which are characteristic of an  $\alpha$ -helical structure of protein (Wallevik 1973, Chmelik *et al.*, 1988, Tayyab *et al.*, 1995, Muzammil *et al.*, 2000, Krishnakumar *et al.*, 2002, Flora *et al.*, 1998). Figure 3.9 shows the representative CD spectra of HSA recorded in the range 170-250 nm with increasing concentration of the squaraine dye **1**. When **1** was added to the solution of HSA, the intensity of negative Cotton effect of HSA at 208 and 222 nm decreased with increasing concentration of dye , finally a new band at 230 nm was obtained. The formation of this new band in the presence of dye **1** indicates the loss of secondary structure of the protein as a result of unfolding of HSA upon the binding of the dye. In contrast, negligible changes in the intensity of the CD bands at 208 and 222 nm were observed with the addition of the dye **2** and **3** (Figure 3.10 and 3.11). Similar observations have been made with BSA. These experiments, further

confirm that dye **1** binds within the protein at a different site as compared to the halogenated dyes **2** and **3**.

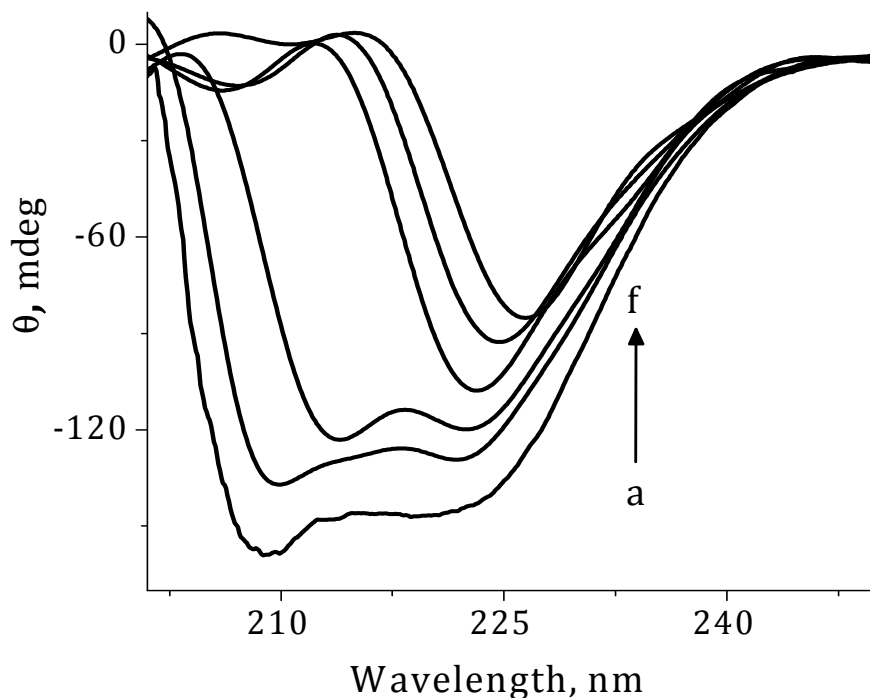


**Figure 3.9.** Circular dichroism spectrum of HSA (0.8  $\mu\text{M}$ ) in the presence of the squaraine dye **1** at 25  $^{\circ}\text{C}$ . [**1**] a) 0 and f) 78  $\mu\text{M}$ .

Further, with a view to quantify the conformation change taking place in the protein upon dye **1** binding, we have calculated the  $\alpha$ -helical content of free and dye complexed HSA at 222 nm using the equation 3.1,

$$\alpha\text{-helix (\%)} = -\{\text{MRE}_{222} - 4000/33000 - 4000\} \times 100 \quad \text{eq. 3.1}$$

where,  $\text{MRE}_{222}$  is the observed Mean Residue Ellipticity value at 222 nm defined as equation 3.2,

$$\text{MRE} = \theta_{\text{obs}}/10nlCp \quad \text{eq. 3.2}$$

where,  $\theta_{\text{obs}}$  is the CD in signal in millidegree,  $n$  is the number of amino acid residues

(585),  $l$  is the path length of the cell (1 cm), and  $C_p$  is the molar concentration of the protein. The MRE of the  $\beta$ -form and random coil conformation cross at 208 nm is 4000 and 33,000 is the MRE value of a pure  $\alpha$ -helix at 208 nm. From the equations, the  $\alpha$ -helicity in the secondary structure of HSA alone was calculated to be 58%. Interestingly, we observed a decrease in the  $\alpha$ -helical content of HSA to *ca.* 23% in the presence of dye **1**, consistent with the CD changes. The observed changes in the CD signals of HSA and BSA with increasing concentrations of the dyes **2** and **3** are consistent with the results obtained using the known site II specific binding agent DP (Figure 3.12), whereas the CD spectra of **1** in the presence of HSA and BSA are similar to that of site I binding agent DNSA with BSA and HSA (Figure 3.13). These results confirm that dyes **2** and **3** bind preferentially at site II, whereas dye **1** binds at

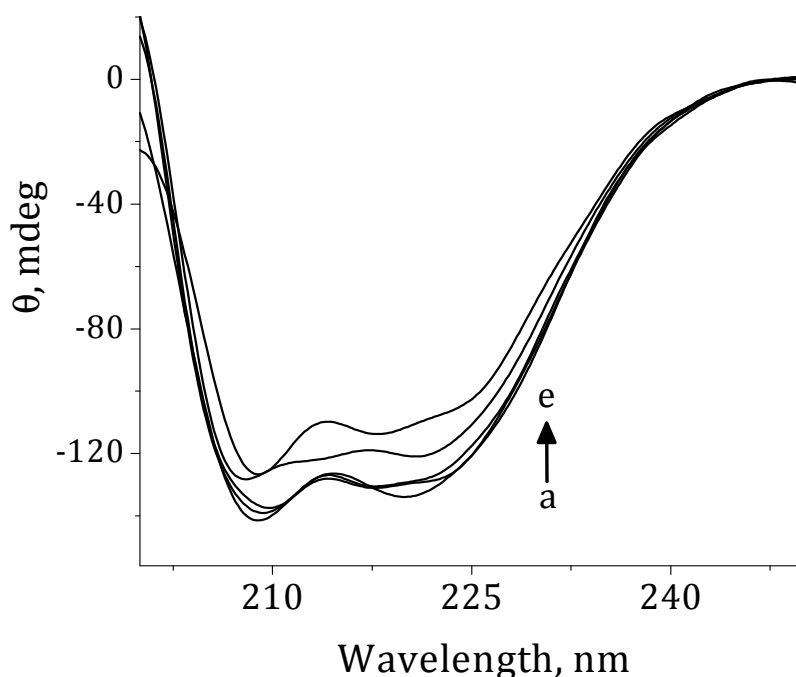


**Figure 3.10.** Circular dichroism spectra of HSA (0.8  $\mu$ M) in the presence of the squaraine dye **2** at 25  $^{\circ}$ C. [**2**] a) 0 and (e) 78  $\mu$ M.

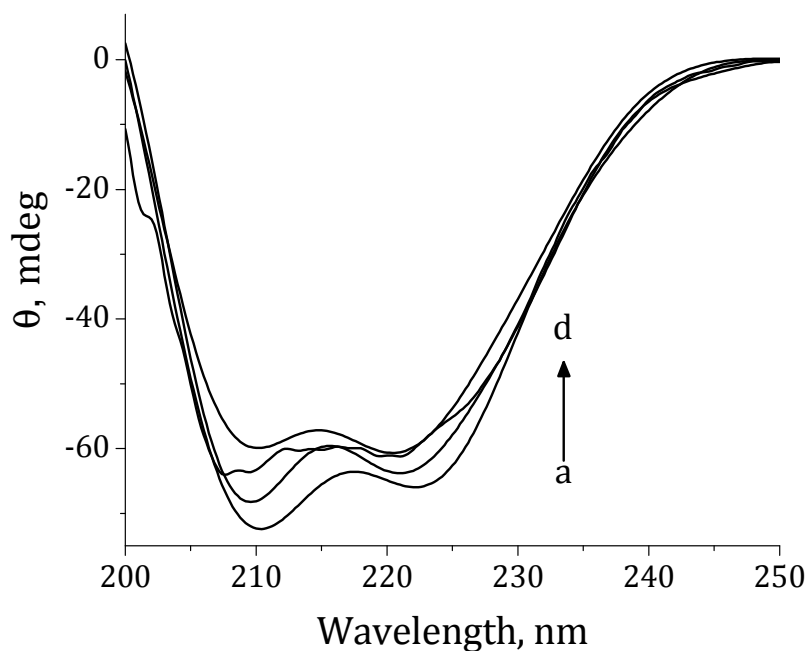


**Figure 3.11.** Circular dichroism spectra of HSA (0.65  $\mu\text{M}$ ) in the presence of the squaraine dye **3** at 25  $^{\circ}\text{C}$ . [**3**] (a) 0 and (d) 78  $\mu\text{M}$ .

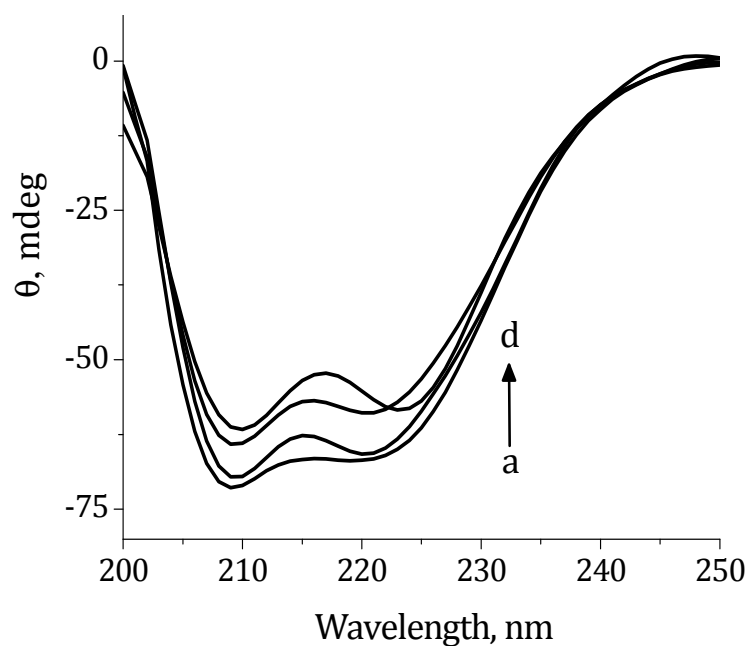


**Figure 3.12.** Changes in the circular dichroism spectrum of HSA (0.65  $\mu\text{M}$ ) with increase in addition of DP at 25  $^{\circ}\text{C}$ . [DP] (a) 0.0 and (f) 0.6 mM.

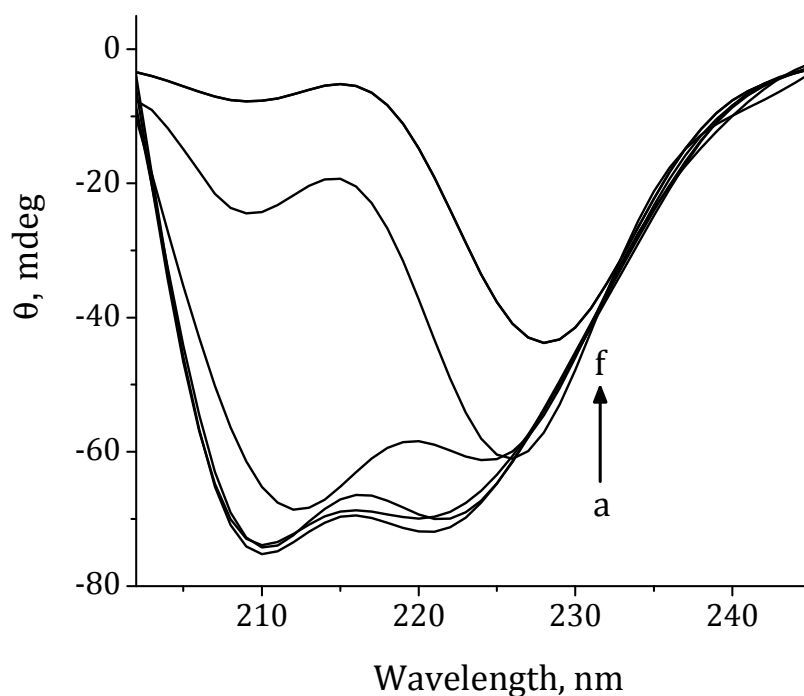


**Figure 3.13.** Changes in the circular dichroism spectrum of HSA (0.65  $\mu\text{M}$ ) with increase in addition of DNSA at 25  $^{\circ}\text{C}$ . [DNSA] (a) 0.0 and (f) 0.71mM.

the same site only with marginal selectivity. The CD spectral studies, thus, clearly indicate the intimate association of these squaraine dyes with the protein and interestingly the site-selective binding of the dyes with the serum albumins can be differentiated by their chiral environments.

### 3.3.3. FLUORESCENCE RESONANCE ENERGY TRANSFER (FRET) STUDIES

Serum albumins HSA and BSA have three fluorophore constituents, namely tryptophan, tyrosine, and phenylalanine (Sytnik *et al.*, 1996). The fluorescence of HSA can be attributed to tryptophan alone, because phenylalanine has a very low fluorescence quantum yield. The fluorescence of tyrosine is known to be quenched completely if it is present in the ionized state or near an amino group or a carboxyl

group, or a tryptophan residue. Thus, the intrinsic fluorescence of HSA is attributed mainly to the sole tryptophan residue (Trp-214) present in the hydrophobic cavity of sub-domain IIA (Sudlow I). Accordingly, if the probes bind at Sudlow site I, this may result in the fluorescence quenching of HSA. No fluorescence quenching mechanism is expected to operate if the probes bind in the hydrophobic cavity of sub-domain IIIA

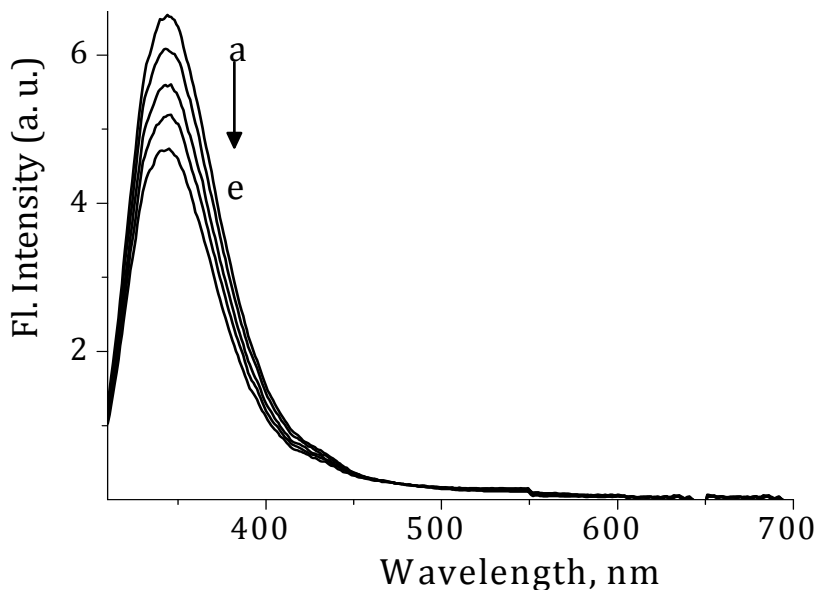


**Figure 3.14.** Emission spectra of tryptophan of HSA (14  $\mu\text{M}$ ) with increase in addition of **2. [2]**, (a) 0, and (e) 19  $\mu\text{M}$ . Excitation wavelength, 295 nm.

(Sudlow II) due to the probes' far location from Trp-214. Tryptophan can thus act as a beacon for the interaction of ligands at the site I of HSA through efficient fluorescence resonance energy transfer (Förster 1948, Sapsford *et al.*, 2006, Sytnik *et al.*, 1996).

To further confirm the site selective interactions of the dyes **1-3**, we have

carried out the excited state intermolecular fluorescence resonance energy transfer (FRET) experiments from tryptophan (donor) to the dyes **1-3** (acceptor). Addition of **2** and **3** to a solution of either HSA or BSA showed no FRET mediated emission, corresponding to the squaraine chromophore at 620 nm, indicating that no energy

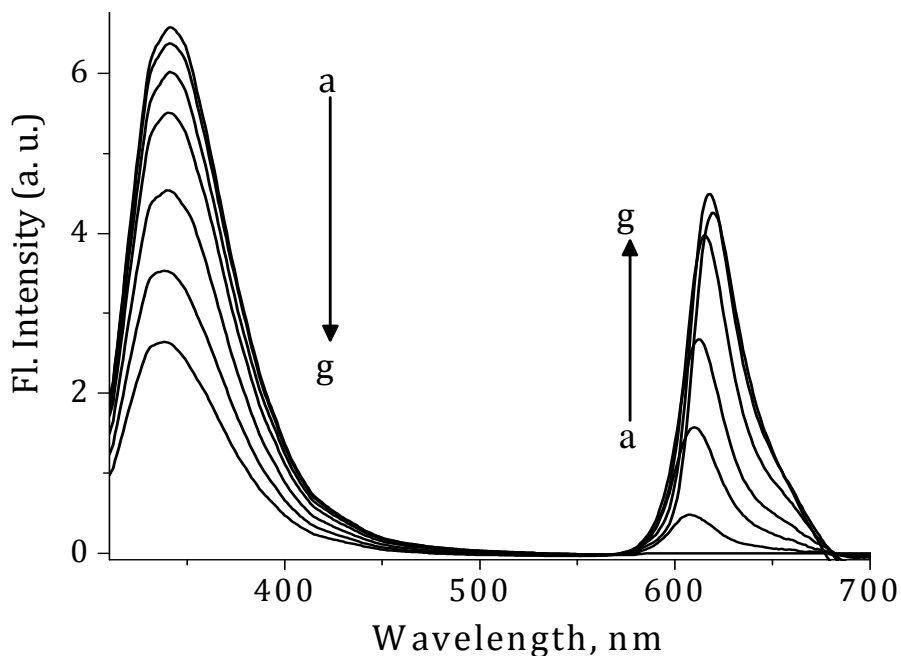
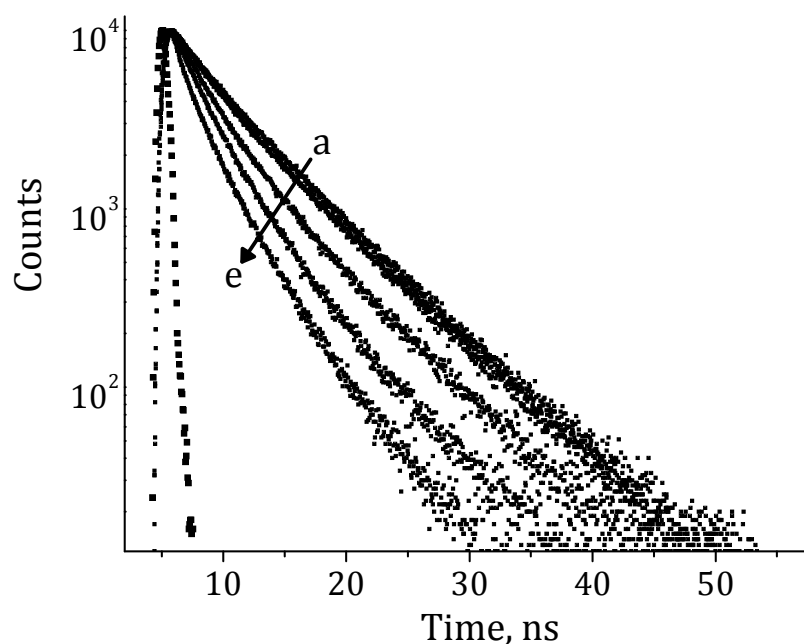


**Figure 3.15.** Emission spectra of tryptophan of HSA (14  $\mu\text{M}$ ) with increase in addition of the dye **1**. [**1**], (a) 0, and (g) 19  $\mu\text{M}$ . Excitation wavelength, 295 nm.

transfer process is involved between tryptophan in HSA and the squaraine moiety in the case of the dyes **2** and **3**. Furthermore, these results confirm that these dyes exhibit negligible binding at site I, but bind predominantly at site II of these proteins (Figure 3.14). Expectedly, the dye **1**, which showed binding distribution at both sites I and II exhibited efficient FRET mediated emission (Figure 3.15).

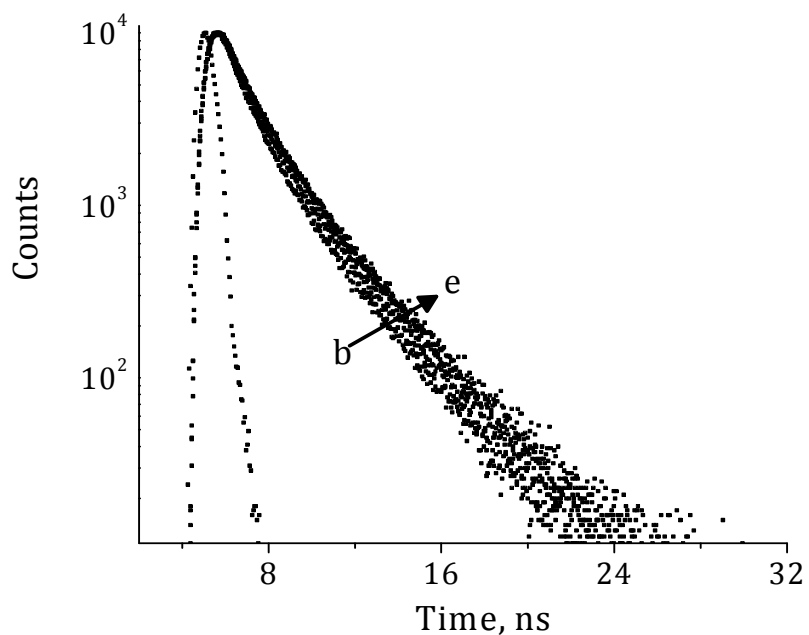
Increase in addition of the dye **1** to a solution of HSA, led to the regular quenching in emission intensity at 340 nm, corresponding to the tryptophan

chromophore, with the concomitant gradual enhancement in FRET mediated emission from the squaraine moiety at 620 nm. Based on the Förster theory (Förster 1948) of excitation energy transfer, the distance between Trp of HSA and the bound squaraine moiety was calculated and is found to be 27 Å. In the case of BSA, we observed a distance of 30 Å. The rate of energy transfer was calculated to be  $k_{\text{HSA}} = 1.19 \times 10^8 \text{ s}^{-1}$  with an efficiency of *ca.* 35% for HSA, while with BSA, relatively a lower value of rate of energy transfer ( $k_{\text{BSA}} = 7.8 \times 10^7 \text{ s}^{-1}$ ) was observed, indicating thereby



**Figure 3.16.** Time-resolved fluorescence decay of **1** (3  $\mu\text{M}$ ) with the increase in addition of HSA. [HSA] (a) 0, (b) 0.18, (c) 0.37, (d) 0.75 and (e) 7  $\mu\text{M}$ .

non-negligible structural differences at the site I of these two transport proteins. Thus, the FRET experiments clearly indicate that the dyes **2** and **3** bind at site II, whereas the dye **1** binds at site I close to Trp moiety in HSA and BSA.



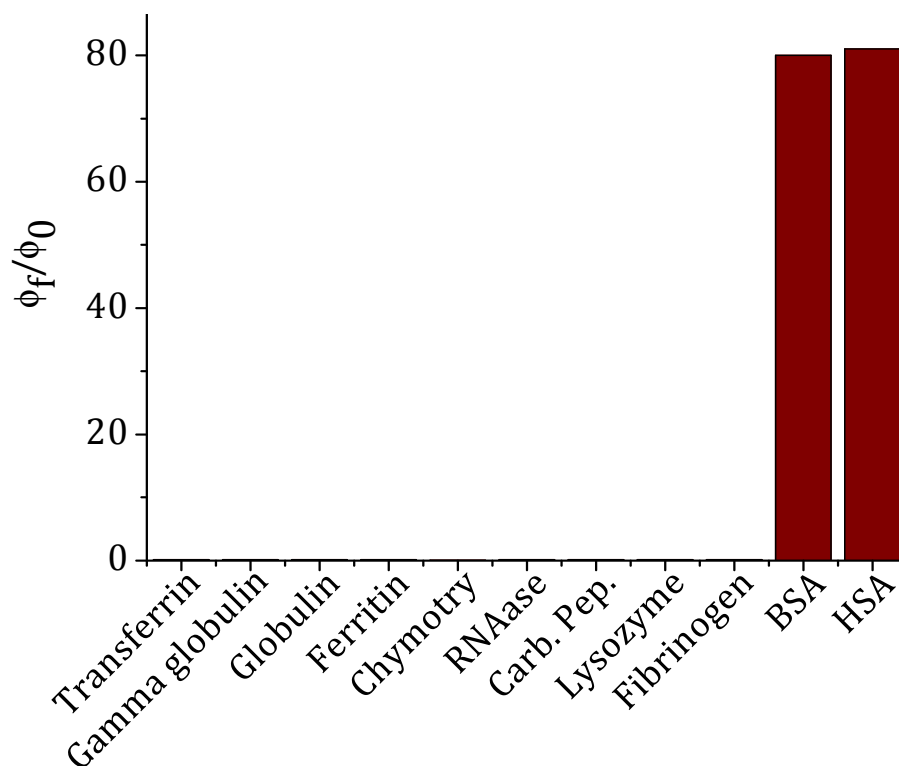
**Figure 3.17.** Time-resolved fluorescence decay of HSA ( $1.5 \times 10^{-5}$  M) with the increase in addition of the dye **1**. [**1**] (a) 0, and (e) 20  $\mu$ M. Excitation wavelength, 280 nm. Emission collected at 624 nm.

Figure 3.16 shows the changes in the lifetime decay of HSA excited at 280 nm and monitored at 335 nm with increasing addition of **1**. HSA alone exhibited a biexponential decay with a lifetime of 3.1 ns (20%) and 6.6 ns (79%), whereas a significantly reduced lifetimes of 2.1 ns (57%) and 4.8 ns (43%) was observed in presence of **1**. In addition, we observed monoexponential decay with a lifetime of 1.5 ns (Figure 3.17), when monitored at 624 nm corresponding to the squaraine moiety bound at site I of HSA under these conditions.

### 3.3.4. INTERACTION OF SQUARINE DYES WITH OTHER PROTEINS

To demonstrate the selectivity of the squaraine dyes under investigation for serum albumins, we have investigated the interactions of dyes **1-3** with other

important transport proteins like ferritin, transferrin, fibrinogen, lysozyme, carboxy peptidase A, ribonuclease A, bovine gamma globulin, gamma globulin and



**Figure 3.18.** Relative changes in the fluorescence quantum yields of the dye **1** ( $3 \mu\text{M}$ ) with increasing concentration of selected proteins ( $0-7 \mu\text{M}$ ) in 2% ethanol-phosphate buffer. Excitation wavelength, 560 nm.

chymotrypsinogen in 2% ethanol-phosphate buffer. Figure 3.18 shows the relative changes in the fluorescence intensity of the dye **1** with the addition of  $7 \mu\text{M}$  of different proteins. As evident from the figure, the addition of other proteins caused negligible changes in the fluorescence emission of the dye **1**. The selectivity of **1** towards serum albumins can be observed visually because the pink color and the fluorescence intensity of **1** remained unchanged upon the addition of these proteins, whereas in the presence of both HSA and BSA, we could observe the color change as

well as “turn on” fluorescence intensity.

### 3.3.5. DETECTION OF SERUM ALBUMINS IN GEL ELECTROPHORESIS

As the squaraine dye **1** exhibited “turn on” fluorescence intensity and visual color change in the presence of serum albumins, it was of our interest to examine its potential use in the detection of protein under SDS-PAGE electrophoresis conditions. Sodium dodecylsulfate-polyacrylamide gel electrophoresis (SDS-PAGE) is a method used for separation and analysis of proteins, and this is achieved by moving

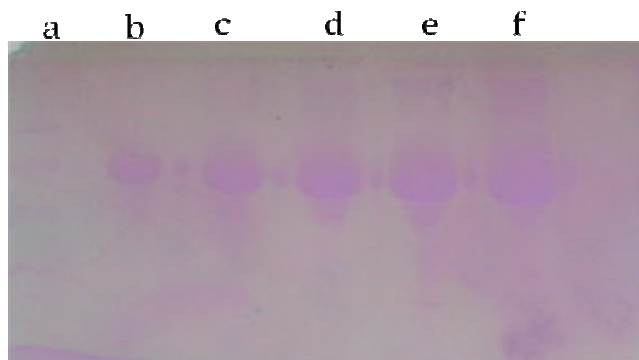


**Figure 3.19.** Recognition of BSA by the squaraine dye **1** (1 mg/20 mL) after gel electrophoresis through visual detection. Staining time is 30 min. Lanes a-f: [BSA] (a) 0.0 and (b-f) 0.05-6 µg/well.

negatively charged protein molecules through a polyacrylamide matrix using an electric field. After electrophoresis, protein can be visualized by staining with a suitable dye. The most common dye used for the protein gel electrophoresis is the Coomassie brilliant blue (CBB). Although CBB staining is an inexpensive method, it has certain disadvantages such as i) the detection limit for BSA is 64 ng per well, ii) it requires destaining and iii) is time consuming (total time required for staining is 105

min). Therefore, it was of our interest to investigate the potential application of the squaraine dye **1** as a staining agent under gel electrophoresis conditions. In this context, we have prepared different concentrations of BSA and carried out the electrophoresis on a 12% SDS-PAGE. After the electrophoresis, the gel was stained with the squaraine dye **1** (Figure 3.19) using different concentrations of proteins and the dye.

The use of the squaraine dye as the protein stain offers several advantages over the existing CBB stain; i) the primary advantage being the rapid and simple staining procedure, ii) the staining procedure of dye **1** requires only 60 min as compared to the 105 min required for CBB and iii) the staining with the dye **1** does not require a destaining step, in contrast to the CBB stain which requires longer destaining time to improve band contrast. Nevertheless, we could not observe any change in the signal intensity, when destaining was carried out with the dye **1** after 24 h. Moreover, the detection limit for this method is about two times higher than that of the CBB staining method. These results demonstrate that the method of using dye **1** is a highly sensitive and speedy staining protocol for the visual detection of proteins under gel electrophoresis conditions.

### **3.3.6. INTERACTION OF SQUARAIN DYES WITH MODIFIED PROTEIN**

Traditional cancer therapy relies on the premise that rapidly proliferating cancer cells are more likely to be killed by a cytotoxic agent than the normal cells. However, these agents have very little or no specificity, which leads to systemic

toxicity, causing undesirable side effects. Therefore, targeted drug-delivery constructs are much desired. In general, a tumor-targeting drug-delivery system consists of a cell surface recognition moiety and a drug connected directly or through a suitable linker. The conjugate itself should be systemically nontoxic, and the linker must be stable in the blood circulation. Upon internalization into the cancer cell, the conjugate should be readily cleaved to generate the active agent thereby improve the selectivity and efficacy.

A variety of receptors have been identified as markers for carcinomas. Among these is the folate receptor ( $\alpha$ -FR), and its substrate folic acid (FA) has the potential to target several types of cancer cells because of its ability to react with this high affinity, membrane-anchored protein. Moreover,  $\alpha$ -FR is over expressed by a wide variety of human tumours, including ovarian, endometrial, breast, lung, renal, and colon. Expression of  $\alpha$ -FR on tumor cell surfaces has led to the exploitation of FA as an important ligand for specific targeting by diagnostic or therapeutic cancer cell agents (Leamon *et al.*, 1992, 1994, 2004, 2001, Atkinson *et al.*, 2001, Goren *et al.*, 2000, Gosselin *et al.*, 2002, Moon *et al.*, 2003). The present study aims at the utilisation of the targeting properties of folic acid with the delivery feature of BSA to develop a targeting delivery vehicle for the squaraine dyes in the cell. In this context, it was our interest to covalently modify the BSA with folic acid and evaluate its ability to interact with various squaraine dyes for applications in PDT.

The folic acid modified BSA was synthesised by using the following procedure. Folic acid was dissolved in anhydrous dimethylsulfoxide and activated with a 5-fold

excess of 1-cyclohexyl-3-(2-morpholinoethyl)-carbodiimide p-toluenesulfonate (CMC) or 1-ethyl-3-(3 dimethylaminopropyl)-carbodiimide (EDC) for 1 h at 23 °C. The activated folate was then reacted with BSA in 0.1 M phosphate buffer (pH 8.5) using a 8:1 folate to BSA ratio. Excess folate and other reactants were then removed from conjugated protein using a Sephadex G-25 column. The concentration of folate-BSA conjugate and the molar ratio of folate to BSA were determined spectroscopically using the Bradford method. It is found that, 1-2 folic acid units are covalently linked to the BSA when EDC was used as the coupling agent, whereas, with CMC the number of folic acid units linked was around 6-7 per BSA molecule. These results are consistent with the literature reports (Turek *et al.*, Leamon and Low 1993).

To further confirm the number of folic acid units attached per BSA, we have performed Matrix-Assisted-Laser Desorption/Ionisation (MALDI) techniques. The BSA alone gave a mass of 66455 g/mol, where as the BSA-folic acid conjugate for EDC and CMC reagents gave an increased mass of 67897 and 70058 g/mol respectively. From the mass obtained, the ratio of folic acid units per BSA was calculated and was found to be 1:3 and 1:8 for the BSA modified using EDC and CMC, respectively. A third method for estimating the difference in conjugations of folic acid to BSA was done by monitoring the BSA conjugates bands on SDS-PAGE and comparing that to pure BSA. The band observed in the SDS-PAGE for EDC-conjugate is approximately the same extent as pure BSA and forms a clear, single band where as the CMC conjugate gave a higher mass band in the gel. These studies indicate that folic acid is covalently linked

to BSA using different coupling agents will result in the formation of BSA-folic acid conjugates in different ratios.

To investigate the utility of the BSA-folic acid conjugate as a delivery system for the squaraine dyes, we have studied the interaction of these dyes in the absence

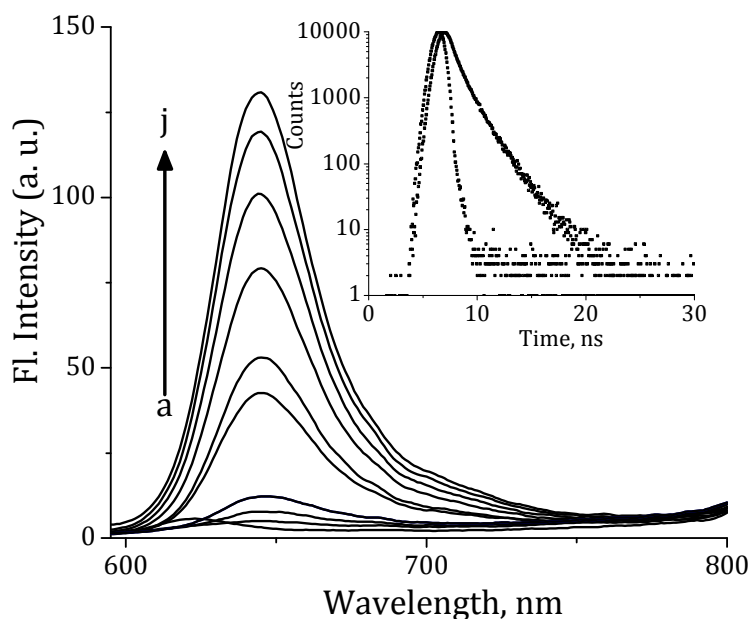


**Figure 3.20.** Fluorescence intensity changes of the dye **2** ( $3.0 \mu\text{M}$ ) with increasing addition of modified BSA-folic acid in 2% ethanol-phosphate buffer (pH=6.8). [Modified BSA] (a) 0 and (m)  $7 \mu\text{M}$ . Excitation wavelength, 575 nm. Inset shows the time-resolved fluorescence decay profiles of **2** ( $3 \mu\text{M}$ ) with the addition of modified BSA( $7 \mu\text{M}$ ).

and presence of modified BSA. The addition of modified BSA showed similar observations in the absorption and fluorescence spectra of the squaraine dyes **1-3** as in the case of BSA and HSA alone. The dye **2** alone in 2% ethanol-buffer showed an emission maximum at 623 nm. Upon the addition of the modified BSA with folic acid, a gradual enhancement in fluorescence intensity, with a bathochromic shift in

emission maxima from 623 to 637 nm was observed. The changes in the fluorescence spectra of the dye **2** with increasing concentration of modified BSA shown in Figure 3.20. The gradual enhancement in fluorescence intensity resulted in a bathochromic shift of 14 nm in the emission maximum. Inset of Figure 3.20 shows the time-resolved decay curve of the dye **2** in the presence of the modified protein. The dye **2**, which showed very low fluorescence lifetime ( $< 50$  ps) in the absence of protein, exhibited biexponential decay with enhanced lifetimes when bound to the modified BSA. Similar observations have been made with the dyes **1** and **3** with the addition of the modified BSA. The results obtained from the absorption fluorescence emission and lifetime studies are consistent essentially with the results obtained with pure BSA. These observations indicate that upon conjugation of the protein with folic acid has negligible influence on the binding ability of the protein with the squaraine dyes.

### **3.4. DISCUSSION**

The squaraine dyes **1**, **2** and **3** under investigation are quite soluble in buffer and interact efficiently with serum albumins and with high selectivity at site II. The quantitative displacement studies shows that dyes **1**, **2** and **3** are displaced from the [dye-serum albumin] complex by DP, a site II binding agent in the order *ca.* 60, 90 and 95% respectively, whereas with DNSA, site I agent, we observed *ca.* 40 10 and 5% displacement of the dyes. The CD studies of BSA and HSA in the presence of the dyes and site specific binding agents further confirm the site selective binding of these dyes. The observed significant changes in the CD signal in the case of the

unsubstituted squaraine dye **1** could be attributed to the conformational clipping of neighbouring domains by **1** and DNSA present at site I, whereas the marginal changes in CD signal observed for the heavy atom substituted dyes **2**, **3**, and DP indicate the absence of such interactions at site II. These results confirm that dyes **2** and **3** bind preferentially at site II, whereas dye **1** binds at site II only with marginal selectivity.

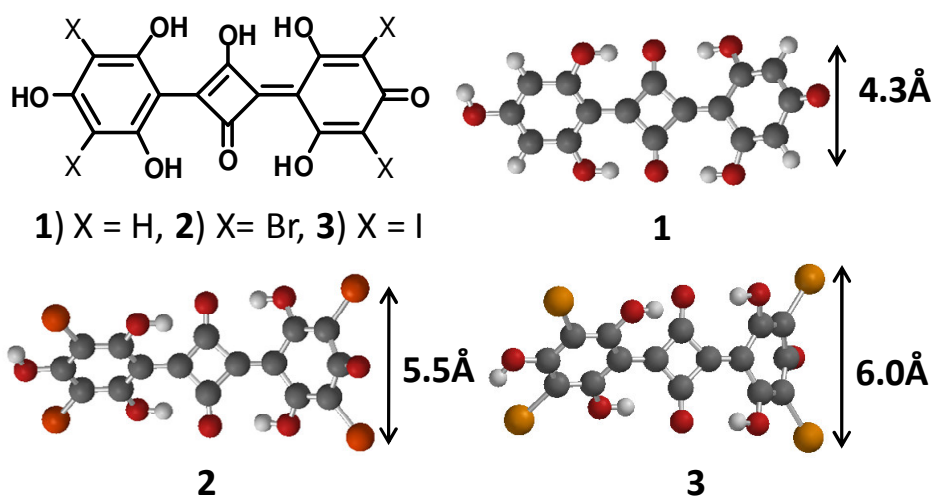


**Figure 3.21.** Structural models indicating the variation in size of the squaraine dyes **1**, **2** and **3**.

The site of binding was further confirmed by FRET experiments. The binding of unsubstituted squaraine dye **1** with serum albumin resulted in the reduction in the fluorescence intensity and lifetime of the Trp-214 residue present in native HSA and BSA, located in the same sub-domain IIA of the protein. Interestingly, an efficient energy transfer from Trp-214 to the squaraine dye was observed when the dye binds at the same site. The distance between the Trp-214 and squaraine dye was calculated using Förster theory agrees well with the reported site I binding agent, such as

dansylamine. Negligible FRET mediated emission was observed in the case of the dyes **2** and **3**, whereas, the efficient FRET mediated emission from the dye **1** showed binding at both sites I and II of the serum albumins. Further, in contrast to the significant spectral changes observed with BSA and HSA, negligible changes were noted in the absorption and emission properties when these dyes were titrated with other relevant proteins. This clearly indicates that these dyes undergo very selective interactions only with serum albumins, HSA and BSA.

The unusual selectivity of the dyes **2** and **3** for site II of the serum albumins can be attributed to the steric factors due to the presence of heavier halogen atoms. This is because of the fact that we observed the substituent size dependent site selectivity in binding of these dyes. The dye **1** having hydrogen atoms and the molecular dimensions of 4.3 Å (Figure 3.21) showed binding at both the sites with a marginal selectivity for site II. In contrast, the dye **2** with bromine atoms and having dimensions of 5.5 Å exhibited ca. 90% selectivity for site II as against 10% at site I. Expectedly, on the basis of higher molecular dimensions of 6.0 Å, the iodo derivative **3**, exhibited binding of ca. 95% at site II of both HSA and BSA. The investigation of interactions of various squaraine dyes with the modified BSA-folic acid conjugate indicate that the presence of folic acid in the serum albumins has negligible influence their efficacy of binding with the protein. These results demonstrate that such modified protein can be exploited as an effective target delivery system for the squaraine dyes thereby to enhance their photodynamic efficacy.

### **3.5. CONCLUSIONS**

In conclusion, we have demonstrated for the first time that steric effects of the substituent play a predominant role in binding of the squaraine dyes with the serum albumins. Interestingly, these dyes with increase in the molecular size exhibited selectivity in binding at site II of the transport proteins involving synergistic effects of hydrophobic, hydrogen bonding and electrostatic interactions. The fluorescence displacement assay and CD studies using the site specific binding agents confirm that the squaraine dyes substituted with heavy atoms show high selectivity towards site II, whereas the unsubstituted squaraine dye binds at site I of the protein. Interestingly, the binding of the dye at the site I results in an efficient energy transfer from Trp-214 to the squaraine dye. The distance between the Trp-214 and squaraine dye calculated using Forster theory agrees well with the reported site I binding agents. The results obtained demonstrate that the squaraine dyes interact with BSA, HSA and modified BSA-folic acid conjugate very efficiently as compared to other proteins and can act as probes for the serum albumins in buffer and under gel electrophoresis conditions.

### **3.6. EXPERIMENTAL SECTION**

#### **3.6.1. GENERAL TECHNIQUES**

The electronic absorption spectra were recorded on a Shimadzu UV-VIS-NIR spectrophotometer. Fluorescence spectra were recorded on a SPEX-Fluorolog F112X spectrofluorimeter. Fluorescence lifetimes were measured using an IBH Picosecond

single photon counting system. The fluorescence decay profiles were deconvoluted using IBH data station software V2.1, fitted with exponential decay and minimizing the  $\chi^2$  values of the fit to  $1 \pm 0.1$ . CD spectra were recorded on Jasco Corporation, J-810 spectropolarimeter.

### 3.6.2. MATERIALS AND METHODS

HSA, BSA, dansylamide were purchased from Sigma, dansylproline from Fluka and used as received. The squaraine dyes **1-3** were dissolved in 2% ethanol-phosphate buffer mixture. For the titration studies, increasing concentration of protein solution in phosphate buffer was added to solution of 3  $\mu$ M of the dyes **1-3**. Solvents used were purified before use. Double distilled water was used in all the studies.

#### 3.6.2.1. Determination of distance between the energy donor and acceptor

The distance between the donor (tryptophan) and acceptor (SQ) pair was determined utilizing the Förster theory of excitation energy transfer. According to this theory, the rate of energy transfer from the excited state donor to the unexcited acceptor is given by the following equation 3.3,

$$k_{ET} = \frac{8.8 \times 10^{-25} F_D \kappa^2 J_{AD}}{n^4 \tau_D R^6} \quad (\text{eq. 3.3})$$

where  $\tau_D$  is the donor fluorescence lifetime,  $\Phi_D$  is the donor quantum yield,  $n$  is the refractive index of the medium between the donor and the acceptor,  $\kappa$  is the dipole –

dipole orientation factor,  $R$  is the distance between the donor and the acceptor, and  $J_{AD}$  is the overlap integral between the donor fluorescence spectra and the acceptor absorbance spectrum, calculated by the equation 3.4,

$$J_{AD} = \int_0^{\infty} F_D(\lambda) \epsilon_A(\lambda) \lambda^4 d\lambda \quad (\text{eq. 3.4})$$

The distance  $R_0$  at which rate of energy transfer is equal to the sum of the rates of all other deexcitation modes of the donor is called the Förster radius obtained by the equation 3.5,

$$R_0 = 0.211 [ F_D k^2 n^{-4} J_{AD} ]^{1/6} \quad (\text{eq. 3.5})$$

In the present work, corrected absorption and fluorescence spectra were employed to calculate  $J_{AD}$  and the integration was performed between 377-587 nm. The efficiency of energy transfer ( $E$ ) was calculated using the equation 3.6,

$$E = \frac{\epsilon_A \lambda_D^{ex}}{\epsilon_D \lambda_D^{ex}} \left[ \frac{F_{AD} \lambda_D^{em}}{F_A \lambda_D^{em}} - 1 \right] \frac{1}{f_D} \quad (\text{eq. 3.6})$$

**NOVEL NAPHTHALIMIDE-DANSYL DYADS AND STUDY OF THEIR INTERACTIONS WITH MONO AND DIVALENT METAL IONS**

---

**4.1. ABSTRACT**

With the objective of understanding the ability of donor acceptor systems to function as bidentate ligands, we have synthesized two dyads, having naphthalimide chromophore as the energy donor and dansyl moiety as the energy acceptor and investigated the interactions with various metal ions through various photophysical, and  $^1\text{H}$  NMR techniques. The absorption spectra of these dyads in various solvents showed peaks corresponding to the individual naphthalimide and dansyl moieties in the near-UV region (300-400 nm), indicating that negligible interactions exist between these chromophores in the ground state. The fluorescence spectra exhibited emission in the visible region with two emission maxima at 376 and 525 nm. The emission at 376 nm corresponds to the naphthalimide moiety, while the emission observed at 525 nm is due to the intramolecular energy transfer (ET) process from the naphthalimide moiety, to the dansyl unit. When titrated with various metal ions, these systems exhibited unusual selectivity for  $\text{Cu}^{2+}$  ions as compared to  $\text{Na}^+$ ,  $\text{Li}^+$ ,  $\text{K}^+$ ,  $\text{Zn}^{2+}$ ,  $\text{Pb}^{2+}$ ,  $\text{Hg}^{2+}$ ,  $\text{Co}^{2+}$ ,  $\text{Fe}^{2+}$ ,  $\text{Cd}^{2+}$ ,  $\text{Mg}^{2+}$  and  $\text{Ba}^{2+}$  ions and signaled the binding event through inhibition of FRET mediated emission at 525 nm, with the concomitant enhancement in the emission intensity of the naphthalimide chromophore at 375 nm. Benesi-Hildebrand analysis of the fluorescence data along with the Job's plot gave a

2:1 stoichiometry for the complex between the dyads and Cu<sup>2+</sup> ions with the association constants in the range 2 - 2.6 x 10<sup>5</sup> M<sup>-1</sup>. The complex formation between the dyads and Cu<sup>2+</sup> ions was further confirmed through MALDI-TOF mass spectral analysis and NMR techniques. The uniqueness of these dyads is that they form stable 2:1 stoichiometric complexes involving the sulphonamide functionality and act as visual fluorescence ratiometric probes for the selective recognition of Cu<sup>2+</sup> ions.

## 4. 2. INTRODUCTION

Optical systems for the sensing and reporting of chemical species are currently of significant importance in chemical, biological and environmental sciences (Ludwig *et al.*, 2002, Ros-Lis *et al.*, 2008, Gokel *et al.*, 2004, de Silva *et al.*, 1997, Desvergne *et al.*, 1997). Of particular interest is the development of specific probes for the detection of transition or heavy metal ions because they play important roles in living systems and have an extremely toxic impact on the environment (Montvydiene *et al.*, 2004, Hylander *et al.*, 2006). Of all metal ions, design of probes for Cu<sup>2+</sup> ions has received considerable attention due to their importance in several biological processes (Kramer *et al.*, 1998, Linder *et al.*, 1996). At higher concentrations, Cu<sup>2+</sup> ions can be highly toxic to the organisms, since they can displace other metal ions that act as cofactors in enzyme-catalyzed reactions (Koval *et al.*, 2006). Also, the unregulated Cu<sup>2+</sup> ions can cause oxidative stress and their concentration in neuronal cytoplasm may contribute to the etiology of Alzheimer's or Parkinson's disease (Barnham *et al.*, 2004, Brown *et al.*, 2004, Millhauser *et al.*, 2004, Gaggelli *et al.*, 2006,

Deraeve *et al.*, 2008, Lee *et al.*, 2008). In this context, the design of functional molecules that selectively bind to  $\text{Cu}^{2+}$  ions and signals the event through sensitive and easily detectable outputs is highly important (Kukrer *et al.*, 1999, Fabbrizzi *et al.*, 1995, Kim *et al.*, 2008, Martinez *et al.*, 2006, Qi *et al.*, 2006, Li *et al.*, 2006, Choi *et al.*, 2006, Silveira *et al.*, 2008). Of the various techniques, the optoelectronic detection has several advantages and the fluorescence based techniques, in particular, offer high sensitivity (Neelakandan *et al.*, 2008, Xu *et al.*, 2005, Neelakandan *et al.*, 2006, Jisha *et al.*, 2006, Ros-Lis *et al.*, 2004, 2005, Constable *et al.*, 1994, Arun *et al.*, 2005, Kuruvilla *et al.*, 2008).

Recently, the development of fluorescence ratiometric probes for metal ions has attracted much attention since they allow the measurement of emission intensities at two different wavelengths (Zhang *et al.*, 2008, Mello *et al.*, 2001, Takakusa *et al.*, 2003, Coskun *et al.*, 2005, Lin *et al.*, 2008, Xu *et al.*, 2005). This method provides a built-in correction for environmental effects (i.e., artifacts as a result of probe concentration variations) as well as increases the dynamic range of emission measurements (Lou *et al.*, 1997, Reise Sousa *et al.*, 1998, Nohta *et al.*, 2000, Okamoto *et al.*, 2004). Since the sensitivity and dynamic range of a ratiometric probe are controlled by the ratio of emission intensities, the design of probes that selectively interact with metal ions and show high ratiometric signals has been challenging. In particular, the design of sensors that give fluorescence enhancement upon  $\text{Cu}^{2+}$  binding is an intriguing challenge since  $\text{Cu}^{2+}$ , due to its inherent paramagnetic nature and hence the complexation generally results in quenching of

the fluorescence intensity of the probe (Varnes *et al.*, 1972, Kemlo *et al.*, 1977, Torrado *et al.*, 1998, Li *et al.*, 2008, Wen *et al.*, 2006). Among various probes for Cu<sup>2+</sup> ions, very few examples are available wherein probes undergoing enhancement in the fluorescent intensity upon complexation with Cu<sup>2+</sup> ions (Ghosh *et al.*, 1996, Yang *et al.*, 2001, Xie *et al.*, 2007, Park *et al.*, 2007). The low sensitivity and the high order of interference by chemically closely related metal ions have thus necessitated the design of highly selective probes for Cu<sup>2+</sup> ions (Li *et al.*, 2007, Zheng *et al.*, 2002, Wen *et al.*, 2006, Grandini *et al.*, 1999). In this context, the development of probes showing fluorescence enhancement in binding to Cu<sup>2+</sup> ions is challenging.

Photoinduced intramolecular energy transfer (ET) between a donor and an acceptor linked through suitable spacer groups is well studied and has been employed effectively in molecular and supramolecular photophysics, biology and molecular devices (Valeur *et al.*, 1992). Systems of particular interest are bichromophoric molecules consisting of a donor able to transfer its excitation energy to an acceptor linked to it by a spacer (Speiser *et al.*, 1996). According to Förster's theory, in a donor-acceptor pair, the energy transfer between the donor and acceptor takes place only when they are at a critical distance and the efficiency of energy transfer depends on distance between the two units (Förster 1948, Lakowicz 2000). Normally, when a bichromophoric system linked through a flexible spacer containing heteroatom binds with metal ions, the distance between the donor and acceptor is altered resulting in changes in the ET process (Abad *et al.*, 2005). The changes in the fluorescence intensity associated with this process have been used successfully as the

signaling event for the detection of various metal ions (Choi *et al.*, 2001).

In this context, it was of our interest to develop novel donor-acceptor based systems as probes for Cu<sup>2+</sup> ions. We have synthesized two dyads **1a** and **1b** and the

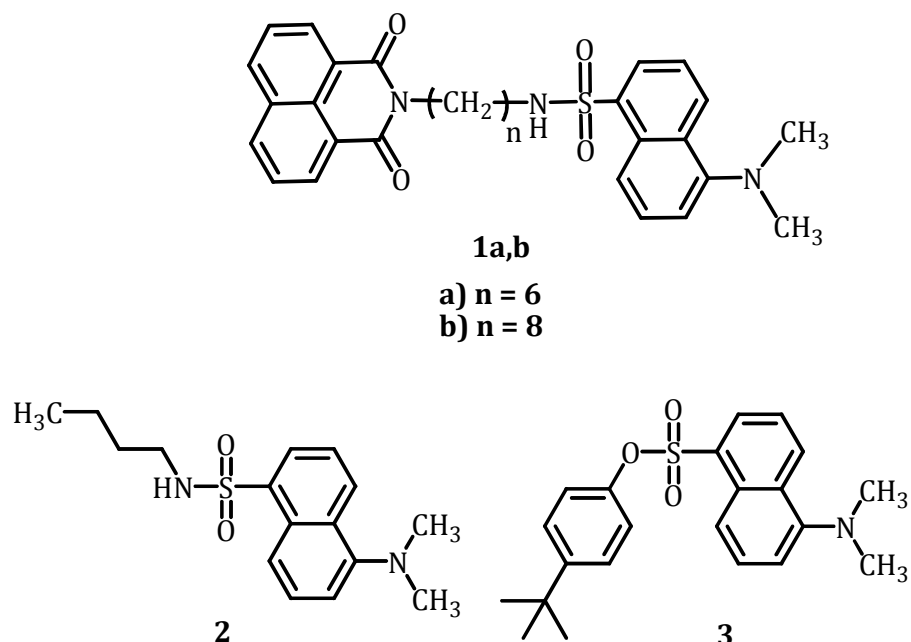


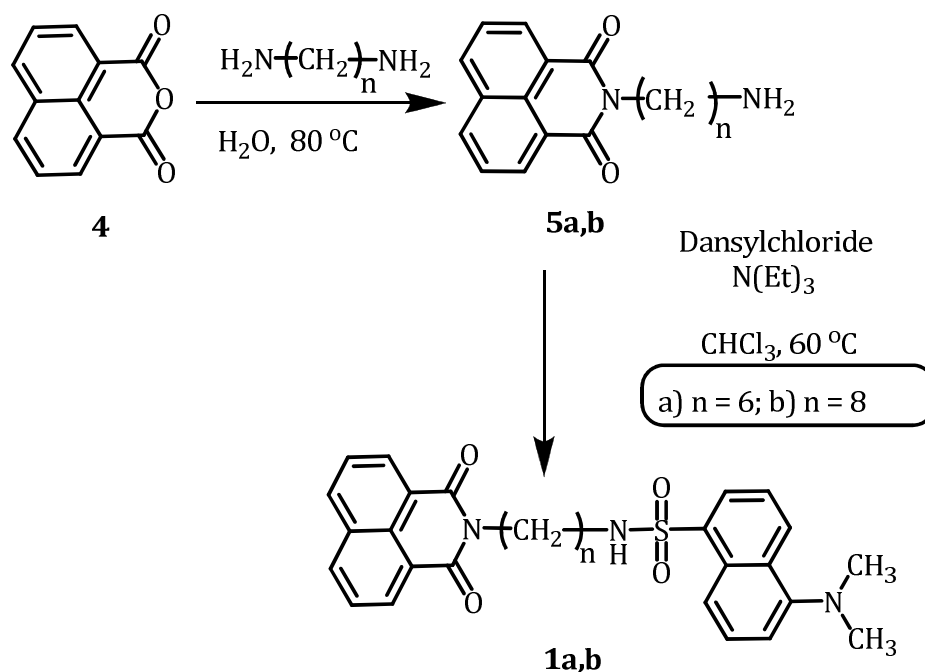
**Chart 4.1**

model compounds **2** and **3** for comparison (Chart 4.1) and have investigated their interactions with various metal ions under different conditions through different photophysical techniques. We designed these dyads because of the fact that their individual units have been investigated as chemosensors (Montalti *et al.*, 2002, Vicinelli *et al.*, 2002, Jiang *et al.*, 2002, Corradini *et al.*, 1997) and fluorescent labels (Daffy *et al.*, 1998, Gunnlaugsson *et al.*, 2003, Zhong *et al.*, 2000) and can, in principle, undergo intramolecular fluorescence resonance energy transfer (FRET) and photoinduced electron transfer (PET) reactions (Abad *et al.*, 2005, Lee *et al.*, 2008, Battistuzzi *et al.*, 1985). Our results demonstrate that these dyads can interact

selectively with Cu<sup>2+</sup> ions as compared to other metal ions and signals the binding event through inhibition of FRET mediated emission, thereby indicating their potential use as sensitive fluorescence ratiometric probes for the selective recognition of Cu<sup>2+</sup> ions.

## 4.3. RESULTS

### 4.3.1. SYNTHESIS OF THE DYADS



**Scheme 4.1**

Synthesis of the chimeric dyads **1a** and **1b** has been achieved in good yields (60-65%) by the reaction of the corresponding  $N$ - $\omega$ -alkylnaphthalimide with dansylchloride (Scheme 4.1), whereas the model compounds **2** (90%) and **3** (50%) were synthesized as per the reported procedure (Ceroni *et al.*, 2002, Pandey *et al.*,

2009) by the reaction of dansyl chloride with butyl amine and *p-tert*-butylphenol, respectively. These products were purified through recrystallization and were characterized on the basis of spectral data and analytical results.

For example, the  $^1\text{H}$  NMR spectrum of the dyad **1a** in  $\text{CD}_3\text{CN}$ , showed the -NH protons as a triplet at  $\delta$  5.70 ppm, while the methylene protons appeared as a quartet and multiplet, respectively at  $\delta$  1.10-3.93 ppm. The protons of the  $-\text{N}(\text{CH}_3)_2$  group appeared as a singlet at  $\delta$  2.80 ppm, whereas the twelve aromatic protons appeared in the range  $\delta$  7.20-8.51 ppm. The  $^{13}\text{C}$  NMR spectrum of the dyad **1a** on the other hand consisted of signals at  $\delta$  25.30- 42.40, corresponding to  $\text{sp}^3$  carbons while the  $\text{N}-\text{CH}_3$  carbon at 44.3 ppm the aromatic carbons appeared between  $\delta$  114.80-151.70,

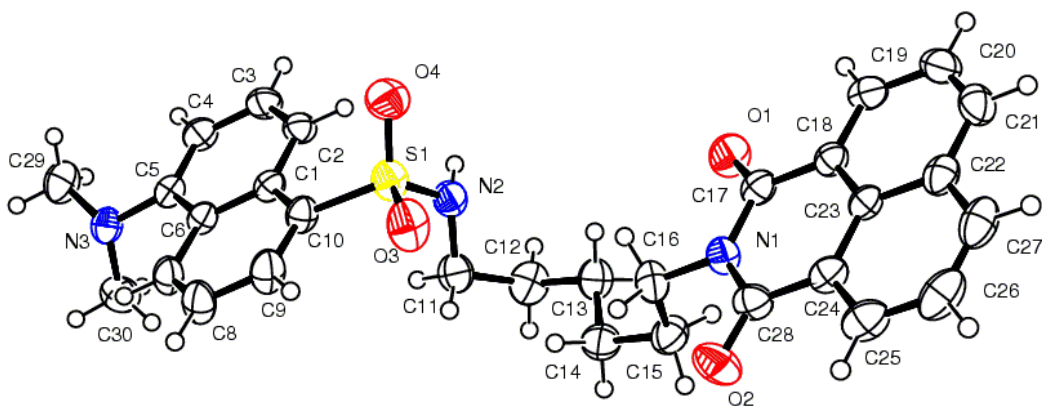


**Figure 4.1.** ORTEP diagram of the dyad **1a**. The thermal ellipsoids are drawn at 50 % probability.

and the carbonyl carbon at  $\delta$  163.60 ppm. Furthermore, the final confirmation of the structures was obtained through single crystal X-ray analysis of the representative example **1a**. Figure 4.1 shows the ORTEP diagram of the dyad **1a** and Table 4.1 summarizes its crystallographic data. The crystal structure shows a distance of 11.6

Å between the naphthalimide and dansyl chromophores, which is well below the critical distance required for an effective energy transfer between the donor and acceptor.

**Table 4.1.** Summary of crystallographic data for the dyad **1a**.

Parameters	<b>1a</b>
Empirical formula	C <sub>30</sub> H <sub>31</sub> N <sub>3</sub> O <sub>4</sub> S
Formula weight	529.64
<i>T</i> , K	293 (2)
$\lambda$ , Å	0.71069
Crystal system	Monoclinic
Space group	P21/c
<i>a</i> , Å	9.175(5)
<i>b</i> , Å	18.652(5)
<i>c</i> , Å	15.823(5)
$\alpha$ , deg	90.00(5)
$\beta$ , deg	100.355(5)
$\gamma$ , deg	90(5)
<i>V</i> , Å <sup>3</sup>	0.163
<i>Z</i>	4
<i>d</i> <sub>calc</sub> , mg/m <sup>3</sup>	1.321
F (000)	1120
Crystal size, mm	0.20 × 0.18 × 0.16
$\mu$ (MoK $\alpha$ ), mm <sup>-1</sup>	0.163

Theta range for data collection, °	1.70 to 28.10
Limiting indices	-12 ≤ h ≤ 11, -24 ≤ k ≤ 24, -20 ≤ l ≤ 20
Reflections collected/ unique	30019/ 6458
Refinement method	Full-matrix least-squares on $F^2$
Data/ restraints/ parameters	6458/ 0/ 349
Goodness-of-fit on $F^2$	1.045
Final R indices [ $I > 2\sigma(I)$ ]	R1 = 0.0415, wR2 = 0.1099
R indices (all data)	R1 = 0.0694, wR2 = 0.1329

---

#### 4.3.2. ABSORPTION AND FLUORESCENCE PROPERTIES

The absorption properties of the dyads have been investigated in various polar and non-polar solvents. Figure 4.2 shows the absorption spectra of the dyads **1a** and **1b** in acetonitrile. These dyads showed absorption maximum at 332 nm with a shoulder at 339 nm. Similar observations have been made in other solvents like methanol, ethanol and toluene. In all these solvents, the absorption spectrum of these dyads is found to be the sum of the individual units; indicating thereby that no significant interaction exist between the naphthalimide and dansyl chromophores in the ground state (Figure 4.3). Inset of Figure 4.2 shows the emission spectra of the dyads **1a** and **1b**. The fluorescence spectra of these dyads exhibited two emission maxima at 375 and 525 nm, when excited at 339 nm, where most of the photons are absorbed by naphthalimide chromophore. Based on the excitation spectral analysis

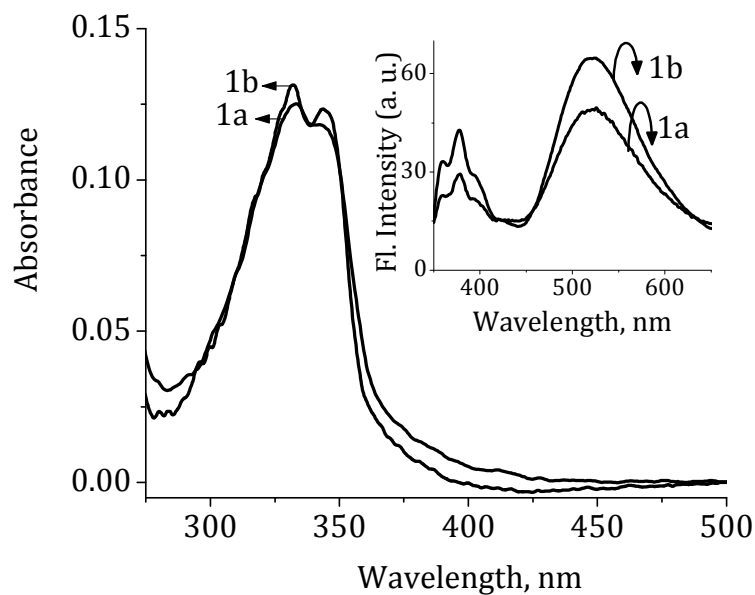


**Figure 4.2.** Absorption and fluorescence emission (inset) spectra of the dyads **1a** and **1b** (3  $\mu$ M each) in acetonitrile. Excitation wavelength, 339 nm.

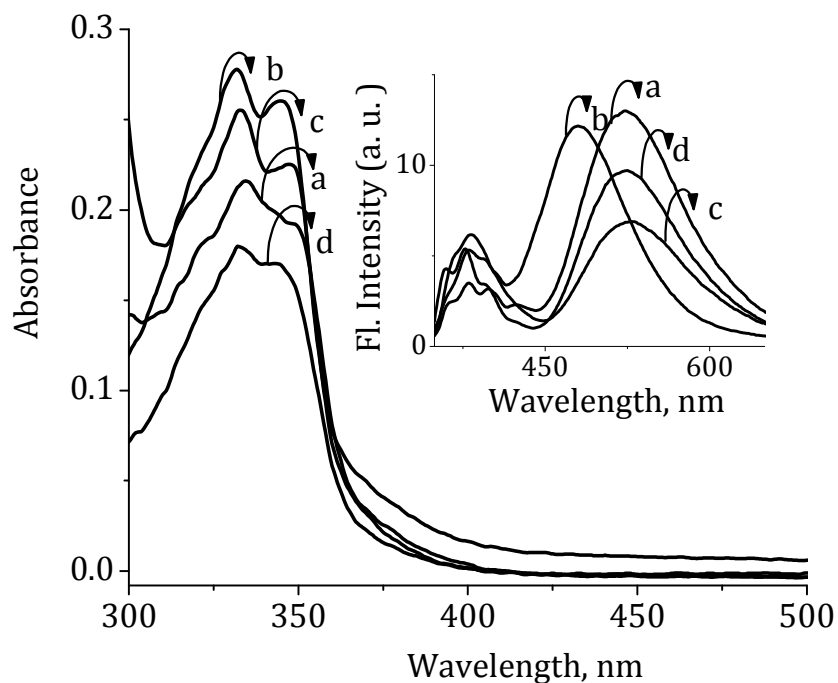


**Figure 4.3.** Absorption and fluorescence spectra (inset) of the dyad **1b** (3  $\mu$ M) in (a) acetonitrile, (b) toluene, (c) methanol and (d) ethanol. Excitation wavelength, 339 nm.

and literature reports, the bands at 375 and 525 nm, respectively, could be assigned to the locally excited state of the naphthalimide chromophore and fluorescence resonance energy transfer (FRET) mediated emission from the dansyl moiety. When compared to the dansyl based model compound **2**, the fluorescence intensity of the dyads **1a** and **1b** is significantly quenched. This is because of the fact that the emission observed at 525 nm in the case of these dyads is due to the existence of FRET from the excited state of the naphthalimide chromophore to the dansyl unit and the photoinduced electron transfer (PET) reaction from the dansyl chromophore to the naphthalimide moiety. The dyad **1b** with longer spacer length, *ie*, octamethylene unit, showed efficient FRET mediated emission with a fluorescence intensity ratio  $I_{525}/I_{375}$  of 1.2, when compared to the ratio of *ca.* 0.5 observed for the dyad **1a** having the shorter hexamethylene group. This can be attributed to increased energy transfer from the naphthalimide chromophore to the dansyl moiety with the increase in spacer length as observed in the case of the donor-acceptor systems.

#### 4.3.3. INTERACTIONS WITH METAL IONS

As the naphthalimide and dansyl based dyads **1a** and **1b** interestingly exhibited intramolecular dual emission, it was of our objective to evaluate their potential use as ratiometric sensors and identify the ideal conditions for the detection of metal ions in the aqueous medium. In this context, we have investigated the interactions of these dyads with various metal ions under different conditions, including the micellar medium. Of all the conditions examined, it has been observed that a solvent

system consisting of a mixture (4:1) of water and acetonitrile containing neutral micelles triton X-100 (TX-100; 2 mM) has been found to be very effective with respect to the stability of dyads as well as the selectivity and sensitivity of the metal ion binding event. For example, Figure 4.4 shows the changes in the absorption spectrum of the dyad **1b** with the addition of copper perchlorate in the micellar

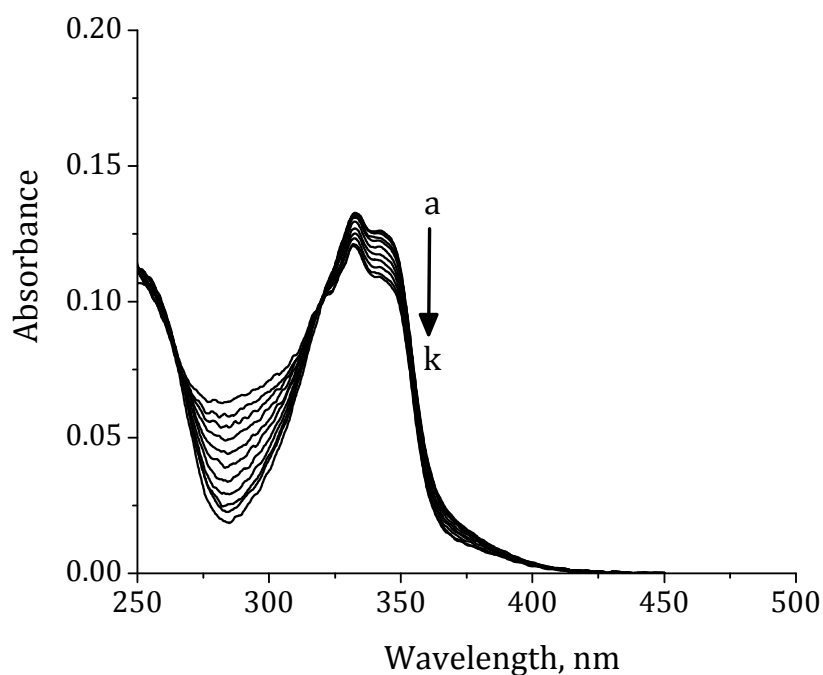


**Figure 4.4.** Changes in the absorption spectrum of the dyad **1b** (3  $\mu\text{M}$ ) in 20% acetonitrile containing 2 mM TX-100 with increase in addition of  $\text{Cu}^{2+}$  ions. [ $\text{Cu}^{2+}$ ] (a) 0 and (k) 20  $\mu\text{M}$ .

medium. With the increasing in concentration of  $\text{Cu}^{2+}$  ions, we observed a decrease in the absorption band at 340 nm with the concomitant increase in the absorbance at 284 nm having isosbestic points at 325 and 360 nm. Interestingly, in the fluorescence spectrum of the dyad **1b**, we observed a regular decrease in the intensity of FRET mediated emission

from the dansyl moiety at 525 nm with the increase in concentration of  $\text{Cu}^{2+}$  ions. Correspondingly, we observed a concomitant increase in the emission intensity of the naphthalimide chromophore at 375 nm with an isoemissive point at 450 nm. Further additions of 20  $\mu\text{M}$  of  $\text{Cu}^{2+}$  ions resulted in the complete quenching of the FRET mediated emission with *ca.* 12-fold increase in the fluorescence intensity ratio of  $I_{375}/I_{525}$ . The significant ‘turn on’ intensity with a blue shift of *ca.* 150 nm led to the visual fluorescence ratiometric detection of  $\text{Cu}^{2+}$  ions by **1b** (insets of Figure 4.5).

Similar observations have been made with the dyad **1a** having a shorter spacer group. In this case, we observed *ca.* 6-fold increase in the fluorescence intensity ratio of  $I_{375}/I_{525}$  with the addition of 20  $\mu\text{M}$  of  $\text{Cu}^{2+}$  ions (Figure 4.6 and Figure 4.7). Of the two systems investigated, the dyad **1b** was found to be very

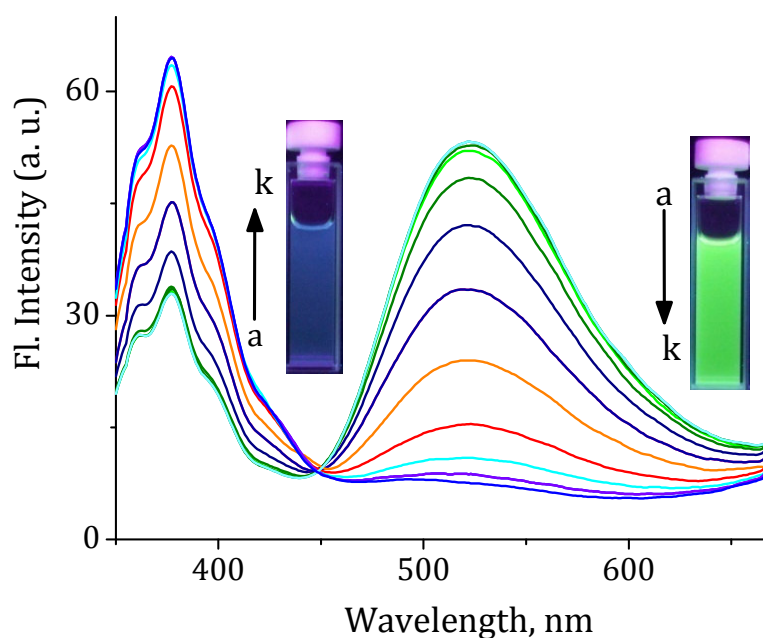


**Figure 4.5.** Changes in the fluorescence spectrum of the dyad **1b** (3  $\mu\text{M}$ ) in 20% acetonitrile containing 2 mM TX-100 with increase in addition of  $\text{Cu}^{2+}$  ions. [ $\text{Cu}^{2+}$ ] (a) 0 and (k) 20  $\mu\text{M}$ . Excitation wavelength, 339 nm.

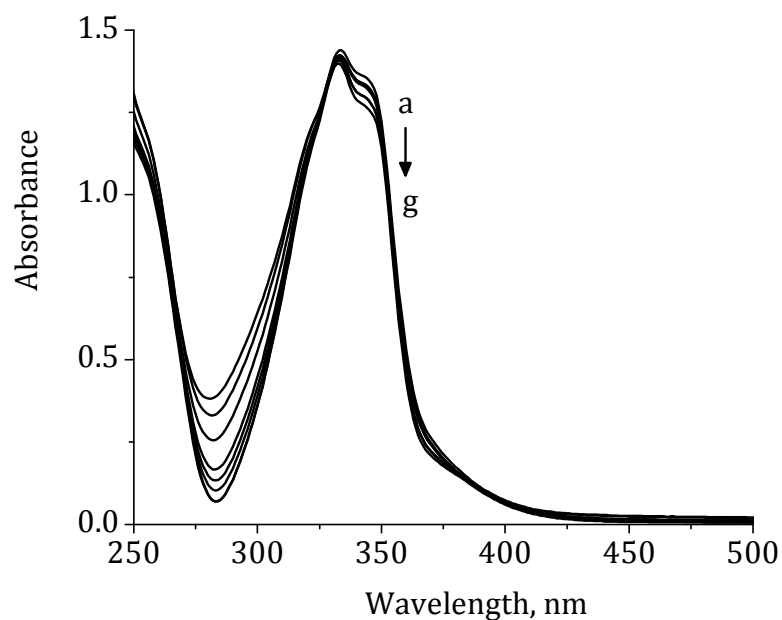


**Figure 4.6.** Changes in the absorption spectrum of the dyad **1a** (3  $\mu\text{M}$ ) in 20% acetonitrile containing 2 mM TX-100 with increase in addition of  $\text{Cu}^{2+}$  ions.  $[\text{Cu}^{2+}]$  (a) 0 and (g) 20  $\mu\text{M}$ .

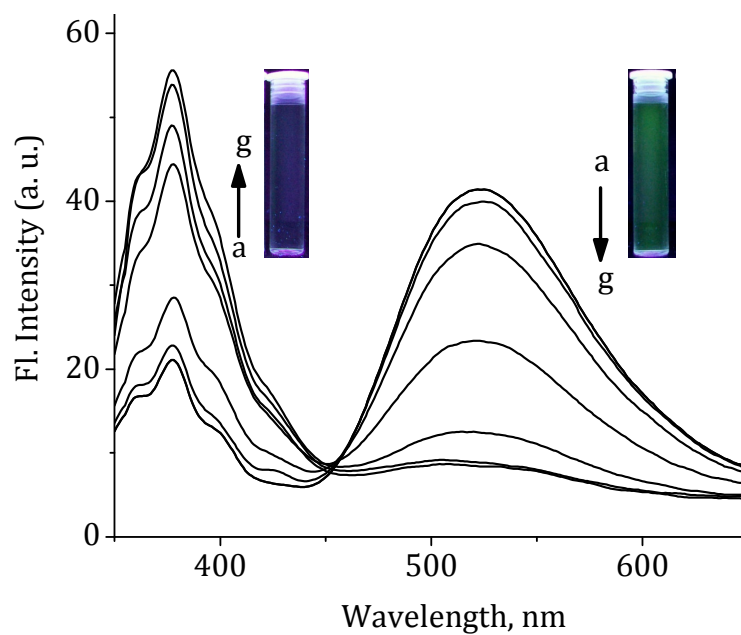


**Figure 4.7.** Changes in the fluorescence spectrum of the dyad **1a** (3  $\mu\text{M}$ ) in 20% acetonitrile containing 2 mM TX-100 with increase in addition of  $\text{Cu}^{2+}$  ions.  $[\text{Cu}^{2+}]$  (a) 0 and (g) 20  $\mu\text{M}$ . Excitation wavelength, 339 nm.

sensitive for the selective recognition of Cu<sup>2+</sup> ions as compared to **1a** because of the efficient FRET mediated emission observed in the former case. The selective quenching of FRET mediated emission at 525 nm alone upon addition of Cu<sup>2+</sup> ions indicate that Cu<sup>2+</sup> ions form stable complex with the dyads. As a consequence, the dansyl moiety becomes incapable of quenching the excited state of the naphthalimide chromophore resulting in the revival of blue naphthalimide emission thereby facilitating the visual detection of Cu<sup>2+</sup> ions.

#### 4.3.4. STOICHIOMETRY OF THE COMPLEXATION

In order to understand the stoichiometry of the complex formed between the dyads and Cu<sup>2+</sup> ions, Jobs plot (Vosburgh *et al.*, 1941, Zeng *et al.*, 2006) for the complex formation was plotted and the binding constant was calculated through Benesi-Hildebrand analysis (Benesi *et al.*, 1949, Yannis *et al.*, 1997, Kim *et al.*, 2008, Hariharan *et al.*, 2007, Hariharan *et al.*, 2007). These analyses gave a 2:1 stoichiometry for the complex formed between the dyad **1b** and Cu<sup>2+</sup> ions with an association constant of ( $K_{ass}$ ) of  $2.6 \pm 0.1 \times 10^5 \text{ M}^{-1}$  (Figure 4.8.). The association constant was further calculated using the curve fitting method (Lin *et al.*, 2008) and the binding constant obtained by this method is in agreement with the value obtained from the Benesi-Hildebrand method. The MALDI-TOF mass spectral analysis of this complex showed a molecular mass of 1141.96 which is in agreement with the calculated molecular mass corresponding to a 2:1 stoichiometric complex between the dyad **1b** and Cu<sup>2+</sup> ions. Similar observations have been made with the

dyad **1a** albeit with lesser sensitivity as compared to the dyad **1b**. In this case, we observed ca. 6-fold increase in the fluorescence ratio of  $I_{375}/I_{525}$  in the presence of  $\text{Cu}^{2+}$  ions with an association constant of  $K_{\text{ass}} = 2 \pm 0.1 \times 10^5 \text{ M}^{-1}$ .

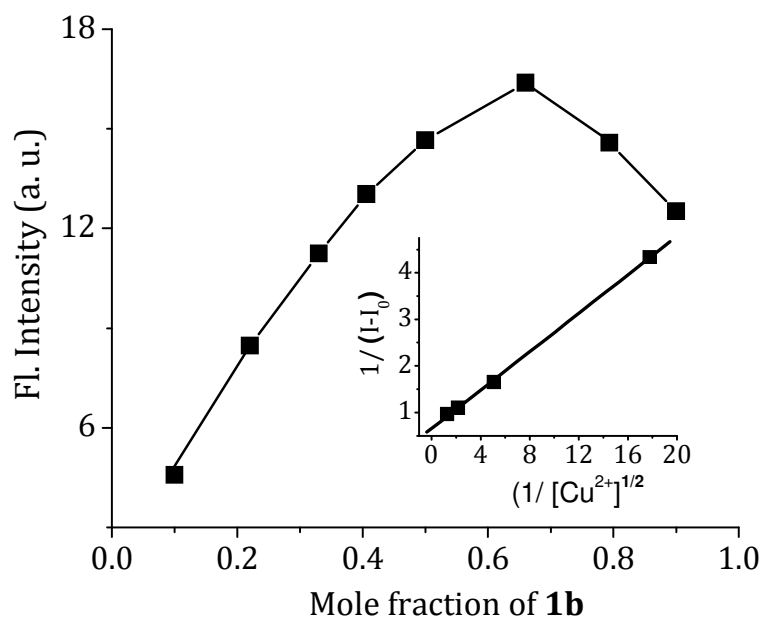


**Figure 4.8.** Job's plot for the complexation of the dyad **1b** with  $\text{Cu}^{2+}$  ions in 20% acetonitrile containing 2 mM TX-100. Inset shows the Benesi-Hildebrand analysis of the emission changes of the dyad **1b** under similar conditions.

#### 4.3.5. REVERSIBILITY OF THE COMPLEXATION

In order to understand the reversibility of the complexation with  $\text{Cu}^{2+}$  ions, ethylenediaminetetraacetic acid (EDTA) was used (Lou *et al.*, 1997, Reise Sousa *et al.*, 1998, Nohta *et al.*, 2000, Okamoto *et al.*, 2004). Figure 4.9 shows the changes in the fluorescence spectra of the **1b** with the consecutive addition of copper ions and EDTA. Initially the dyad shows fluorescence intensity corresponding to dansyl and naphthalimide moiety (trace a in Figure 4.9). With the addition of  $\text{Cu}^{2+}$  ions, the

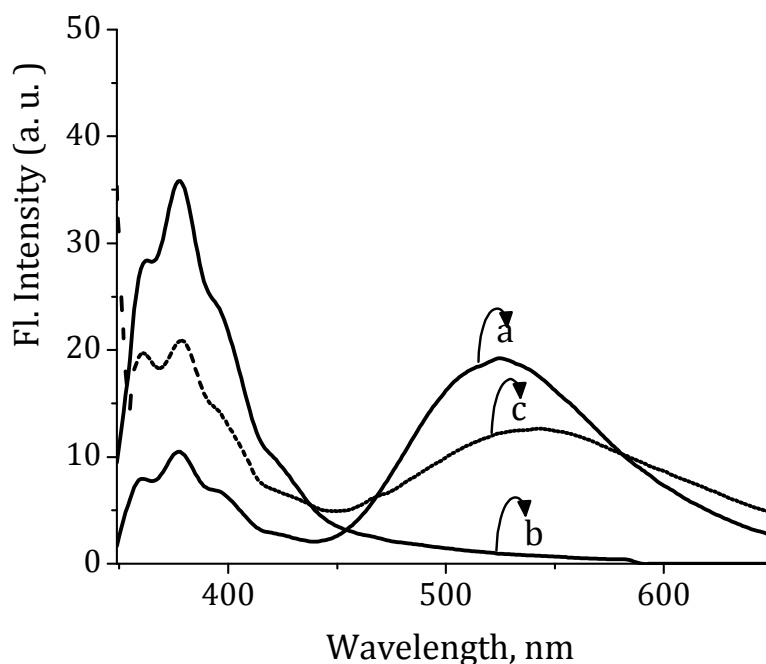


**Figure 4.9.** Emission spectra of **1b** showing reversibility of the complexation in acetonitrile a) **1b** (3  $\mu\text{M}$ ) alone b) [**1b**- $\text{Cu}^{2+}$ ] complex, [ $\text{Cu}^{2+}$ ] 20 mM, and c) [**1b**- $\text{Cu}^{2+}$ ] complex after the addition of EDTA (20  $\mu\text{M}$ ). Excitation wavelength, 339 nm.

decrease in the dansyl emission was observed in the fluorescence intensity as shown by the spectrum (trace b in Figure 4.9) indicating the inhibition of FRET. Interestingly, as can be seen in the figures (trace c in Figure 4.9), the addition of EDTA to the complex results in the revival of the both emission, indicating that the metal ion binding event is reversible in the case of these dyads.

#### 4.3.6. NATURE OF THE COMPLEXATION

To understand the nature of the complex formed as well as the functional groups involved in the coordination, we have analyzed the  $^1\text{H}$  NMR and Fourier transform infrared spectra (FTIR) of the dyads **1a** and **1b** in the presence and

absence of  $\text{Cu}^{2+}$  ions and compared with the model compounds **2** and **3**. For example, with the addition of  $\text{Cu}^{2+}$  ions, we observed a downfield shift of  $\Delta\delta = 0.02$  ppm for the N-H proton of the dyad **1b**, while the peaks corresponding to the aromatic protons showed significant broadening as well as considerable downfield shifts in the range of  $\Delta\delta = 0.03 - 0.07$  ppm (Figure 4.10). In contrast, negligible changes were observed

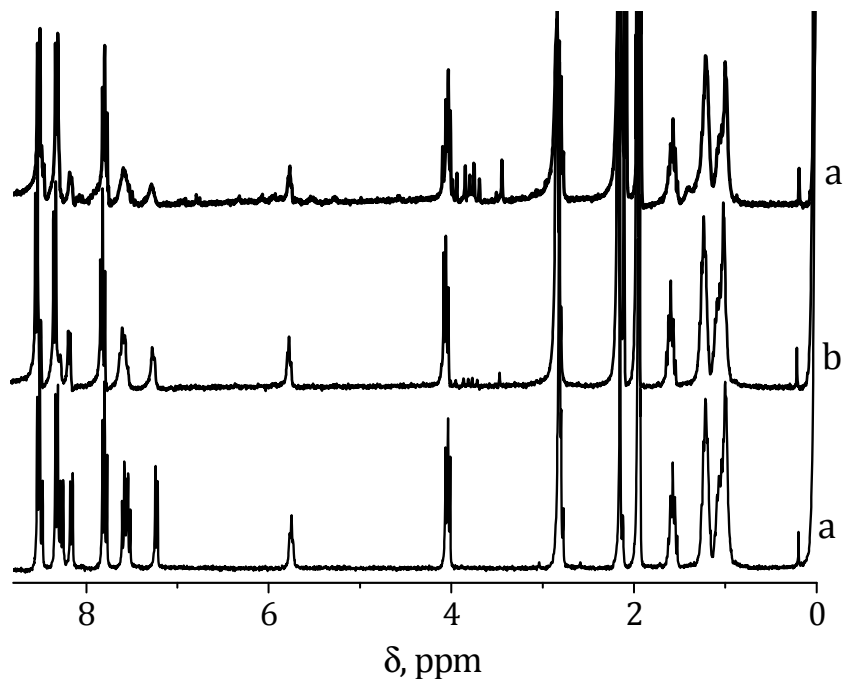


**Figure 4.10.**  $^1\text{H}$  NMR spectra of the dye **1b** (21 mM) in  $\text{CD}_3\text{CN}$  with the increase in addition of  $\text{Cu}^{2+}$  ions in  $\text{CD}_3\text{CN}$ .  $[\text{Cu}^{2+}]$  a) 0, b) 5 and c) 10.5 mM.

in the chemical shift values of *N*-methyl protons of the dansyl unit and methylene protons of the spacer group. In the FTIR spectrum of the dyad **1b**, the characteristic sulphonamide and carbonyl groups stretching frequencies were observed at 1323, 1654 and 1695  $\text{cm}^{-1}$ , while NH stretching frequency appeared at 3284  $\text{cm}^{-1}$  (Figure 4.11). Upon interaction with  $\text{Cu}^{2+}$  ions, we observed significantly decreased

stretching frequencies for both NH and sulphonyl groups, confirming thereby the involvement of these functional groups in the complexation with  $\text{Cu}^{2+}$  ions.

To confirm the role of sulphonamide group of the dyads **1a** and **1b** on their selective complexation with  $\text{Cu}^{2+}$  ions, we have investigated the interactions with the

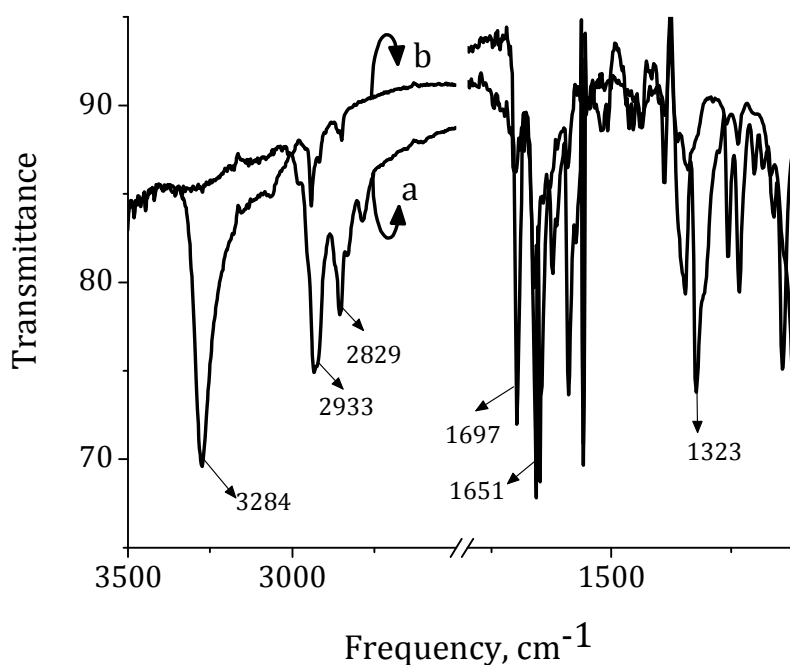


**Figure 4.11.** Fourier transform infrared (FTIR) spectra of dyad **1b**. (a) **1b** alone and (b) **1b** in the presence of  $\text{Cu}(\text{ClO}_4)_2$ .

model compounds **2** and **3**. Of two model derivatives, the compound **2** possess both dialkylamino and sulphonamide groups as in the case of **1a** and **1b**. In contrast, the derivative **3**, in addition to the dialkylamino group and it has been substituted with a sulphonate group instead of the sulphonamide functionality. With increase in addition of  $\text{Cu}^{2+}$  ions to a solution of the model compound **2** ( $100 \mu\text{M}$ ), we observed a absorbance at 286 nm with isosbestic points at 265 and 318 nm (Figure 4.12). At 500  $\mu\text{M}$  of  $\text{Cu}^{2+}$  ions, we observed *ca.* 50% hypochromicity in the absorption spectrum of

the model compound **2**. In the emission spectrum of the compound **2**, we observed regular and significant fluorescence quenching at 525 nm with the addition of  $\text{Cu}^{2+}$  ions (inset of Figure 4.11). In contrast, the model compound **3**, showed negligible

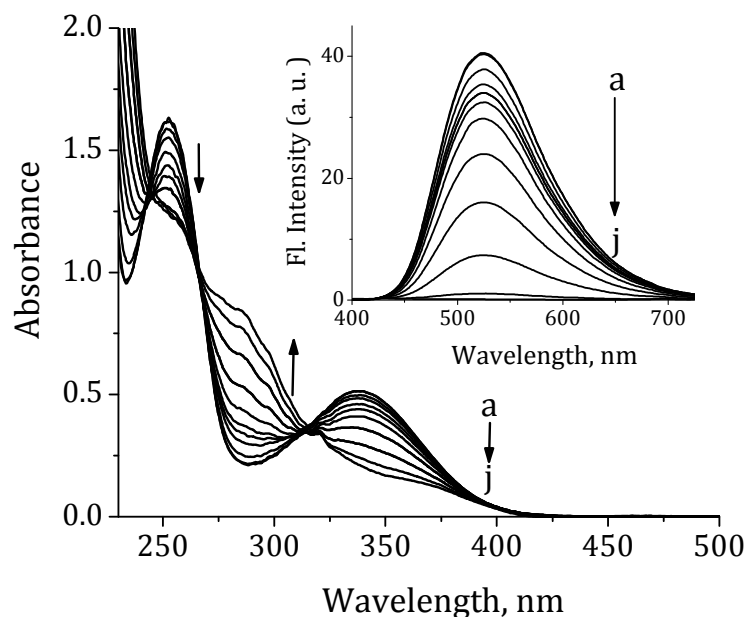


**Figure 4.12.** Changes in absorption and fluorescence (inset) spectrum of the model compound **2** (100  $\mu\text{M}$ ) in acetonitrile with increase in addition of  $\text{Cu}^{2+}$  ions.  $[\text{Cu}^{2+}]$  (a) 0 and (j) 500  $\mu\text{M}$ . Excitation wavelength, 339 nm.

changes in the absorption and fluorescence spectra with the increasing concentration of  $\text{Cu}^{2+}$  ions under identical conditions (Figure 4.13). These results further demonstrate that the complexation between  $\text{Cu}^{2+}$  ions and the dyads **1a** and **1b** and the model compound **2** occur due to the involvement of the sulphonamide group of the dansyl chromophore and rule out the possibility of participation of the dialkylamino group in the binding event.

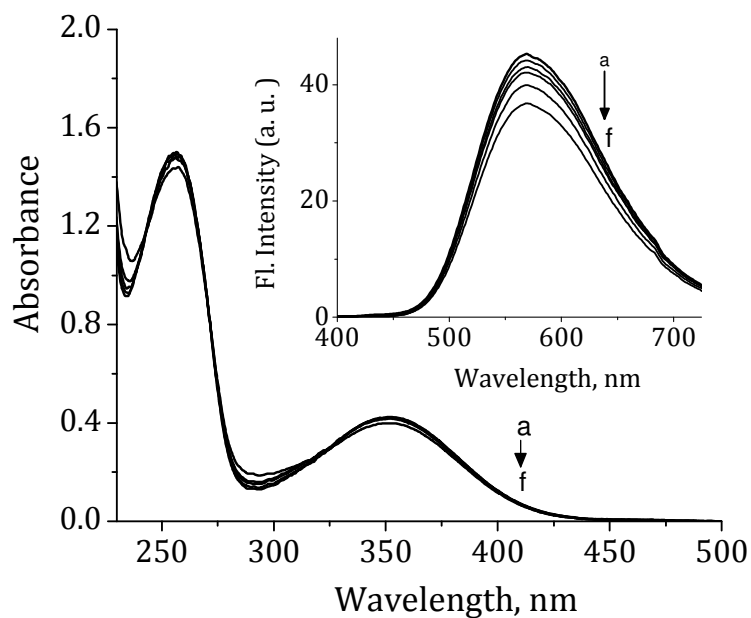


**Figure 4.13.** Changes in the absorption and fluorescence (inset) spectrum of **3** (100  $\mu\text{M}$ ) in acetonitrile with increase in addition of  $\text{Cu}^{2+}$  ions.  $[\text{Cu}^{2+}]$  (a) 0 and (f) 500  $\mu\text{M}$ . Excitation wavelength, 339 nm.

#### 4.3.7. SELECTIVITY OF THE METAL ION COMPLEXATION

To demonstrate the selectivity of the dyads **1a** and **1b** for  $\text{Cu}^{2+}$  ions, we have investigated their interactions with other important monovalent and divalent metal ions such as  $\text{Na}^+$ ,  $\text{Li}^+$ ,  $\text{K}^+$ ,  $\text{Zn}^{2+}$ ,  $\text{Pb}^{2+}$ ,  $\text{Hg}^{2+}$ ,  $\text{Co}^{2+}$ ,  $\text{Fe}^{2+}$ ,  $\text{Cd}^{2+}$ ,  $\text{Mg}^{2+}$  and  $\text{Ba}^{2+}$  ions under identical conditions (Figure 4.14). As can be seen from Figure 4.14, the addition of these metal ions caused negligible changes in the fluorescence intensity of the dyad **1b**. Similar observations have been made with the dyad **1a** in the presence of various metal ions (Figure 4.17). The selectivity of the dyad **1b** towards  $\text{Cu}^{2+}$  ions can be observed visually since the green fluorescence intensity of the dyad **1b** remained unchanged upon addition of these metal ions, while with  $\text{Cu}^{2+}$  ions, we observed the

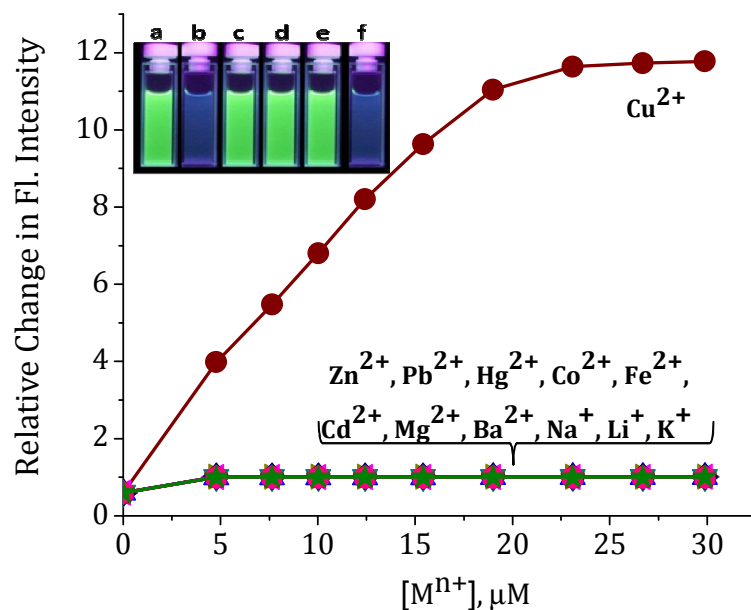


**Figure 4.14.** Relative changes in the fl. intensity of the dyad **1b** (3  $\mu\text{M}$ ) in presence of various metal ions. Inset shows visual observation of fluorescence changes. (a) **1b** alone, (b to d) **1b** in the presence of  $\text{Cu}^{2+}$ ,  $\text{Li}^+$ ,  $\text{Hg}^{2+}$ , (e) equivalent mixture of various metal ions without  $\text{Cu}^{2+}$  (f) equivalent mixture of various metal ions with  $\text{Cu}^{2+}$  ions.

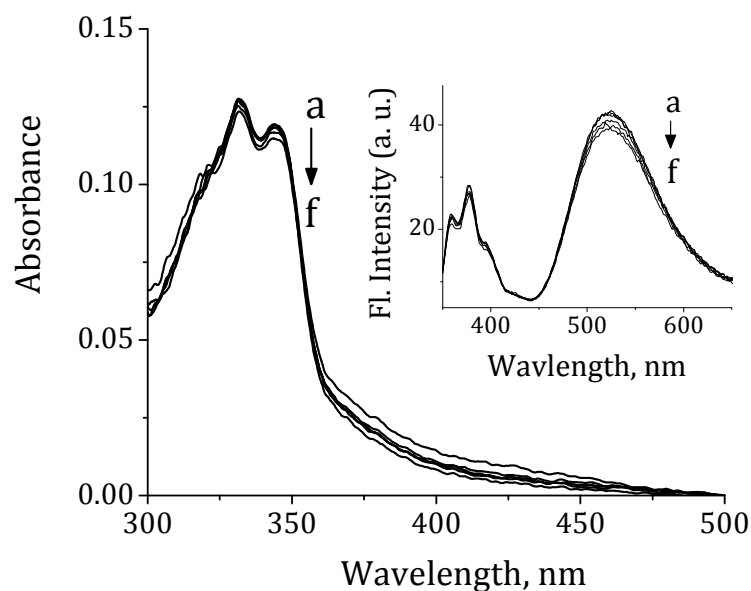


**Figure 4.15.** Absorption and the corresponding fluorescence spectra (inset) of the dyad **1b** (3  $\mu\text{M}$ ) in 20% acetonitrile containing 2 mM TX-100 with the increase in addition of  $\text{Zn}(\text{ClO}_4)_2 \cdot [\text{Zn}^{2+}]$  (a) 0, (f) 20  $\mu\text{M}$ . Excitation wavelength, 339 nm.

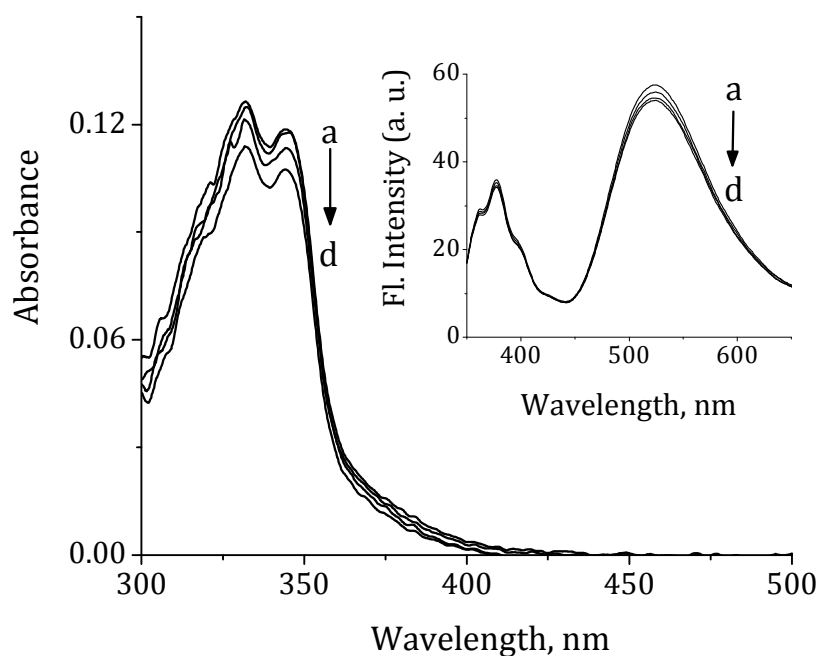


**Figure 4.16.** Absorption and the corresponding fluorescence spectra (inset) of the dyad **1b** (3  $\mu\text{M}$ ) in 20% acetonitrile containing 2 mM TX-100 with the increase in addition of KCl.  $[\text{K}^+]$  (a) 0, (d) 20  $\mu\text{M}$ . Excitation wavelength, 339 nm.

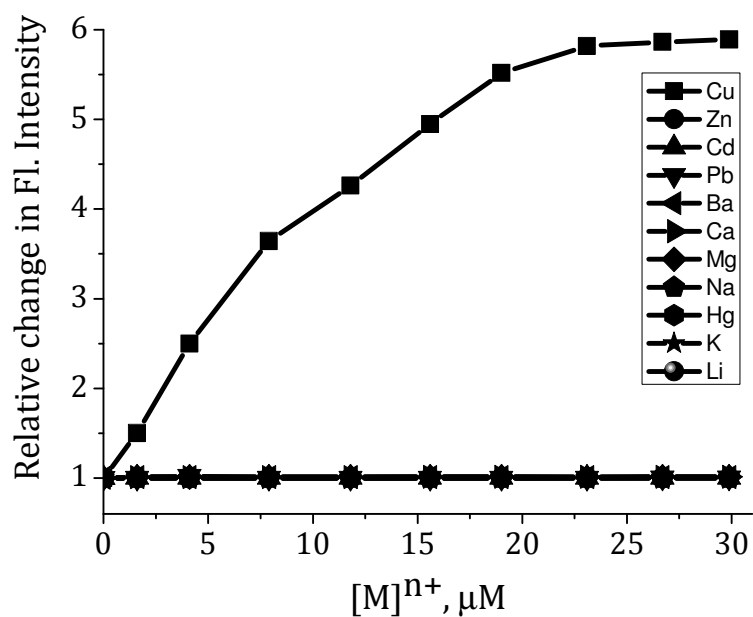


**Figure 4.17.** Relative changes in the fluorescence intensity of the dyad **1a** (3  $\mu\text{M}$ ) in presence of various metal ions.

enhancement in blue fluorescence intensity at 375 nm (inset Figure 4.14). Interestingly, the presence of equimolar concentrations of all other metal ions used for the present studies showed negligible influence on the sensitivity of the detection of Cu<sup>2+</sup> ions by the dyads **1a** and **1b** (Figures 4.15 and 4.16).

#### 4.4. DISCUSSION

The novel dyads **1a** and **1b** having naphthalimide chromophore as the donor and dansyl group as the acceptor moiety showed negligible interactions in the ground state but exhibited efficient FRET reaction in the excited state. The evidence for such a reaction was obtained through excitation spectral analysis, observation of the spacer length dependent energy transfer as well as on the basis of literature reports (Abad *et al.*, 2005). The presence of favorable distance of 11.6 Å between the donor and acceptor units in the case of the dyad **1a** as characterized thorough X-ray crystal analysis further indicate that such a reaction is quite possible in these dyads. In accordance with the above hypothesis, the emission spectrum of the dyads consisted of two emission maxima, one at 375 nm and the other at 525 nm, where the latter band is due to the FRET mediated emission from the dansyl moiety. The observation of significant FRET mediated emission in the case of the dyad **1b** as compared to **1a** could be attributed to the presence of a spacer with an appropriate length for an effective overlap between the donor and acceptor groups. Investigation of the interactions with various metal ions indicates that the dyads **1a** and **1b** undergo selective interactions with Cu<sup>2+</sup> ions as compared to other monovalent and

divalent metal ions. Interestingly, such selective interactions with  $\text{Cu}^{2+}$  ions results in the formation of 2:1 stoichiometric complexes with significant association constants and the complex formation was confirmed through MALDI-TOF mass spectral analysis. The driving force for the selective complexation with  $\text{Cu}^{2+}$  ions is due

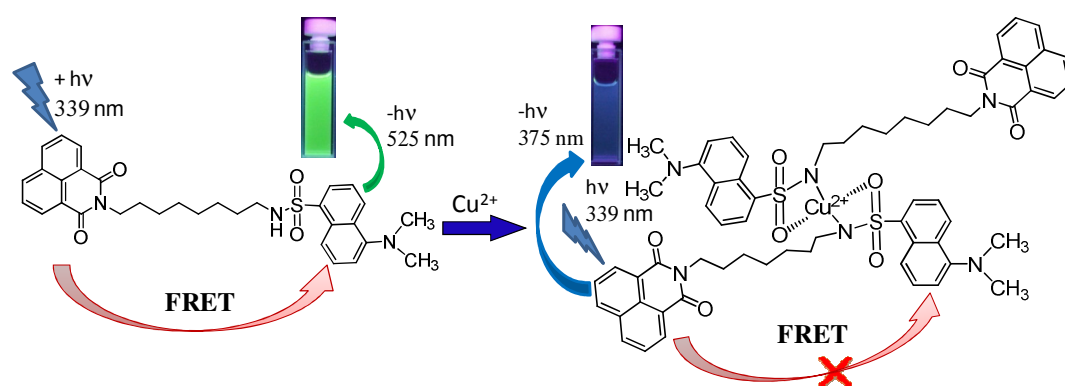


**Figure 4.18.** Schematic representation of the complexation between the dyad **1b** and  $\text{Cu}^{2+}$  ions.

to the presence of sulphonyl and NH groups in these dyads. The involvement of these groups in the complexation was evidenced through absorption, fluorescence,  $^1\text{H}$  NMR and FTIR spectral analysis and further confirmed by studies with the appropriately substituted model compounds **2** and **3**. Uniquely, the complexation of the dyads with  $\text{Cu}^{2+}$  ions involving sulphonamide group alters the interaction between the naphthalimide and dansyl chromophores leading to the disruption of FRET, thereby enabling the visual fluorescence ratiometric detection of  $\text{Cu}^{2+}$  ions.

#### 4.5. CONCLUSIONS

In conclusion, we have developed novel donor and acceptor dyad systems **1a** and **1b** having naphthalimide and dansyl units, which exhibit spacer length

dependent intramolecular energy transfer mediated emission from the dansyl moiety in addition to the emission from the naphthalimide chromophore. These dyads showed selective interactions with  $\text{Cu}^{2+}$  ions as compared to other metal ions and signals the event through inhibition of energy transfer mediated emission intensity. The uniqueness of these dyads is that they form stable complexes with  $\text{Cu}^{2+}$  ions and act as visual fluorescence ratiometric probes for the specific detection of  $\text{Cu}^{2+}$  ions.

## **4.6. EXPERIMENTAL SECTION**

### **4.6.1. GENERAL TECHNIQUES**

The equipment and procedure for spectral recordings are described elsewhere (Kuruville *et al.*, 2005, Avirah *et al.*, 2007, 2008). All melting points are uncorrected and were determined on a Mel-Temp II melting point apparatus. The IR spectra were recorded on a Perkin Elmer Model 882 infrared spectrometer. The electronic absorption spectra were recorded on a Shimadzu UV-3101 or 2401 PC UV-VIS-NIR scanning spectrophotometer. The fluorescence spectra were recorded on a SPEX-Fluorolog F112X spectrofluorimeter.

### **4.6.2. MATERIALS AND METHODS**

1,8-Naphthalic anhydride, 1,6-hexadamine, 1,8-octadamine, dansylchloride,  $\text{Hg}(\text{ClO}_4)_2$ ,  $\text{Pb}(\text{ClO}_4)_2$ ,  $\text{Cu}(\text{ClO}_4)_2$ ,  $\text{Zn}(\text{ClO}_4)_2$ ,  $\text{Ca}(\text{ClO}_4)_2$ ,  $\text{LiClO}_4$ ,  $\text{Cd}(\text{ClO}_4)_2$ ,  $\text{Fe}(\text{ClO}_4)_2$ ,  $\text{Ba}(\text{ClO}_4)_2$ ,  $\text{Co}(\text{ClO}_4)_2$ ,  $\text{NaCl}$ ,  $\text{KCl}$ , triethylamine and  $\text{Mg}(\text{ClO}_4)_2$  were purchased from

aldrich and used as such. The synthesis of *N*-(6-aminoethyl)-1,8-naphthalimide (5a), mp 103-104 °C (mixture mp 104-105 °C), *N*-(8-aminoethyl)-1,8-naphthalimide (5b), mp 163-164 °C (mixture mp 163-164 °C), 5-(*N,N*-dimethylamino)-naphthalene-*N*-butyl-1-sulfonamide (2), mp 96-97 °C (mixture mp 96 °C) and (*N,N*-dimethylamino)-naphthalene-*o*-*tert*-butylphenol-1-sulfonamide (3), mp 109-110 °C (mixture mp 110 °C) was achieved by modifying the reported procedures (Licchelli, *et al.*, 2003, Pandey, *et al.*, 2009).

#### 4.6.2.1. General Procedure for the Synthesis of the Dyads **1a** and **1b**

Dansylchloride (5.0 mmol) was added to a stirred solution of the corresponding *N*-( $\omega$ -aminoalkyl)-1,8-naphthalimide (4.2 mmol) and triethylamine (5.4 mmol) in dry chloroform (15 mL). The mixture was refluxed for 10 h. After cooling the reaction mixture to room temperature (25 °C), the precipitate obtained was filtered off. The clear filtrate solution was evaporated to dryness under vacuum to give a pale yellow residue. The product mixture was chromatographed over silica gel. Elution with a mixture (1:9) of ethyl acetate and hexane gave the dyads **1a** (60%) and **1b** (65%), which were further purified through recrystallization from CH<sub>3</sub>CN.

**Dyad 1a** (60%), mp 121-122 °C, IR (KBr)  $\nu_{\max}$  3248,2927,1693 and 1651 cm<sup>-1</sup>; <sup>1</sup>HNMR (500 MHz, CD<sub>3</sub>CN)  $\delta$  (ppm) 1.1-1.12 (m, 4H), 1.12-1.13 (m, 4H), 1.254 (d, J = 4 Hz, 2H), 2.80 (s, 6H), 3.93 (t, J = 7.5 Hz, 2H), 5.7 (t, J = 5.5 Hz, 1H), 7.20 (d, J = 7.5 Hz, 1H), 7.53-7.59 (m, 2H), 7.78-7.81(m, 2H), 8.14-8.15 (dd, 1H), 8.25 (d, J = 8.5 Hz, 1H), 8.31-8.33 (dd, 2H), 8.47-8.51(m, 3H); <sup>13</sup>C NMR (125.77 MHz, CD<sub>3</sub>CN)  $\delta$  (ppm) 25.3,

25.7, 27.1, 28.5, 29.0, 39.4, 42.40, 44.3, 114.8, 118.7, 122.5, 123.0, 126.7, 127.6, 127.7, 128.7, 129.1, 129.3, 129.6, 130.3, 131.4, 133.7, 135.4, 151.7, 163.6; HRMS – FAB: m/z Calcd for C<sub>30</sub>H<sub>31</sub>N<sub>3</sub>O<sub>4</sub>S: 531.21. Found: 531.23. Anal. Calcd for C<sub>30</sub>H<sub>31</sub>N<sub>3</sub>O<sub>4</sub>S: C, 68.03; H, 5.90; N, 7.93. Found: C, 67.90; H, 6.03; N, 7.89.

**Dyad 1b** (65%) mp 108-109 °C, IR (KBr)  $\nu_{\max}$  3284, 2933, 1697 and 1654 cm<sup>-1</sup>; <sup>1</sup>H NMR (500 MHz, CD<sub>3</sub>CN)  $\delta$  (ppm) 1.05-1.08 (m, 8H), 1.18-1.21 (m, 4H), 1.53-1.59 (m, 2H), 2.80 (s, 6H), 4.01 (t, J = 7.5 Hz, 2H), 5.75 (t, J = 6 Hz, 1H), 7.21 (d, J = 7.5 Hz, 1H), 7.52-7.59 (m, 2H), 7.76-7.80 (m, 2H), 8.14-8.16 (dd, 1H), 8.25 (d, J = 8.5 Hz, 1H), 8.29-8.31 (m, 2H), 8.47-8.49 (d, J = 8.5 Hz, 3H); <sup>13</sup>C NMR (125.77 MHz, CD<sub>3</sub>CN)  $\delta$  (ppm) 27.2, 27.9, 28.9, 29.7, 30.0, 30.1, 41.2, 44.0, 46.0, 116.4, 120.3, 124.1, 124.6, 128.3, 129.3, 130.4, 130.7, 130.9, 131.2, 131.9, 132.9, 135.3, 137.0, 153.3, 165.2; HRMS-FAB Calcd for C<sub>32</sub>H<sub>35</sub>N<sub>3</sub>O<sub>4</sub>S: 559.23. Found: 559.11. Anal. Calcd for C<sub>32</sub>H<sub>35</sub>N<sub>3</sub>O<sub>4</sub>S: C, 68.92; H, 6.33; N, 7.53. Found: C, 68.66; H, 6.51; N, 7.56.

#### 4.6.2.2. Determination of Stoichiometry by Jobs Plot

In the Jobs plot method, the total molar concentration of the two binding partners (e.g. dyad and metal ions) is held constant, but their mole fractions are varied. The fluorescence intensity (or peak area) that is proportional to complex formation is plotted against the mole fractions of these two components. The maximum on the plot corresponds to the stoichiometry of the two species if sufficiently high concentrations are used.

#### 4.6.2.3. Determination of Binding Constant by Benesi-Hildebrand Analysis

The binding affinities of the dyads were calculated using Benesi-Hildebrand equation 4.1 for 1:1 stoichiometry and equation 4.2 for 2:1 stoichiometry, where  $K$  is the equilibrium constant,  $I_0$  is the fluorescence intensity of the free dyad,  $I$  is the observed fluorescence intensity in the presence of metal ions and  $I_s$  is the fluorescence intensity at saturation. The linear dependence on the reciprocal (or its square root) of the metal ion concentration indicates the formation of a 1:1 (or 2:1) complex between the dyad and the metal ion.

$$\frac{1}{(I - I_0)} = \frac{1}{(I - I_{fc})} + \frac{1}{K (I - I_{fc}) [\text{Cu}^{2+}]} \quad (\text{eq. 4.1})$$

$$\frac{1}{(I - I_0)} = \frac{1}{(I - I_{fc})} + \frac{1}{K (I - I_{fc}) [\text{Cu}^{2+}]^{1/2}} \quad (\text{eq. 4.2})$$

Alternatively, the association constants were also calculated using the fluorescence titration data using a reported method (Lin *et al.*, 2008) for a 1:2 metal-ligand binding mode and according to the equation 4.3,

$$\frac{\alpha^2}{(1-\alpha)} = \frac{1}{2KC_F[M]} \quad (\text{eq. 4.3})$$

$$\alpha = \frac{[F-F_0]}{[F_1-F_0]} \quad (\text{eq. 4.4})$$

wherein,  $C_F$  denotes the total concentration of ligand in the system,  $\alpha$  defined as the ratio between the free dyad concentration  $[C]$  and the total concentration of ligand  $C_F$  and was evaluated using the equation 4.4, wherein,  $F_1$  and  $F_0$  are the limiting emission values for  $\alpha = 1$  (in the absence of metal) and  $\alpha = 0$  (probe is complexed with the metal ion), respectively.

## REFERENCES

- Abad, S.; Kluciar, M.; Miranda, M. A.; Pischel, U. Proton-induced fluorescence switching in novel naphthalimide–dansylamide dyads. *J. Org. Chem.* 70, **2005**, 10565–10568.
- Ackers, G. K.; Hazzard, J. H. Transduction of binding energy into hemoglobin cooperativity. *Trends Biochem. Sci.* 18, **1993**, 385–390.
- Amisha Kamal, J. K.; Zhao, L.; Zewail, A. H. Ultrafast hydration dynamics in protein unfolding: Human serum albumin. *Proc. Natl. Acad. Sci. U. S. A.* 102, **2004**, 13411–13416.
- Arunkumar, E.; Forbes, C. C.; Noll, B. C.; Smith, B. D. Squaraine-derived rotaxanes: sterically protected fluorescent near-IR dyes. *J. Am. Chem. Soc.* 127, **2005**, 3288–3289.
- Arun, K. T.; Ramaiah, D. Near-infrared fluorescent probes: Synthesis and spectroscopic investigations of a few amphiphilic squaraine dyes. *J. Phys. Chem. A* 109, **2005**, 5571–5578.
- Arvidson, E. O.; Belfrage, P. Monoglyceride-protein interaction. The binding of monoolein to native human serum albumin. *Acta Chem. Scand.* 23, **1969**, 232–240.
- Ascenzi, P.; Bocedi, A.; Notari, S.; Fanali, G.; Fesce, R.; Fasano, M. Allosteric modulation of drug binding to human serum albumin. *Mini Rev. Med. Chem.* 6, **2006**, 483.
- Atkinson, S. F.; Bettinger, T.; Seymour, L. W.; Behr, J.P.; Ward, C. M. Conjugation of

- folate via gelonin carbohydrate residues retains ribosomal-inactivating properties of the toxin and permits targeting to folate receptor positive cells, *J. Biol. Chem.* 276, **2001**, 27930–27935.
- Avirah, R.R.; Jyothish, K.; Ramaiah, D. Dual-mode semisquaraine-based sensor for selective detection of Hg<sup>2+</sup> in a micellar medium. *Org. Lett.* 9, **2007**, 121-124.
- Avirah, R.R.; Jyothish, K.; Ramaiah, D. Infrared absorbing croconaine dyes: Synthesis and metal ion binding properties. *J. Org. Chem.* 73, **2008**, 274-279.
- Babcock, G. T.; Wickström, M. Oxygen activation and the conservation of energy in cell respiration. *Nature* 356, **1992**, 301–309.
- Balabin, I. A.; Onuchic, J. N. Dynamically controlled protein tunneling paths in photosynthetic reaction centers. *Science* 290, **2000**, 114-117.
- Balbach, J.; Forge, V.; Vannuland, N. A. J.; Winder, S. L.; Hore, P. J.; Dobson, C. M. Following protein folding in real time using NMR spectroscopy. *Nat. Struct. Biol.* 2, **1995**, 865-870.
- Baldo-Enzi, G.; Baiocchi, M. R.; Vigna, G.; Mosconi, C.; Fellin, R. Analbuminaemia: a natural model of metabolic compensatory systems. *J. Inher. Metab. Dis.* 10, **1987**, 317-329.
- Banerjee, A.; Yang, W.; Karplus, M.; Verdine, G. L. A nucleobase lesion remodels the interaction of its normal neighbor in a DNA glycosylase complex. *Nature* 434, **2005**, 612-618.
- Baptista, M. S.; Indig, G. L. Effect of BSA binding on photophysical and photochemical

- properties of triarylmethane dyes. *J. Phys. Chem. B* 102, **1998**, 4678-4688.
- Barnham, K. J.; Masters, C. L.; Bush, A. I. Neurodegenerative diseases and oxidative stress. *Nat. Rev. Drug Discovery*. 3, **2004**, 205-214.
- Battistuzzi G. G.; Grandi, G.; Menabue, L.; Pellacani, G. C.; Sola, M. The effect of a dansyl group on the co-ordinative ability of *N*-protected amino acids. Part 1. Behaviour of the copper(II) ion-*N*-dansylglycinate system in aqueous and methanolic solution. *J. Chem. Soc., Dalton Trans.* **1985**, 2363-2368.
- Beljaars, L.; Molema, G.; Schuppan, D.; Geerts, A.; De Bleser, P. J.; Weert, B.; Meijer, D. K. F.; Poelstra, K. J. Successful targeting to rat hepatic stellate cells using albumin modified with cyclic peptides that recognize the collagen type VI receptor. *J. Biol. Chem.* 275, **2000**, 12743-12751.
- Benesi H. A.; Hildebrand, J. H. A spectrophotometric investigation of the interaction of Iodine with aromatic hydrocarbons. *J. Am. Chem. Soc.* 71, **1949**, 2703-2707.
- Bennhold, H. Das menschliche serum albumin. *Bull. Schweiz. Akad. Med. Wissensch.* 17, **1961**, 62-76.
- Berman, H. M. The past and future of structure databases. *Curr. Opin. Biotechnol.* 10, **1999**, 76-80.
- Bhasikuttan, A. C.; Mohanty, J.; Nau, W. M.; Pal, H. Efficient fluorescence enhancement and cooperative binding of an organic dye in a supra biomolecular host-protein assembly. *Angew. Chem., Int. Ed.* 46, **2007**, 4120-4122.
- Bigelow, R. W.; Freund, H. -J. An MNDO and CNDO / S(S + DES CI) study on the

- structural and electronic properties of a model squaraine dye and related cyanine. *Chem. Phys.* **107**, **1986**, 159-174.
- Binnig, G.; Quate, C. F.; Gerber, Ch. Atomic force microscope. *Phys. Rev. Lett.* **56**, **1986**, 930-937.
- Bohne, C.; Barra, M.; Boch, R.; Abuin, E. B.; Scaiano, J. C. Excited triplet states as probes in organized systems. An overview of recent results. *J. Photochem. Photobiol. A Chem.* **65**, **1992**, 249-265.
- Bonnett, R. *Chemical aspects of photodynamic therapy*; Gordon and Breach Science Publishers: The Netherlands. **2000**.
- Borbat, P. P.; Costa-Filho, A. J.; Earle, K. A.; Moscicki, J. K.; Freed, J. H. Electron spin resonance in studies of membranes and proteins. *Science* **291**, **2001**, 266-269.
- Branden, C.; Tooze, J. *Introduction to protein structure*, Garland Publishing, Inc., New York, **1991**.
- Brenner, S. E.; Chothia, C.; Hubbard, T. J. P. Population statistics of protein structures: lessons from structural classifications. *Curr. Opin. Struct. Biol.* **7**, **1997**, 369-376.
- Brock, A. Binding of digitoxin to human serum albumin: influence of free fatty acids, bile acids, and protein unfolding on the digitoxin-albumin interaction. *Acta Pharmacol. Toxicol.* **38**, **1976**, 497-507.
- Brown, D. R.; Kozlowski, H. Biological inorganic and bioinorganic chemistry of neurodegeneration based on prion and Alzheimer diseases. *Dalton Trans.* **2004**, 1907-1917.

- Brown, J. R. Structure of bovine serum albumin. *Fed. Proc.* 34, **1975**, 591-591.
- Brown, J. R.; Shockley, P. *Serum Albumin: Structure and characterization of its ligand binding site. Lipid-protein interactions*, Vol. 1, pp. 25-68. Wiley, New York, **1982**.
- Caraceni, P.; Gasbarrini, A.; Van Thiel, D. H.; Borle, A. B. Oxygen free radical formation by rat hepatocytes during postanoxic reoxygenation: scavenging effect of albumin. *Am. J. Physiol.* 266, **1984**, G451-G458.
- Carter, D. C.; He, X. M. Structure of human serum albumin. *Science* 249, **1990**, 302-303.
- Carter, D. C.; Ho, J. X. Structure of serum albumin. *Adv. Protein Chem.* 45, **1994**, 152-203.
- Carter, D. C.; He, X. M.; Munson, S. H.; Twigg, P. D.; Gernert, K. M.; Broom, M. B.; Miller, T. Y. Three-dimensional structure of human serum albumin. *Science* 244, **1989**, 1195-1198.
- Ceroni, P.; Laghi, I.; Maestri, M.; Balzani, V.; Gestermann, S.; Gorkab, M.; Vogtle, F. Photochemical, photophysical and electrochemical properties of six dansyl-based dyads. *New. J. Chem.* 26, **2002**, 66-75.
- Chmelik, J.; Anzenbacher, P.; Chmelikova, J. Mechanism of denaturation of human serum albumin by urea. *Collect. Czech. Chem. Commun.* 53, **1988**, 411-422.
- Choi, J. K.; Kim, S. H.; Yoon, J.; Lee, K-H.; Bartsch, R. A.; Kim, J. S. A. PCT-based, pyrene-armed calix[4]crown fluoroionophore. *J. Org. Chem.* 71, **2006**, 8011-8015.
- Choi, M.; Kim, M.; Lee, K. D.; Han, K. N.; Yoon, I. A.; Chung, H. J.; Yoon, J. A new reverse PET chemosensor and its chelatoselective aromatic cadmium. *Org. Lett.*

3, **2001**, 3455-3457.

Chuang, V. T. G.; Otagari, M. Stereoselective binding of human serum albumin. *Chirality*, **18**, **2006**, 159-166.

Cincotta, L.; Foley, J. W.; Cincotta, A. H. Novel red absorbing benzo[a]phenoxazinium and benzo[a]phenothiazinium photosensitizers: in vitro evaluation. *Photochem. Photobiol.* **46**, 1987, 751-758.

Cohen, S. L.; Cramp, D. G.; Lewis, A. D.; Tickner, T. R. The mechanism of hyperlipidaemia in nephrotic syndrome-role of low albumin and the reaction. *Clin. Chim. Acta.* **104**, **1980**, 393-400.

Collman, J. P.; Boulatov, R.; Sunderland, C. J.; Fu, L. Functional analogues of cytochrome c oxidase, myoglobin, and hemoglobin. *Chem. Rev.* **104**, **2004**, 561-588.

Constable, E. C.; Martinez-Manez, R.; Cargill Thompson, A. M. W.; Walker, J. V. Metallosupramolecular complexes containing ferrocenyl groups as redox spectators; synthesis and co-ordination behaviour of the helicand 4',4-bis(ferrocenyl)2,2': 6',2'': 6'',2''': 6''',2'''-quinquepyridine. *J. Chem. Soc., Dalton Trans.* **1994**, 1585-1594.

Corradini, R.; Dossena, A.; Galaverna, G.; Marchelli, R.; Panagia, A.; Sartor, G. Fluorescent chemosensor for organic guests and copper(II) ion based on dansyl diethylenetriamine-modified  $\beta$ -cyclodextrin. *J. Org. Chem.* **62**, **1997**, 6283-6289.

Cottrell, W. J.; Oseroff, A. R.; Foster, T. H. Portable instrument that integrates irradiation with fluorescence and reflectance spectroscopies during clinical

- photodynamic therapy of cutaneous disease. *Rev. Sci. Instrum.* 77, **2006**, 064-302.
- Creighton, T.E. *Proteins: Structures and Molecular Properties*, 2<sup>nd</sup> edn, W. H. Freeman and Company, New York. **1992**.
- Curry, S.; Mandelkow, H.; Brick P.; Franks, N. Crystal structure of human serum albumin complexed with fatty acid reveals an asymmetric distribution of binding sites. *Nat. Stru. Biol.* 5, **1998**, 827-835.
- Daffy, L. M.; de Silva, A. P.; Gunaratne, H. Q. N.; Huber, C.; Lynch, P. L. M.; Werner, T.; Wolfbeis, O. S. Aredicarboximide building blocks for fluorescent photoinduced electron transfer pH sensors applicable with different media and communication wavelengths. *Chem. Eur. J.* 4, **1998**, 1810-1815.
- Dalglish, D. G.; Peacocke, A. R. The circular dichroism in the ultraviolet of aminoacridines and ethidium bromide bound to DNA. *Biopolymers*, 10, **1971**, 1853-1863.
- Das, S.; Kamat, P. V.; la Barre, B. D.; Thomas, K. G.; Ajayaghosh A.; George, M. V. Photophysics and photochemistry of squaraine dyes. 3. Excited-state properties and poly(4-vinylpyridine)-induced fluorescence enhancement of bis(2,4,6-trihydroxyphenyl)squaraine. *J. Phys. Chem.* 96, **1992**, 10327-10330.
- Davila, J.; Harriman, A. Photoreactions of macromolecular dyes bound to human serum albumin. *Photochem. Photobiol.* 51, **1989**, 9-19.
- Deraeve, C.; Boldron, C.; Maraval, A.; Mazarguil, H.; Gornitzka, H.; Vendier, L.; Pitie', M.;

- Meunier, B. Preparation and study of new poly-8-hydroxyquinoline chelators for an anti-Alzheimer strategy. *Chem. Eur. J.* **14**, **2008**, 682-696.
- de Silva, A. P.; Gunaratne, H. Q. N.; Gunnlaugsson, T.; Huxley, A. J. M.; McCoy, C. P.; Rademacher, J. T.; Rice, T. E. Signaling recognition events with fluorescent sensors and switches. *Chem. Rev.* **97**, **1997**, 1515-1566.
- de Silva, A.P.; de Silva, S. A.; Fluorescent signalling crown ethers; 'switching on' of fluorescence by alkali metal ion recognition and binding *in situ*. *J. Chem. Soc., Chem. Commun.* **1986**, 1709-1710.
- Detty, M. R.; Merkel, P. B. Chalcogenapyrylium dyes as potential photochemical therapeutic agents. Solution studies of heavy atom effects on triplet yields, quantum efficiencies of singlet oxygen generation, rates of reaction with singlet oxygen, and emission quantum yields. *J. Am. Chem. Soc.* **112**, **1990**, 3845-3855.
- Detty, M. R.; McKelvey, J. M.; Luss, H. R. Tellurapyrylium dyes as catalysts for oxidations with hydrogen peroxide and as scavengers of singlet oxygen. dihydroxytelluranes as mild oxidizing agents. *Organometallics* **7**, 1988, 1131-1147.
- Dickerson, R.E.; Geis, I. Hemoglobin: Structure, function, evolution, and pathology, The Benjamin/Cummings Publishing Company, Redwood City, CA. **1982**.
- di Prisco, G.; Condò, S.G.; Tamburrini, M.; Giardina, B. Oxygen transport in extreme environments. *Trends Biochem. Sci.* **16**, **1991**, 471-474.
- Dobson, C. M.; Hore, P. J. Kinetic studies of protein folding using NMR spectroscopy.

- Nat. Struct. Biol.* **5**, **1998**, 504-507.
- Dockal, M.; Chang, M.; Carter, D. C.; Ruker, F. Five recombinant fragments of human serum albumin-tools for the characterization of the warfarin binding site. *Protein Sci.* **9**, **2000**, 1455-1465.
- Dockal, M.; Carter, D. C.; Ruker, F. The Three recombinant domains of human serum albumin: Structural characterization and ligand binding properties. *J. Biol. Chem.* **274**, **1999**, 29303-29310.
- Dougherty, D. A. Unnatural amino acids as probes of protein structure and function. *Curr. Opin. Chem. Biol.* **4**, **2000**, 645-652.
- Duff, M. R.; Kumar, C. V. Site-selective photocleavage of proteins by uranyl ions. *Angew. Chem., Int. Ed.* **45**, **2006**, 137-139.
- Fabbrizzi, L.; Poggi, A. Sensors and switches from supramolecular chemistry. *Chem. Soc. Rev.* **24**, **1995**, 197-204.
- Fabian, J.; Nakazumi, H.; Matsuoka, M. Near-infrared absorbing dyes. *Chem. Rev.* **92**, **1992**, 1197-1226.
- Fasano, M.; Curry, S.; Terreno, E.; Galliano, M.; Fanali, G.; Narciso, P.; Notari, S.; Ascenzi, P. The extraordinary ligand binding properties of human serum albumin. *IUBMB Life* **57**, **2005**, 787-796.
- Fehske, K. J., Mtiller, W. E., and Wollert, U. The modification of the lone tryptophan residue in human serum albumin by 2-hydroxy-5-nitrobenzyl bromide. Characterization of the modified protein and the binding of L-tryptophan and

- benzodiazepines to the tryptophan-modified albumin. *Biol. Chem. Hoppe-Seyler* 359, **1978**, 709-717.
- Flora, K.; Brennan, J. D.; Baker, G. A.; Doody, M. A.; Bright, F. V. Unfolding of acrylodan-labeled human serum albumin probed by steady-state and time-resolved fluorescence methods. *Biophys. J.* 75, **1998**, 1084–1096.
- Forker, E. L.; Luxon, B. A. Albumin helps mediate removal of taurocholate by rat liver. *J. Clin. Invest.* 67, **1981**, 1517-1522.
- Foster, J. E. Some aspects of the structure and conformational properties of serum albumin. In "Albumin, structure, function, and uses". V. M. Rosenoer, M. A. Rothschild, eds., pp.53-84. Pergamon, New York, **1977**.
- Förster, Th. Intermolecular energy migration and fluorescence. *Ann. Phys.* 2, **1948**, 55-75.
- Fuchs, E.; Cleveland, D.W. A Structural scaffolding of intermediate filaments in health and disease. *Science* 279, **1998**, 514–519.
- Gaggelli, E.; Kozlowski, H.; Valensin, D.; Valensin, G. Copper homeostasis and neurodegenerative disorders alzheimer's, prion, and parkinson's diseases and amyotrophic lateral sclerosis. *Chem. Rev.* 106, **2006**, 1995-2044.
- Gandin, E.; Lion, Y.; de Vorst, V. Quantum yield of singlet oxygen production by xanthene derivatives. *Photochem. Photobiol.* 37, **1983**, 271-278.
- Gehlhaar, D. K.; Larson, V.; Luty, B. A.; Marrone, T.; et al. Towards understanding the

- mechanisms of molecular recognition by computer simulations of ligand-protein interactions. *J. Mol. Recognit.* **12**, **1999**, 371-389.
- Gellman, S. H., ed. Introduction: Molecular Recognition. *Chem. Rev.* **97**, **1997**, 1231-1232.
- Ghosh, P.; Bharadwaj, P. K.; Mandal, S.; Sanjib, G. Ni(II), Cu(II), and Zn(II) Cryptate-enhanced fluorescence of a trianthrylcryptand: A potential molecular photonic OR operator. *J. Am. Chem. Soc.* **118**, **1996**, 1553-1554.
- Ghuman, J.; Zunszain, P. A.; Petitpas, I.; Bhattacharya, A. A.; Otagiri, M.; Curry, S. Structural basis of the drug-binding specificity of human serum albumin. *J. Mol. Biol.* **353**, **2005**, 38-52.
- Gokel, G. W.; Leevy, W. M.; Weber, M. E. Crown ethers: Sensors for ions and molecular scaffolds for materials and biological models. *Chem. Rev.* **104**, **2004**, 2723-2750.
- Goren, D.; Horowitz, A.T.; Tzemach, D.; Tarshish, M.; Zalipsky, S.; Gabizon, A. Nuclear delivery of doxorubicin via folate-targeted liposomes with bypass of multidrug-resistance efflux pump. *Clin. Cancer Res.* **6**, **2000**, 1949-1957.
- Gosselin, M. A.; Lee, R. J.; Folate receptor-targeted liposomes as vectors for therapeutic agents. *Biotechnol. Annu. Rev.* **8**, **2002**, 103-131.
- Grandini, P.; Mancin, F.; Tecilla, P.; Scrimin, P.; Tonellato, U. Exploiting the self-assembly strategy for the design of selective CuII ion chemosensors. *Angew. Chem. Int. Ed.* **38**, **1999**, 3061-3064.
- Greenstein, J.P.; Winitz, M. *Chemistry of the amino acids*, 3 Vols, John Wiley & Sons,

New York, **1961**

- Gryzunov, T. A.; Syrejshchikova, T. I.; Komarova, M. N.; Misionzhnik, E. Y.; Uzbekov, M. G.; Molodetskich, A. V.; Dobretsov G. E.; Yakimenko, M. N. *Nucl. Instrum. Methods Phys. Res. A* **448**, **2000**, 478–482.
- Gunlaugsson, T.; Clive Lee, T.; Parkesh, R. A highly selective and sensitive fluorescent PET (photoinduced electron transfer) chemosensor for Zn(II). *Org. Biomol. Chem.* **1**, **2003**, 3265-3267.
- Harata, K.; Uedaira, H. The Circular dichroism spectra of the  $\beta$ -cyclodextrin complex with naphthalene derivatives. *Bull. Chem. Soc. Jpn.* **48**, **1975**, 375-378.
- Hariharan, M.; Ramaiah, D. Novel Bifunctional viologen-linked pyrene conjugates: synthesis and study of their interactions with nucleosides and DNA. *J. Phys. Chem. B* **110**, **2006**, 24678-24686.
- Hariharan, M.; Neelakandan, P. P.; Ramaiah, D. Encapsulation of electron donor-acceptor dyads in  $\beta$ -cyclodextrin cavity: Unusual planarization and enhancement in rate of electron-transfer reaction. *J. Phys. Chem. B.* **111**, **2007**, 11940-11947.
- Hariharan, M.; Karunakaran, S.C.; Ramaiah, D. Selective recognition of tryptophan through inhibition of intramolecular charge-transfer interactions in an aqueous medium. *Org. Lett.* **9**, **2007**, 417-420.
- He, X. M.; Carter, D. C. Atomic structure and chemistry of human serum albumin. *Nature* **358**, **1992**, 209-215.
- Henderson, B. S.; Dougherty, T. J.; Eds. *Photodynamic therapy: Basic principles and*

*clinical applications*; New York: Marcel Dekker, **1992**.

Honoré, B. Conformational changes in human serum albumin induced by ligand binding. *Pharmacol. Toxicol.* 66 (Suppl. 2), 7-26, **1990**.

Hylander, L. D.; Goodsite, M. E. Environmental costs of mercury pollution. *Science of the total environment* 368, **2006**, 352-370.

Iglesias, J.; Levine, J. S. Albuminuria and renal injury-beware of proteins bearing gifts. *Nephrol. Dial. Transplant.* 16, **2001**, 215-218,

Ivanov, A. I.; Korolenko, E. A.; Korolik, E. V.; Firsov, S. P.; Zhbakov, R. G.; Marchewka, M. K.; Ratajczak, H. Chronic liver and renal diseases differently affect structure of human serum albumin. *Arch. Biochem. Biophys.* 408, **2002**, 69-77.

Jiang, P.; Chen, L.; Lin, J.; Liu, Q.; Ding, J.; Gao, X.; Guo, Z. Novel zinc fluorescent probe bearing dansyl and aminoquinoline groups. *Chem. Commun.* **2002**, 1424-1425.

Jimenez, M. C., Miranda, M. A., Vaya, I. Triplet excited states as chiral reporters for the binding of drugs to transport proteins. *J. Am. Chem. Soc.* 127, **2005**, 10134-10135.

Jisha, V. S.; Thomas, A. J.; Ramaiah, D. Fluorescence ratiometric selective recognition of Cu<sup>2+</sup> ions by dansyl-naphthalimide dyads. *J. Org. Chem.* 74, **2009**, 6667-6673.

Jisha, V. S.; Arun, K. T.; Hariharan, M.; Ramaiah, D. Site-selective binding and dual mode recognition of serum albumin by a squaraine dye. *J. Am. Chem. Soc.* 128, **2006**, 6024-6025.

Jisha, V. S.; Arun, K. T.; Hariharan, M.; Ramaiah, D. Site-selective interactions:

- Squaraine dye-serum albumin complexes with enhanced fluorescence and triplet yields. *J. Phys. Chem. B* **114**, **2010**, 5912–5919.
- Johnson, W. C. Analyzing protein circular dichroism spectra for accurate secondary structures. *Proteins* **35**, **1999**, 307–312.
- Jyothish, K.; Arun, K. T.; Ramaiah, D. Synthesis of novel quinaldine-based squaraine dyes: Effect of substituents and role of electronic factors. *Org. Lett.* **23**, **2004**, 3965-3968.
- Jyothish, K.; Hariharan, M.; Ramaiah, D. Chiral supramolecular assemblies of a squaraine dye in solution and thin films: concentration-, temperature, and solvent-induced chirality inversion. *Chem. Eur. J.* **13**, **2007**, 5944–5951.
- Kamat, P. V.; Das, S.; Thomas, K. G.; George, M. V. Photochemistry of squaraine dyes. 1. Excited singlet, triplet, and redox states of bis[4(dimethylamino)phenyl]squaraine and bis[4-(dimethylamino)-2hydroxyphenyl] squaraine. *J. Phys. Chem.* **96**, **1992**, 195-199.
- Katchalski-Katzir, E. *In Design and Synthesis of Organic Molecules Based on Molecular Recognition*, G. Van Binst (Ed.), Springer, New York, **1986**.
- Kazmierczak, S. C.; Gurachevsky, A.; Matthes, G.; Muravsky, V. Electron spin resonance spectroscopy of serum albumin: A novel new test for cancer diagnosis and monitoring. *Clin. Chem.* **52**, **2006**, 2129–2134.
- Kelley, D.; McClements, D. J. Interactions of bovine serum albumin with ionic surfactants in aqueous solutions. *Food Hydrocolloids* **17**, **2003**, 73-84.

- Kemlo J. A.; Shepherd, T. M. A. Quenching of excited singlet states by metal ions. *Chem. Phys. Lett.* **47**, **1977**, 158-162.
- Kim, H. J.; Hong, J.; Hong, A.; Ham, S.; Lee, J. H.; Kim, J. S. Cu<sup>2+</sup>-Induced intermolecular static excimer formation of pyrene alkylamine. *Org. Lett.* **10**, **2008**, 1963-1966.
- Kolev, T. M.; Yancheva, D. Y.; Stoyanov, S. I. Synthesis and spectral and structural elucidation of some pyridinium betaines of squaric Acid: Potential materials for nonlinear optical applications. *Adv. Funct. Mater.* **14**, **2004**, 799-805.
- Komatsu, T.; Wang, R-M.; Zunszain, P. A.; Curry, S.; Tsuchida, E. Photosensitized reduction of water to hydrogen using human serum albumin complexed with zinc-protoporphyrin IX. *J. Am. Chem. Soc.* **128**, **2006**, 16297-16301.
- Koonin, E. V.; Tatusov, R. L.; Galperin, M. Y. Beyond complete genomes: from sequence to structure and function. *Curr. Opin. Struct. Biol.* **8**, **1998**, 355-363.
- Koval, I. A.; Gamez, P.; Belle, C.; Selmeczi, K.; Reedijk, J. Synthetic models of the active site of catechol oxidase: mechanistic studies. *Chem. Soc. Rev.* **35**, **2006**, 814-840.
- Kramer, R. Fluorescent Chemosensors for Cu<sup>2+</sup> ions: Fast, selective, and highly sensitive. *Angew. Chem. Int. Ed.* **37**, **1998**, 772-774.
- Kragh-Hansen, U. Molecular aspects of ligand binding to serum albumin. *Pharmacol. Rev.* **33**, **1981**, 17-53.
- Kragh-Hansen, U. Structure and ligand binding properties of human serum. *Dan. Med. Bull.* **37**, **1990**, 57-84.
- Kreil, G. D-Amino acids in animal peptides. *Annu. Rev. Biochem.* **66**, **1997**, 337-345.

- Krishnakumar, S. S.; Panda, D. Spatial relationship between the prodan site, Trp-214, and Cys-34 residues in human serum albumin and loss of structure through incremental unfolding. *Biochemistry* **41**, **2002**, 7443–7452.
- Kubista, M. , Aakerman, B. Nordén, B. Induced circular dichroism in nonintercalative DNA-drug complexes: sector rules for structural applications. *J. Phys. Chem.* **92**, **1988**, 2352-2356.
- Kukrer, B.; Akkaya, E. U. Red to near IR fluorescent signalling of carbohydrates. *Tetrahedron Lett.* **40**, **1999**, 9125-9128.
- Kumar, C. V.; Buranaprapuk, A. Site-specific photocleavage of proteins. *Angew. Chem., Int. Ed. Eng.* **36**, **1997**, 2085-2087.
- Kumar, C. V.; Qin, L.; Das. P. K. Aromatic thioketone triplets and their quenching behaviour towards oxygen and di-t-butylnitroxy radical. A laser-flash-photolysis study. *J. Chem. Soc. Faraday Trans. 2*, **80**, **1984**, 783-793.
- Kumar, C. V.; Buranaprapuk, A.; Sze, H. C.; Jockusch, S.; Turro, N. J. Chiral protein scissors: High enantiomeric selectivity for binding and its effect on protein photocleavage efficiency and specificity. *Proc. Natl. Acad. Sci. U. S. A.* **99**, **2002**, 5810–5815.
- Kumar, C. V.; Chaudhari, A. Proteins immobilized at the galleries of layered  $\alpha$ -zirconium phosphate: Structure and activity studies. *J. Am. Chem. Soc.* **122**, **2000**, 830–837.
- Kumar, C. V.; Buranaprapuk, A. Tuning the selectivity of protein photocleavage:

- Spectroscopic and photochemical studies. *J. Am. Chem. Soc.* **121**, **1999**, 4262–4270.
- Kumar, C. V.; Thota, J. Photocleavage of lysozyme by cobalt (III) complexes. *Inorg. Chem.* **44**, **2005**, 825–827.
- Kumar, C. V.; Tolosa, L. M. Interaction of hydrophobic probes with serum albumin— influence of the side chain and exciplex formation at the binding site. *J. Phys. Chem.* **97**, **1993**, 13914–13919.
- Kurtzhals, P.; Havelund, S.; Jonassen, I.; Kiehr, B.; Larsen, U. D.; Ribøl, U.; Markussen, J. Albumin binding of insulins acylated with fatty acids: characterization of the ligand-protein interaction and correlation between binding affinity and timing of the insulin effect in vivo. *Biochem. J.* **312**, **1995**, 725–731.
- Kuruvilla, E.; Nandajan, P.C.; Schuster, G. B.; Ramaiah, D. Acridine–viologen dyads: selective recognition of single-strand DNA through fluorescence enhancement. *Org. Lett.* **10**, **2008**, 4295–4298.
- Kuruvilla, E.; Ramaiah, D. Selective interactions of a few acridinium derivatives with single strand DNA: Study of photophysical and DNA binding interactions. *J. Phys. Chem. B* **111**, **2007**, 6549–6556.
- Lakowicz, J. R. ed Topics in fluorescence spectroscopy: Protein fluorescence. Kluwer Academic/ Plenum, New York, Vol.6. **2000**.
- Langlots, R.; Ali, H.; Brasseur, N.; Wagner, J. R.; van Lier, I. R. Biological activities of phthalocyanines-IV. Type II sensitized photooxidation of L-Tryptophan and

- cholesterol by sulfonated metallo phthalocyanines.. *Photochem. Photobiol.* 44, **1986**, 117-123.
- Lapicque, F.; Muller, N.; Payan, E.; Dubois, N. Protein binding and stereoselectivity of nonsteroidal anti-inflammatory drugs. *Clin. Pharmacokinet.* 25, **1993**, 115-125.
- Law, K. Y. *J. Imaging Sci.* 31, **1987**, 83.
- Law, K. Y. Organic photoconductive materials: recent trends and developments. *Chem. Rev.* 93, **1993**, 449-486.
- Leamon, C. P.; Low, P. S. Folate-mediated targeting: from diagnostics to drug and gene delivery. *Drug Discovery Today* 6, **2001**, 44-51.
- Leamon, C. P.; Low, P. S. Cytotoxicity of momordin-folate conjugates in cultured human cells. *J. Biol. Chem.* 267, **1992**, 24966–24971.
- Leamon, C. P.; Low, P. S. Endocytosis of folate-protein conjugates: Ultrastructural localization in KB Cells. *J. Cell. Sci.* 106, **1993**, 423-30.
- Leamon, C. P.; Low, P.S. Selective targeting of malignant cells with cytotoxin-folate conjugates. *J. Drug Target.* 2, **1994**, 101–112.
- Leamon, C. P.; Reddy, J. A. Folate-targeted chemotherapy, *Advanced Drug Delivery Reviews.* 56, **2004**, 1127– 1141.
- Lee, J. C.; Gray, H. B.; Winkler, J. R. Copper (II) binding to  $\alpha$ -Synuclein, the parkinson's protein. *J. Am. Chem. Soc.* 130, **2008**, 6898-6899.
- Lee, M. H.; Kim, H. J.; Yoon, S.; Park, N.; Kim, J. S. Metal ion induced FRET OFF–ON in tren/dansyl-appended rhodamine. *Org. Lett.* 10, **2008**, 213-216.

Lehninger *Principles of biochemistry*, CBS Publishers and Distributors, New Delhi.

**1984.**

Lhiaubet-Vallet, V.; Sarabia, Z.; Bosca, F.; Miranda, M. A. Human serum albumin-mediated stereodifferentiation in the triplet state behavior of (S)-and (R)-carprofen. *J. Am. Chem. Soc.* **126**, **2004**, 9538-9539.

Li, G.-K.; Xu, Z.-X.; Chen, C.-F.; Huang, Z.-T. A highly efficient and selective turn-on fluorescent sensor for Cu<sup>2+</sup> ion based on calix[4]arene bearing four iminoquinoline subunits on the upper rim. *Chem. Commun.* **2008**, 1774-1776.

Li, K. L.; Thakur, A. K.; Kapoor, A. L. Structural requirements for binding of nonsteroidal anti-inflammatory drugs to human serum albumin. *J. Pharm. Sci.* **77**, **1988**, 251-254.

Li, Y.; Cao, L.; Tian, He. Fluoride ion-triggered dual fluorescence switch based on naphthalimides winged zinc porphyrin. *J. Org. Chem.* **71**, **2006**, 8279-8282.

Li, Y.; Zheng, H.; Li, Y.; Wang, S.; Wu, Z.; Liu, P.; Gao, Z.; Liu, H.; Zhu, D. Photonic logic gates based on control of FRET by a solvatochromic perylene bisimide. *J. Org. Chem.* **72**, **2007**, 2878-2885.

Lim, M. H.; Lippard, S. J. Copper complexes for fluorescence-based NO detection in aqueous solution. *J. Am. Chem. Soc.* **127**, **2005**, 12170-12171.

Lim, M. H.; Lippard, S. J. Fluorescent nitric oxide detection by copper complexes bearing anthracenyl and dansyl fluorophore ligands. *Inorg. Chem.*, **45**, **2006**, 8980-8989.

- Lin, W.; Yuan, L.; Long, L.; Guo, C.; Feng, J. A fluorescent cobalt probe with a large ratiometric fluorescence response via modulation of energy acceptor molar absorptivity on metal ion binding. *Adv. Funct. Mater.* **18**, **2008**, 2366-2373.
- Linder M. C.; Hazegh-Azam, M. Copper biochemistry and molecular biology. *Am. J. Clin. Nutr.* **63**, **1996**, 797S- 811S.
- Lou, J.; Hatton, T. A.; Laibinis, P. E. Fluorescent probes for monitoring temperature in organic solvents. *Anal. Chem.* **69**, **1997**, 1262-1264.
- Lucas, L. H.; Price, K. E.; Larive, C.K. Epitope mapping and competitive binding of HSA drug site II ligands by NMR diffusion measurements. *J. Am. Chem. Soc.* **126**, **2004**, 14258-14266.
- Ludwig, R.; Dzung, N. T. K. Calixarene-based molecules for cation recognition. *Sensors* **2**, **2002**, 397-416.
- Lyon, C. E.; Suh, E. S.; Dobson, C. M.; Hore, P. J. Probing the exposure of tyrosine and tryptophan residues in partially folded proteins and folding intermediates by CIDNP pulse-labeling. *J. Am. Chem. Soc.* **124**, **2002**, 13018-13024.
- Mallick, A.; Haldar, B.; Chattopadhyay, N. Spectroscopic investigation on the interaction of ICT probe 3-Acetyl-4-oxo-6, 7-dihydro-12H indolo-[2,3-a] quinolizine with serum albumins. *J. Phys. Chem. B* **109**, **2005**, 14683-14690.
- Martinez-Manez, R.; Sancenon, F. Fluorogenic and chromogenic chemosensors and reagents for anions. *Chem. Rev.* **103**, **2003**, 4419-4476.
- Martinez, R.; Zapata, F.; Caballero, A.; Espinosa, A.; Tarraga, A.; Molina, P. 2-Aza-1,3-

- butadiene derivatives featuring an anthracene or pyrene unit: Highly selective colorimetric and fluorescent signaling of Cu<sup>2+</sup>cation. *Org. Lett.* **8**, **2006**, 3235-3238.
- Mazzaglia, A.; Anelini, N.; Lombardo, D.; Micali, N.; Patane, S.; Villari, V.; Scolaro, L. M. amphiphilic cyclodextrin carriers embedding porphyrins: charge and size modulation of colloidal stability in heterotopic aggregates. *J. Phys. Chem. B* **109**, **2005**, 7258–7265.
- McPherson, A. Macromolecular crystals. *Sci. Am.* **260**, **1989**, 62–69.
- Meister, A. Biochemistry of the amino Acids, 2<sup>nd</sup> edn, Vols 1 and 2, Academic Press, Inc., New York. **1965**.
- Meyer, B.; Peters, T. NMR Spectroscopy techniques for screening and identifying ligand binding to protein receptors. *Angew. Chem. Int. Ed.* **42**, **2003**, 864 – 890.
- Michel, H.; Behr, J.; Harrenga, A.; Kannt, A. Cytochrome c oxidase: Structure and spectroscopy. *Annu. Rev. Biophys. Biomol. Struct.* **27**, **1998**, 329–356.
- Millhauser, G. L. Copper binding in the prion protein. *Acc. Chem. Res.* **37**, **2004**, 79-87.
- Montalti, M.; Prodi, L.; Zaccheroni, N.; Falini, G. Solvent-induced modulation of collective photophysical processes in fluorescent silica nanoparticles. *J. Am. Chem. Soc.* **124**, **2002**, 13540-13546.
- Momenteau, M.; Reed, C. A. Synthetic heme-dioxygen complexes. *Chem. Rev.* **94**, **1994**, 659-698.
- Montvydiene, D.; Marciulioniene, D. Assessment of toxic interactions of heavy metals

- in a multicomponent mixture using *Lepidium sativum* and *Spirodela polyrrhiza*. *Environmental Toxicology* **2004**, 351-358.
- Moon, W.K.; Lin, Y.; O'Loughlin, T.; Tang, Y.; Kim, D. E.; Weissleder, R.; Tung, C.H.; Enhanced tumor detection using a folate receptor-targeted near-infrared fluorochrome conjugate. *Bioconjugate Chem.* 14, 2003, 539– 545.
- Moser, J. G. *Photodynamic tumor therapy: 2<sup>nd</sup> and 3<sup>rd</sup> Generation Photosensitizers*; Harwood Academic Publishers: Amsterdam, **1998**.
- Müller, W. E.; Wollert, U. Circular dichroism studies on the interaction of four structurally related long-acting sulfonamides with human and bovine serum albumin. *Biochem. Pharmacol.* 25, **1976**, 1459-1464.
- Muzammil, S.; Kumar, Y.; Tayyab, S. Anion-induced stabilization of human serum albumin prevents the formation of intermediate during urea denaturation. *Protein* 40, **2000**, 29–38.
- Nair, A. K.; Neelakandan, P. P.; Ramaiah, D. A supramolecular Cu(II) metallocyclophane probe for guanosine 5'-monophosphate. *Chem. Commun.* **2009**, 6352–6354.
- Neelakandan, P. P.; Ramaiah, D. DNA-assisted long-lived excimer formation in a cyclophane. *Angew. Chem. Int. Ed.* 47, **2008**, 8407-8411.
- Neelakandan, P. P.; Hariharan, M.; Ramaiah, D. A supramolecular ON-OFF-ON fluorescence assay for selective recognition of GTP. *J. Am. Chem. Soc.* 128, **2006**, 11334-11335.
- Nishizawa, S.; Watanabe, M.; Uchida, T.; Teramae, N. Fluorescence ratio sensing of

- alkali metal ions based on control of the intramolecular exciplex formation. *J. Chem. Soc., Perkin Trans. 2*, 1999, 141-144
- Nohta, H.; Satozono, H.; Koiso, K.; Yoshida, H.; Ishida, J.; Yamaguchi, M. Highly Selective fluorometric determination of polyamines based on intramolecular excimer-forming derivatization with a pyrene-labeling reagent. *Anal. Chem.* **72**, **2000**, 4199-4204.
- Nordén, B., Tjerneld, F. Structure of methylene blue–DNA complexes studied by linear and circular dichroism spectroscopy. *Biopolymers* **21**, **1982**, 1713-1734.
- Okamoto, A.; Ichiba, T.; Saito, I. Pyrene-labeled oligodeoxynucleotide probe for detecting base insertion by excimer fluorescence emission. *J. Am. Chem. Soc.* **126**, **2004**, 8364-8385.
- Oswald, B.; Patsenker, L.; Duschl, J.; Szmecinski, H.; Wolfbeis, O. S.; Terpetsching, E. Synthesis, spectral properties, and detection limits of reactive squaraine dyes, a new class of diode laser compatible fluorescent protein labels. *Bioconjugate Chem.* **10**, **1999**, 925-931.
- Pal, S. K.; Zewail, A. H. Dynamics of water in biological recognition. *Chem. Rev.* **104**, **2004**, 2099-2124.
- Pandey, R. K.; Constantine, S.; Tsuchida, T.; Zheng, G.; Medforth, C. J.; Aoudia, M.; Kozyrev, A. N.; Rodgers, M. A. J.; Kato, H.; Smith, K. M.; Dougherty, T. J. Synthesis, photophysical properties, in vivo photosensitizing efficacy, and human serum albumin binding properties of some novel bacteriochlorins. *J. Med. Chem.* **40**,

**1997**, 2770-2779.

Pandey, S.; Azam, A.; Pandey, S.; Chawla, H. M. Novel dansyl-appended calix[4]arene frameworks: fluorescence properties and mercury sensing. *Org. Biomol. Chem.* **7**, **2009**, 269-279.

Park, S. M.; Kim, M. H.; Choe, J.-I.; No, K. T.; Chang, S.-K. Cyclams bearing diametrically disubstituted pyrenes as Cu<sup>2+</sup>- and Hg<sup>2+</sup>-selective fluoroionophores. *J. Org. Chem.* **72**, **2007**, 3550-3553.

Perutz, M.F. Myoglobin and haemoglobin: role of distal residues in reactions with heme ligands. *Trends Biochem. Sci.* **14**, **1989**, 42-44.

Peters, T. All about albumin: Biochemistry, genetics and medical applications Academic, San Diego. **1995**.

Ponting, C. P.; Russell, R. R. The natural history of protein domains. *Annu. Rev. Biophys. Biomol. Struct.* **31**, **2002**, 45-71.

Prockop, D. J.; Kivirikko, K. I. Collagens, molecular biology, diseases, and potentials for therapy. *Annu. Rev. Biochem.* **64**, **1995**, 403-434.

Qi, X.; Jun, E. J.; Xu, L.; Kim, S.-J.; Hong, J. S. J.; Yoon, Y. J.; Yoon, J. New BODIPY derivatives as OFF-ON fluorescent chemosensor and fluorescent chemodosimeter for Cu<sup>2+</sup>: Cooperative selectivity enhancement toward Cu<sup>2+</sup>. *J. Org. Chem.* **71**, **2006**, 2881-2884.

Rahman, M. H.; Yamasaki, K.; Shin, Y.-H.; Lin, C. C.; Otagiri, M. Characterization of high affinity binding sites of non-steroidal anti-inflammatory drugs with respect to

- site-specific probes on human serum albumin. *Biol. Pharm. Bull.* **16**, **1993**, 1169-1174.
- Ramaiah, D.; Joy, A.; Chandrasekhar, N.; Eldho, N. V.; Das, S.; George, M. V. Halogenated squaraine dyes as potential photochemotherapeutic agent. Synthesis and study of photophysical properties and quantum efficiencies of singlet oxygen generation. *Photochem. Photobiol.* **65**, **1997**, 783-790.
- Ramaiah, D.; Eckert, I.; Arun, K. T.; Weidenfeller, L.; Epe, B. Squaraine dyes for photodynamic therapy: Study of their cytotoxicity and genotoxicity in bacteria and mammalian cells. *Photochem. Photobiol.* **76**, **2002**, 672-677.
- Ramaiah, D.; Eckert, I.; Arun, K. T.; Weidenfeller, L.; Epe, B. Squaraine dyes for photodynamic therapy: Mechanism of cytotoxicity and DNA damage induced by halogenated squaraine dyes plus light (>600 nm). *Photochem. Photobiol.* **79**, **2004**, 99-104.
- Ramaiah, D.; Arun, K. T.; Das, S.; Epe, B. US 6770787, **2004**.
- Reise Sousa, A. T.; Castanheira, E. M. S.; Fedorov, A.; Martinho, J. M. G. Kinetic study of the reactions of Ca(<sup>1</sup>S) and Sr(<sup>1</sup>S) atoms with Cl<sub>2</sub> in the temperature ranges from respectively 303–1038 K and 303–991 K. *J. Phys. Chem. A* **102**, **1998**, 6406-6410.
- Resch-Genger, U.; Grabolle, M.; Cavaliere-Jaricot, S.; Nitschke, R.; and Nann, T. Quantum dots versus organic dyes as fluorescent labels. *Nat. Methods* **5**, **2008**, 763–775.
- Richardson, J.S. The anatomy and taxonomy of protein structure. *Adv. Prot. Chem.* **34**,

**1981**, 167–339.

Roberts S. M. Molecular recognition—chemical and biochemical problems, Royal Society of Chemistry, Cambridge. **1989**.

Roda, A.; Cappelleri, G.; Aldini, R.; Roda, E.; Barbara, L. Quantitative aspects of the interaction of bile acids with human serum albumin. *J. Lipid Res.* **23**, **1982**, 490-495.

Rodger, A.; Norden, B. Circular dichroism and linear dichroism; Oxford University Press. **1997**.

Rodgers, M. A. J. Photodynamic therapy of tumors and other diseases; Jori, G., Perria, C., Eds.; Liberia Progetto: Padova, p 22. **1985**.

Ros-Lis, J. V.; Garcia, B.; Jimenez, D.; Martinez-Manez, R.; Sancenon, F.; Soto, J.; Gonzalvo, F.; Vallendecabres, M. C. Squaraines as fluoro-chromogenic probes for thiol-containing compounds and their application to the detection of biorelevant thiols. *J. Am. Chem. Soc.* **126**, **2004**, 4064-4065.

Ros-Lis, J. V.; Martinez-Manez, R.; Sancenon, F.; Soto, J.; Spieles, M.; Rurack, K. Squaraines as reporter units: Insights into their photophysics, protonation, and metal-ion coordination behaviour. *Chem. Eur. J.* **14**, **2008**, 10101-10114.

Ros-Lis, J. V.; Martinez-Manez, R.; Rurack, K.; Sancenon, F.; Soto, J.; Spieles, M. Highly selective chromogenic signaling of Hg<sup>2+</sup> in aqueous media at nanomolar levels employing a squaraine-based reporter. *Inorg. Chem.* **43**, **2004**, 5183-5185.

Ros-Lis, J. V.; Marcos, M. D.; Martinez-Manez, R.; Rurack, K.; Soto, J. A regenerative

chemodosimeter based on metal-induced dye formation for the highly selective and sensitive optical determination of Hg<sup>2+</sup> Ions. *Angew. Chem., Int. Ed.* **44**, **2005**, 4405-4407.

Rugar, D.; Hansma, P. K. *Atomic force microscopy. Phys. Today* **43**, **1990**, 23-24.

Sajimon, M. C.; Ramaiah, D.; Suresh, C. H.; Adam, W.; Lewis, F. D.; George, M. V. Photochromic dibenzobarrene: Long-lived triplet biradical intermediates. *J. Am. Chem. Soc.* **129**, **2007**, 9439-9445.

Samori, P. *Scanning probe microscopies beyond imaging*; Wiley-VCH: Weinheim, **2006**.

Sapsford, K. E.; Berti, L.; Medintz, I. L. Materials for fluorescence resonance energy transfer analysis: Beyond traditional donor-acceptor combinations. *Angew. Chem., Int. Ed.* **45**, **2006**, 4562-4589.

Schneider, H.-J.; Blatter, T.; Zimmermann, P. Host-guest complexes with closed, half-open, and stretched receptors: Hydrophobic cavity effects and induced pole-dipole interactions. *Angew. Chem. Int. Ed. Engl.* **29**, **1990**, 1161-1162.

Schneider, H.-J.; Yatsimirsky, A. K. Selectivity in supramolecular host-guest complexes. *Chem. Soc. Rev.* **37**, **2008**, 263-277.

Schwuger, M. J.; Bartnik, F. G. In *Anionic surfactants*; Gloxhuber, C., Ed.; Surfactant Science Series; Marcel Dekker: New York, Vol.10. **1980**.

Serganov, A.; Keiper, S.; Malinina, L.; Tereshko, V.; Skripkin, E.; Hobartner, C.; Polonskaia, A.; Phan, A. T.; Wombacher, R.; Micura, R.; Dauter, Z.; Jaschke, A.;

- Patel, D. J. Structural basis for diels-alder ribozyme-catalyzed carbon-carbon bond formation. *Nat. Struct. Mol. Biol.* **12**, **2005**, 218-224.
- Sen, P.; Roy, D.; Mondal, S. K.; Sahu, K.; Ghosh, S.; Bhattacharyya, K. Solvation dynamics of DCM in a DPPC vesicle entrapped in a sodium silicate derived sol-gel matrix. *J. Phys. Chem. B* **109**, **2005**, 3319-3323.
- Sheffield, W. P. Current Drug Targets CardioVasc. *Haematol. Disord.* **1**, **2001**, 1-22.
- Siam, M.; Blaha, G.; Lehner, H.. Maximum binding capacity of serum albumin for bilirubin is one, as revealed by circular dichroism. *J. Chem. Soc., Perkin Trans 2*, **1998**, 853-856.
- Silveira, V. C. D.; Luz, J. S.; Oliveira, C. C.; Graziani, I.; Ciriolo, M. R.; Ferreira, A.M.D.C. Double-strand DNA cleavage induced by oxindole-Schiff base copper(II) complexes with potential antitumor activity. *J. Inorg. Biochem.* **102**, **2008**, 1090-1103.
- Simard, J. R.; Zunszain, P. A.; Ha, C. E.; Yang, J. S.; Bhagavan, N. V.; Petitpas, I.; Curry, S.; Hamilton, J. A. Locating high-affinity fatty acid-binding sites on albumin by x-ray crystallography and NMR spectroscopy. *Proc. Natl. Acad. Sci. U. S. A.* **102**, **2005**, 17958-17963.
- Simard, J. R.; Zunszain, P. A.; Hamilton, J. A.; Curry, S. Location of high and low affinity fatty acid binding sites on human serum albumin revealed by NMR Drug-competition Analysis. *J. Mol. Biol.* **361**, **2006**, 336-351.
- Sollenne, N. P.; Means, G. E. Characterization of a specific drug binding site of human

- serum albumin. *Mol. Pharmacol.* 15, **1979**, 754-757.
- Spector, A. A. Structure and lipid binding properties of serum albumin, in "Methods in Enzymology"(J. P. Segrest and J. J. Albers, eds.), Vol. 128, pp. 320-339. Academic Press, Orlando, Florida, **1986**.
- Spector, A. A. Fatty acid binding to plasma albumin. *J. Lipid Res.* 16, **1975**, 165-179.
- Speiser, S. Photophysics and mechanisms of intramolecular electronic energy transfer in bichromophoric molecular systems: Solution and supersonic jet studies. *Chem. Rev.* 96, **1996**, 1953-1976.
- Stewart, A. J.; Blindauer, C. A.; Berezenko, S.; Sleep, D.; Sadler, P. J. Interdomain zinc site on human albumin. *Proc. Natl. Acad. Sci. U. S. A.* 100, **2003**, 3701-3706.
- Sudlow, G.; Brikket, D. J.; and Wade, D. N. The characterization of two specific drug binding sites on human serum albumin. *Mol. Pharmacol.* 11, **1975**, 824-832.
- Sudlow, G.; Birkett, D. J.; and Wade, D. N. Further characterization of specific drug binding sites on human serum albumin. *Mol. Pharmacol.* 12, **1976**, 1052-1061.
- Sugio, S.; Kashima, A.; Mochizuki, S.; Noda, M.; Kobayashi, K. Crystal structure of human serum albumin at 2.5 Å resolution. *Protein. Eng.* 12, **1999**, 439-446.
- Suzuki, Y.; Yokoyama, K. Design and synthesis of intramolecular charge transfer-based fluorescent reagents for the highly-sensitive detection of proteins. *J. Am. Chem. Soc.* 127, **2005**, 17799-17802.
- Switzer, S.; Eder, H. A. Transport of lysolecithin by albumin in human and rat plasma. *J. Lipid Res.* 6, **1965**, 506-511.

- Sytnik, A.; Litvinyuk, I. Energy transfer to a proton-transfer fluorescence probe: tryptophan to a flavonol in human serum albumin. *Proc. Natl. Acad. Sci. U. S. A.* **93**, **1996**, 12959-12963.
- Szacilowski, K.; Macyk, W.; Drzewiecka-Matuszek, A.; Brindell, M.; Stochel, G. Bioinorganic photochemistry: Frontiers and mechanisms. *Chem. Rev.* **105**, **2005**, 2647-2694.
- Tanford, C. *The hydrophobic effect: Formation of micelles and biological membranes*, 2nd ed., pp 155-157, Wiley, New York, **1980**.
- Tayyab, S.; Siddiqui, M. U.; Ahmad, N. Experimental determination of the free energy of unfolding of proteins. *Biochem. Ed.* **23**, **1995**, 162-164.
- Torrado, A.; Walkup, G. K.; Imperiali, B. Exploiting polypeptide motifs for the design of selective Cu(II) ion chemosensors. *J. Am. Chem. Soc.* **120**, **1998**, 609-610.
- Triebs, A.; Jacob, K. Cyclotrimethine dyes derived from squaric Acid. *Angew. Chem. Int. Ed. Engl.* **4**, **1965**, 694-695.
- Tsuchida, T.; Zheng, G.; Panday, R. K.; Potter, W. R.; Bellnier, D. A.; Henderson, B. W.; Kato, H.; Dougherty, T. J. Correlation between site II-specific human serum albumin (HSA) binding affinity and murine in vivo photosensitizing efficacy of some photofrins components. *Photochem. Photobiol.* **66**, **1997**, 224-228.
- Turek, J. J.; Leamon, C. P.; Low, P. S. Endocytosis of folate-protein conjugates: ultrastructural localization in KB cells. *J. Cell. Sci.* **106**, **1993**, 423-430.

- Turfan, B.; Akkaya, E.U. Modulation of boradiazaindacene emission by cation-mediated oxidative PET. *Org. Lett.* **4**, **2002**, 2857–2859.
- Turro, N. J.; Lei, X. G.; Ananthapadmanabhan, K. P.; Aronson, M. Spectroscopic probe analysis of protein-surfactant interactions: The BSA/SDS System. *Langmuir* **11**, **1995**, 2525-2533.
- Turro, N. J. *Modern Molecular Photochemistry*; Benjamin/Cummings: Menlo Park, CA, **1978**.
- Ueno, A.; Osa T. In *Photochemistry in Organized and Constrained Media*; Ramamurthy, V. Ed.; VCH Publishers: New York, 1991, pp 739-782.
- Valeur, B.; Bourson, P. J. Tuning of photoinduced energy transfer in a bichromophoric coumarin supermolecule by cation binding. *J. Phys. Chem.* **96**, **1992**, 6545-6549.
- Varnes, A. V.; Dodson, R. B.; Whery, E. L. Interactions of transition-metal ions with photoexcited states of flavines. Fluorescence quenching studies. *J. Am. Chem. Soc.* **94**, **1972**, 946-950.
- Vaya, I.; Bueno, C. J.; Jimenez, M. C.; Miranda, M. A. Use of triplet excited states for the study of drug binding to human and bovine serum albumins. *ChemMedChem.* **1**, **2006**, 1015-1020.
- Vicinelli, V.; Ceroni, P.; Maestri, M.; Balzani, V.; Gorka, M.; Vögtle, F. Luminescent lanthanide ions hosted in a fluorescent polylysine dendrimer. Antenna-like sensitization of visible and near-infrared emission. *J. Am. Chem. Soc.* **124**, **2002**, 6461-6468.

- Vijai, K.; Forster, J. The amphoteric behavior of bovine plasma albumin. Evidence for masked carboxylate groups in the native protein. *Biochemistry* 6, **1967**, 1152-1159.
- Voet, D.; Voet, J. G. *Biochemistry*: 2<sup>nd</sup> edition, John Wiley and Sons, New York, **1995**.
- Vosburgh, W. C.; Cooper, G. R. Complex ions. I. The identification of complex ions in solution by spectrophotometric measurements. *J. Am. Chem. Soc.* 63, **1941**, 437-442.
- Wallace, K. J.; Gray, M.; Zhong, Z.; Lynch, V. M.; Anslyn, E. V. An artificial siderophore for the detection of iron(III). *Dalton Trans.* **2005**, 2436-2441.
- Wallevik, K. Reversible denaturation of human serum albumin by pH, temperature, and guanidine hydrochloride followed by optical rotation. *J. Biol. Chem.* 248, **1973**, 2650-2655.
- Wang, C. S.; Bass, H.; Whitmer, R.; McConathy, W. J. Elongation, desaturation, and esterification of essential fatty acids by fetal rat brain in vivo. *J. Lipid Res.* 34, **1993**, 2091-2098.
- Watanabe, A., S; Matsuzaki, H.; Moriwaki, K.; Suzuki, K.; Nishiguchi, S. Problems in serum albumin measurement and clinical significance of albumin microheterogeneity in cirrhotics. *Nutrition* 20, **2004**, 351-357.
- Watanabe, S.; Saito, T. Conformational effects in the interaction of phenylbutazone with albumin studied by circular dichroism. *Biochem. Pharmacol.* 43, **1992**, 931-935.

- Weisiger, R.; Gollan, J.; Ockner, R. Receptor for albumin on the liver cell surface may mediate uptake of fatty acids and other albumin-bound substances. *Science* **211**, **1981**, 1048-1050.
- Wen, Z.-C.; Yang, R.; He, H.; Jiang, Y.-B. A highly efficient and selective turn-on fluorescent sensor for Cu<sup>2+</sup> ion based on calix[4]arene bearing four iminoquinoline subunits on the upper rim. *Chem. Commun.* **2006**, 106-108.
- Wen, Z.-C.; Yang, R.; He, H.; Jiang, Y.-B. A highly selective charge transfer fluoroionophore for Cu<sup>2+</sup>. *Chem. Commun.* **2006**, 106-108.
- Wieder, M. E.; Hone, D. C.; Cook, M. J.; Handsley, M. M.; Gavrilovic, J.; Russell, D. A. Intracellular photodynamic therapy with photosensitizer-nanoparticle conjugates: cancer therapy using a 'Trojan horse.' *Photochem. Photobiol. Sci.* **5**, **2006**, 727-734.
- Xie, J.; Menand, M.; Maisonneuve, S.; Metivier, R. Synthesis of Bispyrenyl Sugar-Aza-Crown Ethers as New Fluorescent Molecular Sensors for Cu(II). *J. Org. Chem.* **72**, **2007**, 5980-5985.
- Xu, L. C.; Rodriguez, V. V.; Logan, B. E. Residence time, loading force, pH, and ionic strength affect adhesion forces between colloids and biopolymer-coated surfaces. *Langmuir* **21**, **2005**, 7491-7500.
- Xu, Z.; Xiao, Y.; Qian, X.; Cui, J.; Cui, D. Ratiometric and selective fluorescent sensor for Cu<sup>II</sup> based on internal charge transfer (ICT). *Org. Lett.* **7**, **2005**, 889-892.
- Yang, J.-S.; Lin C.-S.; Hwang, C.-Y. Cu<sup>2+</sup>-Induced blue shift of the pyrene excimer

- emission: A new signal transduction mode of pyrene probes. *Org. Lett.* **3**, **2001**, 889-892.
- Yannis, L. L. Multiple complex formation of fluorescent compounds with cyclodextrins: Efficient determination and evaluation of the binding constant with improved fluorometric studies. *J. Phys. Chem. B* **101**, **1997**, 4863-4866.
- Zeng, L.; Miller, E. W.; Pralle, A.; Isacoff, E.Y.; Chang, C. J. A selective turn-on fluorescent sensor for imaging copper in living Cells. *J. Am. Chem. Soc.* **128**, **2006**, 10-11.
- Zhang, R. M.; and Snyder, G. H. Dependence of formation of small disulfide loops in two-cysteine peptides on the number and types of intervening amino acids. *J. Biol. Chem.* **264**, **1989**, 18472-18479.
- Zhang, X.; Xiao, Y. A Ratiometric Fluorescent Probe Based on FRET for Imaging Hg<sup>2+</sup>Ions in Living Cells. *Angew. Chem. Int. Ed. Engl.* **47**, **2008**, 8025-8029.
- Zheng, Y.; Gattás-Asfura, K. M.; Konka, V.; Leblanc, R. M. A dansylated peptide for the selective detection of copper ions. *Chem. Commun.* **2002**, 2350-2351.
- Zhong, D. P.; Pal, S. K.; Zewail A. H. Femtosecond studies of protein-DNA binding and dynamics: Histone I. *ChemPhysChem.* **2**, **2001**, 219-227.
- Zhong, D. P.; Douhal, A.; Zewail, A. H. Femtosecond studies of protein–ligand hydrophobic binding and dynamics: Human serum albumin. *Proc. Natl. Acad. Sci. U. S. A.* **97**, **2000**, 14056-14061.
- Zhong, Z.; Anslyn, E. V. A colorimetric sensing ensemble for heparin. *J. Am. Chem. Soc.* **124**, **2002**, 9014-9015.

## LIST OF PUBLICATIONS OF Ms. V. S. JISHA

1. Site-Selective Binding and Dual Mode Recognition of Serum Albumin by a Squaraine Dye, **V. S. Jisha**, K. T. Arun, M. Hariharan and D. Ramaiah, *J. Am. Chem. Soc.* **2006**, *128*, 6024-6025.
2. Novel Ratiometric Fluorescence Sensor for Cupric Ions through Inhibition of Intramolecular Energy Transfer, **V. S. Jisha**, A. J. Thomas and D. Ramaiah, *J. Org. Chem.* **2009**, *74*, 6667-6673.
3. Site-Selective Interactions: Squaraine Dye-Serum Albumin Complex with Enhanced Fluorescence and Triplet Yields, **V. S. Jisha**, K. T. Arun, M. Hariharan and D. Ramaiah, *J. Phys. Chem. B.* **2010**, *114*, 5912-5919.
4. Novel Porphyrin Derivatives for Photodynamic Therapy (PDT): A Process for the Preparation Thereof and their use as PDT Agents and Fluorescence Probes for Biological Applications, D. Ramaiah, C. K. Suneesh, **V. S. Jisha**, T. K. Chandrasekhar, A. Srinivasan, M. R. Pillai, S. A. Nair, P. S. Saneesh Babu, Ch. Mohan Rao and K. Sridhar Rao, a patent application filed in India and abroad, *No. 0147NF2009, dated September 14, 2009.*

## PAPERS PRESENTED AT CONFERENCES

1. Site-Selective Binding and Dual Mode Recognition of Serum Albumin by a Squaraine Dye, **V. S. Jisha**, K. T. Arun, M. Hariharan and D. Ramaiah, a poster presented at "*Photo-Rad Chem, Mahatma Gandhi University, Kottayam, India, 2007*, February 8-11.
2. Site Selective Binding and Dual Mode Recognition of Serum Albumin by a Squaraine Dye, **V. S. Jisha**, K. T. Arun, M. Hariharan and D. Ramaiah, a poster presented at "*10<sup>th</sup> National Symposium in Chemistry,*" Indian Institute of Science, Bangalore, India, **2008**, February 1-3.
3. Study of Interactions of a Few Novel Squaraine dyes with Serum Albumins, **V. S. Jisha**, K. T. Arun, M. Hariharan and D. Ramaiah, a poster presented at "*Recent Trends in Molecular Materials Research,*" DST-JSPS Conference, Trivandrum, **2008**, January 20-22.